Characterization of the retinal degeneration and glial activation of neuronal ceroid lipofuscinosis mouse models *Cln3*$^{\Delta ex7-8}$ and *Cln6*^{nclf} and the beneficial effects of dietary supplementation

DISSERTATION ZUR ERLANGUNG DES
DOKTORGRADES DER NATURWISSENSCHAFTEN (DR. RER. NAT.)
DER FAKULTÄT BIOLOGIE UND VORKLINISCHE MEDIZIN
DER UNIVERSITÄT REGENSBURG

vorgelegt von

Myriam Mirza

aus

Montreal, Canada

2013

Promotionsgesuch wurde eingereicht am: 25 June, 2013

Die Arbeit wurde angeleitet von: Prof Dr. Thomas Langmann

Unterschrift:

What is a scientist after all? It is a curious man looking through a keyhole, the keyhole of nature, trying to know what's going on.

Jacques Yves Cousteau

Dedicated to those which suffer or have suffered
from the merciless hands of neuronal ceroid lipofuscinosis

Table of Contents

1. Introduction 1

1.1 Structure and Function of the Mammalian Retina 1

1.2 Müller Cells 2

1.3 Microglia cells 3

1.3.1 Microglia in the CNS and Retina 3

1.3.2 Function of the Microglia Cells 4

1.3.3 Activation and Morphological Plasticity of Microglia Cells 4

1.4 Inherited Diseases of the Eye 6

1.4.1 Microglia in Retinal Degeneration 7

1.4.2 Müller Cells in Retinal Degeneration 8

1.5 Neuronal Ceroid Lipofuscinosis (NCL) 9

1.5.1 Characteristics of NCL 9

1.5.2 NCL as a Lysosomal Storage Disorder 10

1.5.3 Characteristics of CLN3 Mutations 11

1.5.4 Characteristics of CLN6 Mutations 12

1.5.5 Animal Models of CLN3 and CLN6 13

1.5.6 Retinal Degeneration in NCL 14

1.5.7 Glial Activation in NCL 15

1.6 Glial Attenuation with Natural Compounds 16

1.6.1 Curucmin 16

1.6.2 Luteolin 16

1.6.3 DHA 17

1.7 Aim of the Thesis 17

2. Materials 19

2.1 Mouse Models 19
2.2 Oligonucleotides for real-time RT-PCR 19
2.3 Enzymes 20
2.4 Antibodies 20
2.4 Chemical and Kit System 20
2.5 Dietary Supplementation 22
2.6 Electroretinograms 22
2.7 Buffers and Solutions 22
2.8 Basic Materials 23
2.9 Machines and Software 24
3 Methods 26
3.1 Mouse Lines and Husbandry 26
3.2 Mouse Genotyping 26
3.2.1 DNA Extractions 26
3.2.2 Photometric determination of DNA concentration 26
3.2.3. DNA amplification with PCR 26
3.2.4 DNA amplification for Sequencing 27
3.2.5 DNA Separation and Analysis 28
3.2.6 Sequence Analysis 29
3.3 Retinal Preparations for Experiments 29
3.3.1 Cryo-embedding and Sections 29
3.3.2 Whole Retinal Flat Mounts 29
3.3.3 Morphometry Experiments 30
3.4 Morphological and Immunohistological Analyses of Prepared Retinae 30
3.4.1 Hematoxylin and Eosin Stain 30
3.4.2 Immunohistochemical Stain of Retinal Sections 30

3.4.3 Immunohistochemical Stain of Retinal Flat Mounts 31
3.4.4 TUNEL Assay 31
3.4.5 Microscopy 31
3.4.6 Retinal Morphometry Analysis 32
3.5 Behaviour and Retinal Function Studies 32
3.5.1 Optomotry 32
3.5.1 Rotarod 34
3.5.2 Electroretinograms 34
3.6 RNA Gene Expression Analysis 34
3.6.1 RNA Isolation 35
3.6.2 Photometric determination of RNA concentration 35
3.6.3 Reverse Transcription 35
3.6.4 TaqMan technology 36
3.6.5 Relative Quantification 37
3.7 Food Supplementation Study 38
3.8 Statistics 38
4. Results 39
4.1 Characterization of the *Cln3*$^{\Delta ex7-8}$ Retina 39
4.1.1 Histological Characterization of the *Cln3*$^{\Delta ex7-8}$ Retina and Immunohistological Evaluation of Müller and Microglia Cells. 39
4.1.2 Functional Characterization of the *Cln3*$^{\Delta ex7-8}$ Retina 41
4.1.3 *CRB*^{rd8} Mutation present in the *Cln3*$^{\Delta ex7-8}$ and Wild Type Background 44
4.1.4 End of *Cln3*$^{\Delta ex7-8}$ Study 44
4.2 Characterization of the *Cln6*^{nclf} Retina 44
4.2.1 Morphological Characterization of the *Cln6*^{nclf} Retina 44
4.2.2 Quantification of Retinal Degeneration 47
4.2.3 Behavioural and Functional Characterization of the *Cln6*^{nclf} Retina and Mouse Model 49

4.2.4 Transcriptional Changes in Stress and Inflammatory Gene Markers in the *Cln6*^{nclf} Retina 51

4.3 CLN6^{nclf} Dietary Supplementation Study 53

4.3.1 Supplementation effect on *Cln6*^{nclf} Retinal Histology and Microglia 54

4.3.2 Retinal Morphometry of Supplemented Retinas 55

4.3.3 Retinal Function of Supplemented Retinas 56

4.3.4 Transcriptional changes affected by Supplementation 58

5. Discussion 60

5.1 Comparison of retinal Degeneration in NCL Models 60

5.2 Microglia and Müller Cells in NCL Retinal Degeneration 62

5.2.1 Glial Activation in *Cln3*$^{\Delta ex7-8}$ Retina 63

5.2.2 Glial Activation in *Cln6*^{nclf} Retina 64

5.3 Immuno-modulation and Neuronal Degeneration Rescue via Dietary Supplements 66

5.4 Perspective 70

5.4.1 Cln3 and Cln6: Different but Similar? 70

5.4.2 Müller Cells, Microglia and Modulation via Natural Compounds 71

6. Summary 73

7. Zusammenfassung 75

8. References 77

List of Tables 93

List of Figures 94

List of Abbreviations 96

List of Publications 101

Conference Contributions 102

Curriculum Vitae 104

Grateful Acknowledgements 107

1. Introduction

1.1 Structure and Function of the Mammalian Retina

The eye is the optical camera of the body which transmits and focuses light onto a complex highly-structured neuronal tissue called the retina. The retina is located in the proximal segment of the eye and is the first station of the neuronal visual system (Fig 1A). The mammalian retina allows for the perception of color, shape and motion through complex signaling pathways which are ultimately amplified and extracted before being transmitted to the midbrain and thalamus via the optic nerves. Signal processing is carried out by five main classes of retinal cells which are segregated into alternate, anatomically distinctive layers (Fig 1B): photoreceptors, bipolar cells, amacrine cells, horizontal cells and ganglion cells (Fig 1C) (Sung and Chuang, 2010).

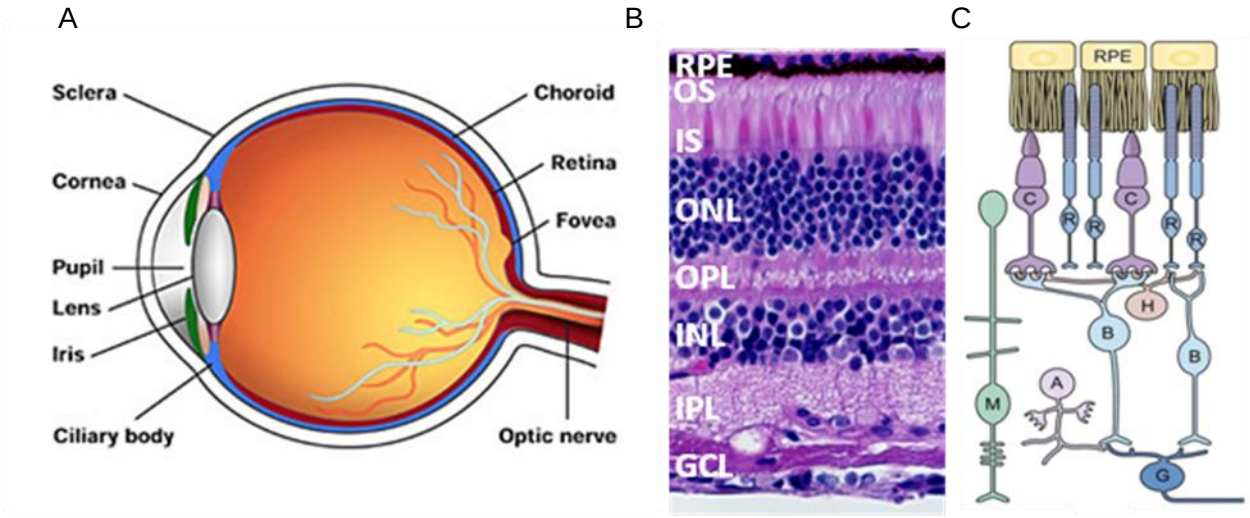

Figure 1. Gross anatomy of the eye ball and detailed cross-section of the human retina. A. The retina lines the back of the eye ball. B. Stained cross-section of the retina highlighting the different layers of the retina. RPE: retinal pigment epithelium, OS: outer segment, IS: inner segment, ONL: outer nuclear layer, OPL: outer plexiform layer, INL: inner nuclear layer, IPL: inner plexiform layer, GCL: ganglion cell layer. C. Schematic overview of the organization of the retinal cells. R: rod, C: cones, H: horizontal cells, B: bipolar cells, A: amacrine cells, M: Müller cells, G: ganglion cell. Eye ball adapted from: http://sparemed.blogspot.de/2011/05/good-vs-bad-eyeball.html Retinal cross section modified from: http://pathology.wustl.edu/research/corbolab/projects.htm Schematic diagram of retinal cells adapted from Sung and Chuang, 2010

Visual perception begins when light crosses the retina, which is approximately 0.2mm in thickness, and reaches the light-sensitive photoreceptor cells (Yau and Hardie, 2009). The retina contains two type of photoreceptor cells: rods and cones. In humans, the cone-photoreceptors are

specialized in day- and color vision and enriched in fovea, whereas rod photoreceptors mediate vision in dim light and are located predominantly in peripheral areas of the retina. The human retina contains approximately 110 million rod- and 6 million cone-photoreceptors (Klinke and Toth, 2003). The photoreceptors are juxtaposed to the outermost layer of the retinal pigment epithelium (RPE) which is known to play a critical role in their regeneration. The RPE is responsible for the maintenance of retinal homeostasis, the formation of the outer blood-retinal barrier and absorption of scattered or unabsorbed light. RPE cells also phagocytose membranous discs which are shed by photoreceptor outer segments (Dunn et al., 1996), recycle the light sensitive pigment rhodopsin and provide nutrients to the photoreceptors. The nuclei of the photoreceptors constitute the tightly packed outer nuclear layer (ONL) which are connected to the outer segments (OS) by the connecting cilium (Horst et al., 1990). Visual perception begins when the chromophore conjugated with opsin, absorbs a photon in the OS of a photoreceptor. The photo-excited visual pigment initiates a signal transduction cascade which leads to the closure of cation channels and results in a hyperpolarisation of the cell membrane. This photo-transmission is forwarded to inner retinal cells such as the horizontal or bipolar cells via synapses in the outer plexiform layer (OPL). The cell bodies of the inner retinal cells are found in the inner nuclear layer (INL). Signals from the inner retinal cells are further relayed to the ganglion cells in the ganglion cell layer (GCL) via synpases found in the inner plexiform layer (IPL) (Sung and Chuang, 2010). Amacrine cells in the INL laterally modify signals from the horizontal cells to the ganglion cells, whose axons build the optic nerve which further transmits information to the midbrain (Masland, 1988). Between the stratified layers of the retina exist two other cell types which are important for the maintenance and health of the retina: the Müller glia cells and microglia cells.

1.2 Müller Cells

Astrocytes are macroglias which are found in the brain in various forms, with one form existing in the mammalian retina called Müller cells (Reichenbach and Bringmann, 2010). Müller cells are specialized radial glial cells which span the entire thickness of the retina in columns contacting all retinal neuronal somas and processes (Bringmann et al., 2006). This anatomical link is important for information processing as well as neuronal survival. Among many other roles, Müller cells maintain the structural stability of the retina, regulate extracellular homeostasis of relevant ions, remove metabolic waste and metabolize glucose to lactate which is preferentially taken up by photoreceptors as a fuel for their oxidative metabolism (Poitry-Yamate et al., 1995; Newman and

Reichenbach, 1996). Müller cells can also modulate immune and inflammatory responses and buffer mechanical deformations of the retina tissue (Lu et al., 2006; Bringmann et al., 2009; Reichenbach and Bringmann, 2010). However, the main cell type which modulate immune and inflammatory responses are the microglia.

1.3 Microglia cells

In contrast to macroglia cells which arise from primitive neuroepithelium together with neurons, microglia originate from myeloid precursors in the yolk sac during very early embryonic development before the formation of the blood brain barrier (Ginhoux et al., 2010). Like macrophages, microglia are mononuclear phagocytes and act as the resident immune cells of the central nervous system (CNS) (Kreutzberg, 1996). They make up 10% of total glial population in the CNS, are found ubiquitously and serve as sensors and executers of innate immunity within the CNS (Vaughan and Peters, 1974; Graeber and Streit, 2001).

1.3.1 Microglia in the CNS and Retina

Microglia cells were first described by Del Rio Hortega in 1919 as unique cells in the CNS with an elongated soma bearing processes extending from both poles of the cell (Del Rio Hortega, 1919). This phenotype is termed as ramified microglia. In this form, microglia are able to scan the environment using their processes allowing them to quickly identify changes or injuries in tissues (Raivich, 2005). Moreover, the highly motile microglial ramifications have been shown to continuously scan the CNS microenvironment with estimates that the complete brain parenchyma is monitored every few hours (Davalos et al., 2005; Nimmerjahn et al., 2005). Depending on their location in the CNS, microglia can have major morphological differences with regard to the size and orientation of their ramifications. The density of microglial cells also seems to be determined by region-specific cues. Such heterogeneity of microglia density and morphology might be linked to functional heterogeneity of microglia (Davoust et al., 2008). In the adult retina, microglia are normally found in the OPL and IPL (Hume and Gordon, 1983) at the margin adjacent to the nuclear layers (Ebert et al., 2009; Karlstetter et al., 2010). From their location in the brain and retina, microglia can assess the homeostatic state of the tissue and carry out their functions.

1.3.2 Function of the Microglia Cells

Microglia cells exert many physiological functions in the developing and adult CNS. These include the induction of apoptosis in specific subpopulations of developing neurons, the control of synaptogenesis, the synthesis of neurotrophic factors and the regulation of synaptic transmissions (Elkabes et al., 1996; Marin-Teva et al., 2004; Roumier et al., 2004; Coull et al., 2005). In order to carry out their function to maximum efficiency, microglia exist individually and keep their distance from one another while covering their own surveillance territory. This microglia immune network is different from other neuroglia which have established syncytial networks (Graeber, 2010). It is therefore likely that microglia communicate using auto- and paracrine mechanisms (Liu et al., 2009).

Microglia also communicate with neurons which signal microglia about their status via use of different ligands, neurotransmitters and neurotrophins (Kettenmann et al., 1990; Biber et al., 2007; Pocock and Kettenmann, 2007). Two characterized ligands, CD200 and CX3CL1 (CX3C chemokine ligand 1, also known as fractalkine) , which are found to be constitutively expressed on the neuronal membrane surface have their corresponding receptors, CD200R and CX3CR1, expressed on microglial surface (Hoek et al., 2000; Biber et al., 2006). Signals between aforementioned ligands and receptors provide suppressive signals to microglia, preventing harmful activation as well as maintenance of homeostatic state (Carter and Dick, 2004; Cardona et al., 2006). Furthermore, CD200 and CX3CL1 stimulate microglia migration and protrusion movements, controlling surveillance frequency and vigilance in healthy tissues (Carter and Dick, 2004). However, upon detection of injury or subtle alterations in their microenvironment, such as imbalances in ion homeostasis, microglia cells undergo morphological changes and enter an 'active' state (Kettenmann et al., 1990).

1.3.3 Activation and Morphological Plasticity of Microglia Cells

One of the most remarkable features of microglia is their high level of morphological and functional plasticity in response to activating stimuli. Under a number of pathological conditions, ramified microglia will activate and undergo a graded morphological transformation resulting in shorter, thicker processes and larger soma size (Kreutzberg, 1996). By the end of such a process, fully activated microglia, also called reactive microglia, harbor a similar morphology to activated macrophages (Fig 2). Microglia become more motile and actively move to site of injury as well as

increase in local density, either by *in situ* proliferation or recruitment of myeloid cells from the blood stream. This results in a greater defense system of the tissue which can protect and restore tissue homeostasis (Xu et al., 2007; Soulet and Rivest, 2008; Graeber, 2010).

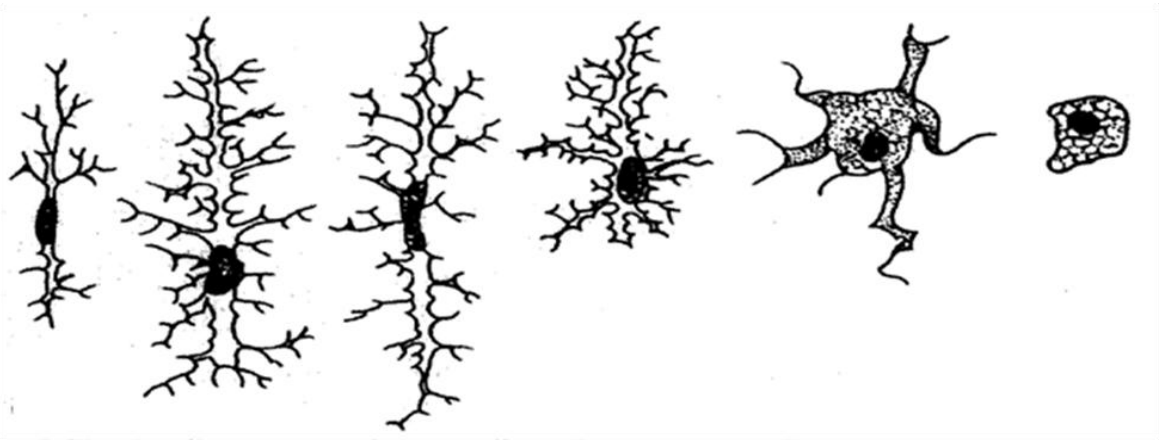

Figure 2. Microglia activation occurs in a graded manner. On the left: Ramified microglia are thin with protrusion extending from both poles of the cell. Upon alterations in the microenvironment, microglia undergo graded morphological changes including thicker somas, shorter protrusions, smaller cell size, rounded amoeboid cell shape with short thick protrusions and finally a fully phagocytic activated cell. Adapted from Kreutzberg, 1996.

Activated microglia are found to exert functions commonly assigned to all tissue-resident macrophages under inflammatory conditions. These include notably phagocytosis, antigen presentation and secretion of pro-inflammatory cytokines such as interleukin (IL)-6 , IL-1 or tumor necrosis factor α (TNF-α), as well as reactive oxygen intermediates and nitric oxide (Banati et al., 1993; Bauer et al., 1994; Minghetti and Levi, 1998; Perry, 1998). In addition, microglia up-regulate cell surface molecules including major histocompatibility markers (MHC class I and II) F4/80, complement receptor 3 (CD11b/CD18, OX42) and Griffonia simplicifolia isolectin B4 (Gordon et al., 1988; Perry, 1998; Langmann, 2007a; Lynch, 2009). These markers are classical microglia markers used to detect microglia by immunohistochemistry and immunofluorescence-staining procedures (Kreutzberg, 1996; Streit et al., 1999). The magnitude of microglial activation is influenced by the type and duration of the stimulus, the current CNS microenvironment and exposure to prior and existing stimuli (Schwartz et al., 2006; Perry et al., 2007; Ransohoff and Perry, 2009).

The type of stimulus which activates microglia is very important. In response to certain cytokines such as interferon-γ (IFNγ) and tumor necrosis factor-R (TNFR) or after recognition of pathogen-associated molecular patterns (PAMPs), microglia enter a 'classically' activated state normally

associated with strong immune defense (Laskin, 2009). In contrast, interleukin-10 (IL-10) or transforming growth factor-β (TGFβ) trigger 'alternatively' activated microglia which is associated with resolution of inflammation through phagocytosis of apoptotic neutrophils, reduced production of pro-inflammatory cytokines, and increased expression of mediators important in tissue remodeling, angiogenesis, and wound repair (Duffield, 2003; Van Ginderachter et al., 2006).

Microglia activation occurs very early in response to injury, often preceding reactions of any other cell type (Gehrmann et al., 1995). Time-lapse *in vivo* imaging have shown that microglia appear minutes following injury, polarizing their processes toward the site of injury (Nimmerjahn et al., 2005). Based on these studies as well as many others, microglial response to injury is generally thought to constitute the initial step of a generalized inflammatory response. Once the cause of stimulation has been removed, signals from neurons as well as the microenvironment will efficiently regulate neuroimmune response allowing the tissue to return to homeostatic state. This is in part regulated by the balance of 'classically' and 'alternatively' activated microglia. However, these neuromodulatory mechanisms may become deficient and/or dysregulated under excessive or prolonged inflammatory stimulation induced by disease and injury. In such cases, the microglial function which was initially important for host defense and neuroprotection, can have detrimental and neurotoxic effects (Block et al., 2007). It is now recognized that overly active microglia, normally of the 'classically' active class, are associated with the pathogenesis of several neurodegenerative disorders including Alzheimer's disease, amyotrophic lateral sclerosis (ALS), Parkinson's disease and several retinal degenerative diseases (Boillee et al., 2006; Kim and Joh, 2006; El Khoury et al., 2007).

1.4 Inherited Diseases of the Eye

Inherited retinal dystrophies are a heterogeneous group of disorders where an underlying inherited gene defect leads to impaired retinal function. They can be classified according to mode of inheritance, site of retinal dysfunction, age of onset, associated systemic syndromes or the underlying gene defect (Sundaram et al., 2012). To date, the Retnet (Retinal Information Network) database lists 232 genes which lead to retinal disease (https://sph.uth.edu/retnet/home.htm). Age-related Macular Degeneration (AMD), is the leading cause of vision loss in industrialized countries and is caused by genetic predisposition as well as environmental factors. Achromatopsia and Retinitis Pigmentosa (RP) together define a large class of monogenic diseases that affect vision

in humans, caused by a wide variety of mutations that disrupt visual transduction and photoreceptor maintenance. Due to the high oxygen consumption that is required for retinal light absorption, photoreceptors in particular, are greatly susceptible to injury and perturbations often resulting in cell death. In most cases, loss of vision is usually caused by photoreceptor loss which occurs though apoptotic mechanisms and/or non-apoptotic mediated cell death (Portera-Cailliau et al., 1994; Sancho-Pelluz et al., 2008).

In the mouse model of X-linked juvenile retinoschisis, Retinoschisis-deficient (Rs1h-/Y) mice develop massive photoreceptor degeneration very early in postnatal development, accompanied by splitting or schisis of retinal layers (Weber et al., 2002; Ebert et al., 2009). The *rd1* (retinal degeneration) mouse model, which is a relevant RP model, has early rod photoreceptor degeneration starting at postnatal day 10 which has been attributed to apoptotic mechanisms (Chang et al., 1993) as well oxidative stress (Sanz et al., 2007). Photoreceptor cell death due to apoptosis and oxidative stress has also been reported in AMD animal models as well as patients (Curcio et al., 1996; Winkler et al., 1999; Dunaief et al., 2002). However, recent studies in AMD, Rs1h-/Y and *rd1* mouse models now show significant induction of inflammatory markers as well as activation of microglial and Müller cells, which also play a major role in retinal disease progression and degeneration (Gupta et al., 2003; Patel and Chan, 2008; Ding et al., 2009; Ebert et al., 2009).

1.4.1 Microglia in Retinal Degeneration

Microglia activation has also been shown to contribute to retinal degeneration in a number of studies (Langmann, 2007). Both genetic or retinal dystrophies caused by external factors usually harbor active phagocytic microglia at lesion sites/site of cell loss. Numerous studies have shown that microglial activation is not simply a side-effect of heredity photoreceptor dystrophies, but an active contributor to retinal degeneration (Thanos, 1991; Schuetz and Thanos, 2004; Zeiss and Johnson, 2004; Karlstetter et al., 2010).

Studies done on the aforementioned retinoschisis, Rs1h-/Y, mice using DNA-microarray analyses, identified several transcripts from activated microglia cells preceding gene expression patterns related to apoptosis (Gehrig et al., 2007). Furthermore, microglial transformation from ramified to an ameoboid phagoctyic morphology coincided with cell death (Ebert et al., 2009). This suggests early microglial activation as a key event preceding/triggering photoreceptor death (Gehrig et al.,

2007; Langmann, 2007). Increased expression of the microglia-activating chemokines MCP-1, MCP-3, as well as high levels of microglia-secreted TNFα were also observed in the retina of *Rd* mice. These observations coincided with prominent microglial migration into the ONL well before photoreceptor apoptosis (Zeiss et al., 2004; Zeng et al., 2005). Diseased retinas from human AMD and RP patients have also revealed the presence of activated microglia in the ONL, bearing phagocytised fragments from dead photoreceptors (Gupta et al., 2003). Studies done by Joly et al. could show both resident and bone-derived macrophages co-operating to remove apoptotic photoreceptors in blue-light injured mouse retinas, indicating recruitment of peripheral macrophages (Joly et al., 2009). In the retinal microenvironment, recruited macrophages transform phenotypically into microglia-like cells and actively contribute to the inflammatory processes (Kaneko et al., 2008). These studies, among many others, imply early microglial activation as an active cause or additive effect of retinal degeneration. However, the molecular mechanism of microglial activation and whether the functional consequences are destined to be detrimental or protective is unclear. It is important to note, that morphology does not accurately reflect the activation state of microglia. As mentioned above, different patterns of activation lead to distinct functional profiles, which may be associated with the common 'activated' morphology (Schwartz et al., 2006). Nonetheless, in most diseases, there is a greater presence of neurotoxic microglia compared to the neuroprotective counterpart.

1.4.2 Müller Cells in Retinal Degeneration

Like microglia cells, Müller cells can also become 'activated' or 'reactive' in response to pathological alterations in the retina. This reaction, also known as Müller cell gliosis, is one part of a complex retinal response to pathogens which also includes inflammatory and immune responses. Reactive gliosis may be a cellular attempt to protect retinal tissue from further damage and promote tissue repair by releasing neurotropic factors and antioxidants (Schutte and Werner, 1998). However, some factors which are released by Müller cells, such as vascular endothelial growth factor (VEGF), may at first have neuroprotective effects but later contribute to disease progression by inducing vascular leakage and neovascularozation (Miller et al., 1994; Yasuhara et al., 2004). Notably, Müller cells up-regulate glial intermediate filaments vimentin and glial fibrillary acidic protein (GFAP). These are sensitive and non-specific responses to retinal disease and/or injury, which are used as early indicators of retinal stress (Bignami and Dahl, 1979; Lewis and Fisher, 2003). These intermediates are also expressed by some astrocytes when pathogens or

insults occur in the brain. Along with GFAP and vimentin, inflammatory factors such as monocyte chemoattractant protein-1 are also up-regulated and can recruit microglia to site of injury (Nakazawa et al., 2006; Nakazawa et al., 2007b). Microglia, in turn, release oxygen free radicals and cytokines which contribute to photoreceptor apoptosis. A study using GFAP- and vimentin-deficient mice with induced retinal detachment showed reduced microglial infiltration and decreased photoreceptor apoptosis (Nakazawa et al., 2007a). Similar results were also found after experimental blue-light retinal injury in GFAP- and vimentin- deficient rats (Iandiev et al., 2008). In severe cases of gliosis, proliferation of Müller cells contributes to neuronal cell death by impairing tissue homeostasis, which in turn increases the susceptibility of neurons to stressful stimuli in diseased retinas (Fisher et al., 1991).

1.5 Neuronal Ceroid Lipofuscinosis (NCL)

One particular disease which is an inherited degeneration of the retina and CNS is Neuronal Ceroid Lipofuscinosis (NCL), First identified in 1826 by Dr. Otto Christian Stengel, NCL is defined as a progressive degenerative disease of the brain and most cases, retina, in association with intracellular accumulation of storage material known as ceroid lipofuscin. Despite over 100 years of research and the vast accumulation of knowledge on genes, proteins and pathways, there is no treatment for NCL (Haltia, 2003, 2006; Haltia and Goebel, 2012).

1.5.1 Characteristics of NCL

Collectively, the NCLs are the most common cause of progressive encephalopathies in children (Haltia, 2006; Kollmann et al., 2013). Incidence is estimated to be 1:25 000-50 000 in the USA (according to The National Institute of Neurological Disorders and Stroke) and ranging between 1:25 000 and 1:200 000 in European countries (e.g. Norway, Germany and Italy)(Williams, 2011). Up to date, almost 400 causative mutations have been reported in 13 CLN genes (Table 1) (NCL Mutation and Patient Database, http://www.ucl.ac.uk/ncl /mutation.shtml). Symptoms of NCL disease include epileptic seizures, ataxia, mental and motor regression, myoclonus and/or visual failure (Warrier et al., 2013). Although there are various kinds of NCL, they do share some common traits: 1) the accumulation of auto-fluorescent, electrondense granules in most nerve cells and, to a lesser extent, in many other cell types, 2) varying degrees of cerebral/cerebellar neurodegeneration (Haltia and Grobel, 2012). It is now becoming evident that severe up regulation

inflammatory processes, microglia and astrocytes are also part of the NCL pathogenesis. Although the relative timing and rate of disease progression differs between different forms of NCL, all end inevitably with the premature death of the affected individual.

The NCLs are subdivided into categories based on molecular genetic findings, age of onset and the ultra structure appearance of storage material (Table 1). The NCLs are normally classified as congential, infantile, late-infantile, juvenile and adult form (Haltia and Goebel, 2012). NCL diagnosis is based on genetic or enzymatic tests from a blood, skin biopsy or saliva samples. Prerequisite for NCL diagnosis is the existence of intracellular storage material, which can be studied using electron microscopy on lymphocytes from skin/rectal biopsies. Monitoring electroencephalogram (EEG), electroretinogram (ERG), measuring the visual and/or somatosensory evoked potentials (VEPs, SEPs) or performing neuroradiological analyses may also assist the diagnosis of certain forms of NCL (Kousi et al., 2012).

1.5.2 NCL as a Lysosomal Storage Disorder

The NCLs are considered as inherited lysosomal storage disorders (LSDs). Lysosomes are primarily characterized as acidic organelles which contain the primary hydrolysis machinery of the cell required for the degradation of proteins, lipids, and carbohydrates, and whole organelles. Lysosomes are globular or tubular-shaped vacuoles with variable electron-dense constituents. Their lumen is acidic (pH 4.5 – 5) and contains membrane sheets and intraluminal vesicles. LSDs are mostly recessively inherited, fatal diseases characterized by a progressive accumulation of un-degraded metabolite(s) in the lysosome but also in other intracellular and extracellular locations. Several types of macromolecules have been identified to be stored in LSDs, including sphingolipids, mucopolysaccharides, oligosaccharides, glycoproteins, lipids, sulfatides, and specific proteins and amino acids (Futerman and van Meer, 2004; Ballabio and Gieselmann, 2009). Most of the LSDs are due to mutations in soluble lysosomal hydrolases but can be caused by a multitude of mutations which cause functional impairment (Ruivo et al., 2009).

Most of the NCL proteins are, in fact, present in the lysosomes where ceroid lipopigments accumulate. Lipofuscin and ceroid are fluorescent storage material largely composed of protein, which in most NCLs is the subunit c of mitochondrial F1-F0-ATP synthase. In certain subtypes, mainly in infantile and congenital disease, the main protein components of the storage material are

sphingolipid activator proteins (saposins) A and D. However, the role NCL proteins play in lysosomes or else-where in the cells as well as NCL disease mechanism is largely unknown (Haltia, 2003; Seehafer and Pearce, 2006).

Table 1: The neuronal ceroid lipofuscinosis classified according to clinical onset, affected gene, protein function, protein location, storage component and first identification of causative gene

Disease	Onset	Gene Affected	Function	Location	Storage component	First identification
CLN1	Infancy	Palmitoyl protein thioesterase 1 (PPT1)	Palmitoyl-thioesterase	Lysosome	Saposin A/D	(Vesa et al., 1995)
CLN2	Late-infancy	Tripeptidyl peptidase 1 (TPP1)	Serine protease	Lysosome	subunit c	(Sleat et al., 1997)
CLN3	Juvenile	CLN3	Unknown	Lysosome Endosome	subunit c	(Consortium, 1995)
CLN4	Adulthood	Cysteine-string protein alpha (CSPα), DNAJC5	Chaperone	Plasma Membrane	Saposin A/D	(Noskova et al., 2011)
CLN5	Late-infancy	CLN5	Unknown	Lysosome	subunit c	(Savukoski et al., 1998)
CLN6	Late-infancy	CLN6	Unknown	ER	subunit c	(Wheeler et al., 2002)
CLN7	Late-infancy	MFSD8	Unknown	Lysosome	n.d.	(Siintola et al., 2007)
CLN8	Late-infancy	CLN8	Unknown	ER-Golgi intermediate compartment	subunit c	(Ranta et al., 1999)
CLN 10	Congenital	Cathepsin D (CTSD)	Aspartyl endopeptidase	Lysosome	subunit c	(Siintola et al., 2006; Steinfeld et al., 2006)
CLN 11	Adult	Progranulin GRN	Unknown	Extracellular	Saposin D	(Smith et al., 2012)
CLN 12	Juvenile	ATP13A2	Unknown	Lysosome	n.d.	(Bras et al., 2012)
CLN 13	Adult	Cathepsin F (CTSF)	Cysteine protease	Lysosome	n.d.	(Smith et al., 2013)
CLN14	Infantile	Potassium channel tetramerization domain-containing protein 7 (KCTD7)	Unknown	Cytosolic	n.d.	(Staropoli et al., 2012)

Table 1: List of CLN genes which carry NCL causing mutations. Abbreviations. CLN1 ect: Ceroid lipofuscinosis 1 ect.; n.d.: not described. References: Kollmann et al., 2013, Warrier et al., 2013, NCL Mutation and Patient Database, http://www.ucl.ac.uk/ncl/mutation.shtml

1.5.3 Characteristics of CLN3 Mutations

Mutations in the CLN3 gene result in juvenile neuronal ceroid lipofuscinosis (JNCL, Batten disease, OMIM#204200). World wide, JNCL represents the most common form of NCL. Currently, 57

mutations have been characterized in the CLN3 gene (NCL Mutation and Patient Database). The most common mutation is a 1.02 kb deletion of exon 7 and 8 which results in a severely truncated protein with residual function, (Kitzmuller et al., 2008). JNCL usually begins with visual failure due to retinal degeneration at 5–10 years of age. Mental retardation develops slowly and is followed by epilepsy and deterioration of motor skills. Juvenile NCL is also connected to different psychiatric symptoms like aggressiveness, depression and sleep problems. The clinical course is largely variable and the death occurs between 20-30 years of age. At autopsy, the cerebral cortex is narrowed and the weight of the brain is decreased (Haltia, 2003). Unfortunately, because neurological symptoms often begin years after occurrence of visual problems, JNCL patients are considered as otherwise normal children with vision loss often mistaken as a maculopathies (Collins et al., 2006). This significantly delays accurate patient diagnosis.

The CLN3 gene is located on chromosome 16p12 and encodes a hyrophobic transmember protein of 438 amino acids called battenin. CLN3 is normally detected in endosomal/lysosomal structures in neurons and gets transported to synaptosomes (Kyttala et al., 2004). CLN3 functions are postulated to include lysosomal acidification, membrane fusion, vesicular transport, autophagy and proteolipid modification (Jalanko and Braulke, 2009; Kollmann et al., 2013). However, the precise function of CLN3 remains elusive, making it difficult to evaluate the impact of the mutations on the resultant peptides (Kollmann et al., 2013).

1.5.4 Characteristics of CLN6 Mutations

Mutations in the CLN6 gene cause a variant late infantile NCL (vLINCL; OMIM#601780) (Gao et al., 2002; Wheeler et al., 2002), as well as an adult form termed Kufs type A disease (OMIM#204300) (Arsov et al., 2011). At present, 68 disease-causing mutations have been described (NCL Mutation and Patient Database). The most common mutation, which leads to vLINCL, is a 1-bp insertion in exon 4 (c.316insC) causing a frame shift mutation and premature stop codon resulting in a truncated protein (Kurze et al., 2010). The age of onset for vLINCL caused by CLN6 mutations is between 18 months and 8 years of age with the most common presenting features being motor delay, dysarthria and ataxia. Addition symptoms include mental regression, speech impairments and in approximately 50 percent of cases seizures and loss of vision (Mole et al., 2005; Moore et al., 2008). Disease progression is rather variable with death occurring between 5 to 30 years of age (Pena et al., 2001; Jalanko and Braulke, 2009).

The CLN6 gene on chromosome 15q23 encodes an endoplasmatic reticulum (ER) resident transmembrane protein 331 amino acids long, named linclin or CLN6p. CLN6 is conserved across vertebrates showing no sequence homology with other proteins. Mutations in CLN6 do not have an impact on normal distribution or its ability to dimerize (Mole et al., 2004; Kurze et al., 2010). Instead, is it postulated that mutations exert their pathogenic effect on the stability and function of mutant polypeptides, possibly reducing rate of synthesis and stability compared to wild type peptides (Kurze et al., 2010). CLN6p has also been shown to interacts with collapsin response mediator protein-2 (CRMP-2) which controls axon growth (Benedict et al., 2009). Recent studies have now shown the CLN6^{nclf} mutation also results in disruption of the autophagy-lysosome degradation pathway suggesting the CLN6 protein may be important for fusing autophagosomes and lysosomes (Thelen et al., 2012).

1.5.5 Animal Models of CLN3 and CLN6

Animal models exist for all subtypes of NCL disorders (NCL Animal Models Database http://www.ucl.ac.uk/ncl/animal.shtml). These are either spontaneously occurring or engineered and they have been described in organisms ranging from the single celled yeast to larger animal models such as sheep and dog (Cooper et al., 2006).

Orthologs of CLN3 can be found across many species and have been studied in *Drosophila Melanogastor*, *C. elegans*, unicellular yeasts *Saccharomyces cerevisiae* and *Schizosaccharomyces pombe* and mouse models. Pioneering work done on CLN3-deficiency yeast models, *btn1*, significantly contributed to understanding CLN3 function (Pearce and Sherman, 1997; Gachet et al., 2005; Rakheja et al., 2008). In order to better understand CLN3 mutations in mammals, four mouse models of JNCL have been established and characterized to varying degrees (Cooper, 2006). All mouse models display recessive features of JNCL including accumulation of ceroid lipofuscin, brain gliosis, neurological dysfunction and neurodegeneration. The *Cln3*$^{\Delta ex7/8}$ knock-in mouse represents the only genetically accurate JNCL mouse model, and therefore may be most predictive of the earliest molecular and cellular consequences of CLN3 mutation in JNCL (Cotman et al., 2002) and the only one which has been fully phenotyped (Strapoli et al., 2012).

In contrast to the engineered CLN3 models, CLN6 disease occurs naturally in mouse, sheep and dog (Jolly et al., 1989; Gao et al., 2002; Wheeler et al., 2002; Tammen et al., 2006; Katz et al., 2011). The

CLN6 mutant mouse model, *Cln6*^{nclf}, possesses an identical mutation (c.307insC) to the most common CLN6 human mutation mentioned. The course of the *Cln6*^{nclf} neurodegenerative phenotype also recapitulates the human CLN6 disease with homozygous mice developing progressive retinal atrophy, cerebral atrophy, spastic limb paresis starting at eight months, paralysis and premature death at one year of age (Bronson et al., 1998; Wheeler et al., 2002; Sharp et al., 2003; Siintola et al., 2005).

1.5.6 Retinal Degeneration in NCL

Vision loss is typically evident in patients with NCL at early age making ophthalmologists often the first specialists seen by patients (Birch, 1999). Retinas of NCL patients are normally affected by two different pathological processes, 1- accumulation of disease specific lipopigments in the neuronal perikarya and retinal pigment epithelium cells, 2- progressive degeneration of the neuronal elements, commencing at the photoreceptors. At autopsy, patients eyes normally exhibit severe atrophy of the entire retina (Goebel, 1992).

Many NCL models also exhibit varying levels of retinal degeneration and vision problems. Among them are mutant forms of CLN1, CLN3, CLN5, CLN6, CLN8 and CLN10, which have been studied using electroretinograms (ERGs). ERGs are a good method for measuring retinal cell function and can be used on both patients and animals. Briefly, ERGs measure electrical responses from the retina upon light stimulation which are recorded as waves; the a-wave which is the first negative component, indicating the general health of the photoreceptors, followed by the b-wave which is has a large positive amplitude, reflecting the health of the inner layers of the retina (Creel, 2013).

Retinal studies in the Cln8^{mnd} mouse showed reduced ERG amplitudes in both the a- and b-wave starting at two months until the signals became barely recordable by five months of age. These functional measurements were accompanied by obvious morphological retinal degeneration which appeared four months before motor paralysis starts (Chang et al., 2002). ERG studies done on *Cln3*$^{\Delta ex7\text{-}8}$ mice past nine months of age showed a reduction in the b-wave whilst maintaining a relatively normal a-wave function, indicating that the inner retina is the most affected region (Strapoli et al., 2011). Ppt1$^{-/-}$ (CLN1) mice, a model for the infantile form of human NCL, showed only moderate changes in retinal morphology and reduction in the b-wave amplitudes (Lei et al., 2006). Retinal degeneration in *Cln6*^{nclf} mice have also been studied, showing retinal degeneration

starting at four months of age resulting in loss of the ONL by nine months of age (Bronson et al., 1998).

1.5.7 Glial Activation in NCL

Neuropathology, genome wide expression profiling and cellular analyses in several NCL mouse models have firmly established hyperactivity of the immune system prior to neurodegenerative events as a potential early disease mechanism (Elshatory et al., 2003; Chattopadhyay et al., 2004; Kopra et al., 2004; Jalanko et al., 2005; Jalanko et al., 2006). Autopsy material from patients with different forms of NCL also show consistent and regionally specific pattern of astrocytosis and microglial activation in the brain (Tyynela et al., 2004).

Early prominent activation of astrocytes and microglia were first observed in CLN6-deficient South Hampshire sheep (Oswald et al., 2005). Activated astrocytes appeared in developing white matter 40–20 days before birth and astrocytic activation within the gray matter 20 days before birth. Clusters of activated microglia were detected in upper cortical gray matter layers 12 days after birth defining regions most vulnerable to neurodegeneration, which starts at two months of age (Oswald et al., 2005). *Cln6*^{nclf} mouse brains also show localized reactive astrocytes and microglia, most prominent in the thalamocortical system, starting between five to six months of age (Bronson et al., 1998; Thelen et al., 2012).

Increased reactive astrocytes is the fist histopathological change observed in specific regions of the Ppt1$^{-/-}$ mouse brain, starting at 3 months of age. These regions also suffer significant neuronal loss subsequent to gliosis (Kielar et al., 2007; Macauley et al., 2009). However, when these mice were crossed with GFAP$^{-/-}$ Vimentin$^{-/-}$ mice, resulting in loss of astrocytes in the brain, it resulted in an accelerate brain degeneration (Macauley et al., 2011). These experiments highlight the protective and deleterious effects gliosis can have. Moreover, studies done by Groh et al., in which lymphocytes were inactivated in Ppt1$^{-/-}$ mice, showed a substantial disease attenuation, unequivocally defining immune cells as pathogenic mediators in infantile NCL (Groh et al., 2013).

Studies done on *Cln3*$^{-/-}$ and *Cln3*$^{\Delta ex7\text{-}8}$ mice also showed selective loss of inhibitory interneurons and early low level glial activation preceding neuron loss most pronounce in the thalamocortical system (Pontikis et al., 2004; Pontikis et al., 2005).

1.6 Glial Attenuation with Natural Compounds

The presence of glial activation in numerous degenerative diseases has resulted in the search for therapeutic interventions which can modulate astrocyte and microglia activity while reducing inflammatory marker expression and simultaneously support neuronal survival. Therapeutic strategies include targeting ligands which activate microglia (Jin et al., 2007; Veiga et al., 2007), enhancing protective endogenous mechanisms (Zhu et al., 1999) and immuno-modulation with natural compounds (Ebert et al., 2009; Dirscherl et al., 2010; Karlstetter et al., 2011).

1.6.1 Curucmin

Curcumin ((E,E)-1,7-bis(4-hydroxy-3-methoxyphenyl)-1,6-heptadiene-3,5-dione), derived from the plant *Curcuma longa,* is a major constituent of tumeric which has been used as herbal medicine in India and China for centuries (Ammon and Wahl, 1991). Curcumin has been show to inhibit the defense program of microglia by diminishing the production of nitric oxide and secretion of pro-inflammatory cytokines (Jung et al., 2006; Jin et al., 2007). It has also been shown to protect dopaminergic neurons against microglia-mediated neurotoxicity (He et al., 2010). Curcumin supplementation in a rat model of acute-light damage had functional and structural protection of photoreceptors along with decreased inflammatory gene expression (Mandal et al., 2009). Curcumin treated activated microglia become neuroprotective and can rescue neurons from apoptosis *in vitro* (Yang et al., 2008) as well as reduce microglial migration (Karlstetter et al., 2011).

1.6.2 Luteolin

Luteolin (3',4',5,7-tetrahydroxyflavone) is a flavonoid abundant in parsley, green pepper, celery, and chamomile tea (Lopez-Lazaro, 2009). It has been shown to suppress pro-inflammatory cytokine IL-6 production in macrophages by blocking nuclear factor kappa B (NFkB) and activator protein 1 signaling pathways (Chen et al., 2007). Like curucmin, it has also been shown to inhibit production of nitric oxide (Hu and Kitts, 2004). Supplementation studies done on aged mice between 22-24 months of age showed reduced microglia activity in the hippocampus as well as reduced inflammatory marker expression (Jang et al., 2010). Luteolin treatment also attenuates microglial activation and induces a neuroprotective phenotype *in vitro* (Chen et al., 2008; Dirscherl et al., 2010).

1.6.3 DHA

Docosahexaenoic acid (DHA, 22:6n-3), a polyunsaturated fatty acid enriched in fish oil also dampens microglial nitric oxide production (Antonietta Ajmone-Cat et al., 2012) and attenuates microglial reactivity in a mouse model of inherited retinal degeneration (Ebert et al., 2009). DHA is highly enriched in the retina and is a precursor for neuroprotectin D1, promoting the survival of photoreceptors and RPE cells (Mukherjee et al., 2007). DHA has also been shown to inhibit the synthesis of inflammatory products by microglia allowing better survival of neural progenitor cells (Antonietta Ajmone-Cat et al., 2012). Furthermore, it has been previously reported that patients with juvenile NCL have reduced DHA levels in plasma and cerebral cortex, which may contribute to retinal and brain degeneration (Kohlschutter et al., 1993b).

1.7 Aim of the Thesis

Despite all the studies done on glial activation in the NCL brain, the presence of glial activation in the retina and whether it is the cause of retinal degeneration has not been studied. It is postulated that retinal glial activation in CLN mouse models represents an early event before the onset of overt neurodegenerative symptoms which leads to retinal dystrophy and blindness. Furthermore, therapeutic targeting of retinal glia cells and inflammatory processes could delay neuronal degeneration, hence improving symptoms. Results from immuno-modulation of the retina could be a basis to further evaluate the potential of immune-related therapies in the brain.

The aim of this study was divided into three parts.

1. Characterize the visual function and retinal degeneration of two NCL mouse models, *Cln3*$^{\Delta ex7\text{-}8}$ and *Cln6*^{nclf} , using optokinietic and electroretinogram measurements, as well as histological assessment.

2. Analysis retinal microglia and Müller cell activation in relation to progressive neurodegeneration using immunohistochemistry as well as glial and inflammatory marker gene expression.

3. Select one mouse line with the most prominent glial activation, which best correlates to onset of retinal degeneration, and do supplementation studies with curcumin, luteolin and

DHA in order to attenuate inflammatory processes resulting in reduced retinal degeneration.

2. Materials

All materials, software and machines used in this thesis were provided by the Institute of Human Genetics at the University Clinic Regensburg, unless otherwise specified.

2.1 Mouse Models

Table 2: Mouse models used in thesis studies

Mouse Model	Origin	Mutation	Genetic Background	Reference
***Cln3*$^{\Delta ex7-8}$**	Charité Berlin, Dr. Klaus Ruther	Knock-In	C57BL/6N	Cotmann et al., 2002
***Cln3*$^{+/+}$**	Charité Berlin, Dr. Klaus Ruther		C57BL/6N	
***Cln6*^{nclf}**	Charité Berlin, Dr. Klaus Ruther	c.316insC	C57BL/6J	Bronson et al., 1998
***Cln6*$^{+/+}$**	Charité Berlin, Dr. Klaus Ruther		C57BL/6J	
Wild type	Charles River (Sulzfeld, Germany)	inbreed	C57BL/6N	

Table 2: List of animals used in study, origin, mutation, genetic background and reference.

2.2 Oligonucleotides for real-time RT-PCR

Table 3: List of oligonucleotides (Metabion) and probes (Roche) used for quantitative real time RT-PCR.

Gene	Accession #	Primer	Sequence (5'-3')	Probe
ATPase	NM_016774	F R	GGCACAATGCAGGAAAGG TCAGCAGGCACATAGATAGCC	77
Casp8	NM_009812	F R	TGAACAATGAGATCCCCAAAT CAAAAATTTCAAGCAGGCTCA	11
Cd68	NM_009853	F R	CTCTCTAAGGCTACAGGCTGCT TCACGGTTGCAAGAGAAACA	27
Cd95	NM_007987	F R	AAACCAGACTTCTACTGCGATTCT GGGTTCCATGTTCACACGA	76
C1qa	NM_007572.2	F R	GGAGCATCCAGTTTGATCG CATCCCTGAGAGGTCTCCAT	16
Edn2		F R	TGGCTTGACAAGGAATGTGT GCCGTAGGGAGCTGTCTGT	29
Egr1	NM_20157	F R	CCTTCCAGGGTCTGGAGAA ACTGAGTGGCGAAGGCTTTA	3
Gfap	NM_010277	F R	ACAGACTTTCTCCAACCTCCAG CCTTCTGACACGGATTTGGT	64
Nclf	NM_001033175.2	F R	GGCGAAGAAGGTGAAGATGA AGAGCCACATGCCAGGAC	104
Tgfb1	NM_011577.1	F R	TGGAGCAACATGTGGAACTC CAGCAGCCGGTTACCAAG	72
Tnfα		F R	CTGTAGCCCACGTCGTAG TTGAGATCCATGCCGTTG	25

Table 3. Primer and probes for TaqMan assays

2.3 Enzymes

Table 4: Overview of enzymes used in experiments

Enzyme	Use	Firm, Article #
Antartctic Phophatase	Sequencing	NEB, M02895
DNAse I recombinant	TUNEL-Assay	Roche; 04536282001
Exonucleaase	Sequencing	USB, 70073
House Taq-polymerase	Mouse Genotyping	Dr. Ulrike Friedrich (Institute for Human Genetic, Regensburg)
Revert AidTM M-MuLV ReverseTranscritpase	Reverse transcription	Fermentas; EP0442
***Taq* Polymerase**	Mouse genotyping	Genaxxon; M3454
***Taq* Polymerase**	PCR and sequencing	Qiagen; 105476

Table 4. Enzymes: use and firm of purchase

2.4 Antibodies

Tables 5.and 6: List of primary and secondary antibodies used

Primary Antibody	Species	Dilution	Firm, Article #
F4/80	Rat monoclonal	1:600	Acris, BM4007S
GFAP	Rabbit, polyclonal	1:600	Sigma, G9269
Iba1	Rabbit, polyclonal	1:500	Wako, 01-1974

Table 5. Primary antibody, species, dilution and firm of purchase

Secondary Antibody	Species	Dilution	Firm, Article #
Goat anti-Rat IgG Alexa Fluor 594	Rat	1:800	Invitrogen; A11007
Goat anti-Rabbit IgG Alexa Fluor 488	Rabbit	1:1000	Invitrogen; A11008

Table 6. Secondary antibody, species, dilution and firm of purchase

2.4 Chemical and Kit System

Table 7 and 8: List of chemicals and kit-systems used

Chemical	Use	Firm, Article #
30% H2O2	Different	Merck, 1.07209
Biozym LE Agarose	Agarose gel	Biozym, 840004
Boric Acid	1x TBE buffer	Merck; 1.00165
Bromophenol blue	10x-DNA loading buffer	Sigma, B-6131
BSA	Immunohistochemistry, flat mounts	Applichem, A6588
Dako mounting medium	Stained tissue preservation	Dako, S3023
DAPI	Immunohistochemistry	Invitrogen, D1306
dNTPs	Genotyping/ sequencing	Genaxxon, M3018 - M3021

Chemical	Use	Firm, Article #
EDTA	10x TBE buffer	Merck, 1.08418.1000
Eosin Y	HE stain	Applichem, A0822
Ethanol	Different	J.T. Baker, UN 1170
Ethidium Bromide	Agarose gel	Applichem, A2273
Glycerin	10x DNA loading buffer	Applichem, A3561
HCl	Different	Merck,1090571000
Hematoxylin	HE stain	Sigma, HHS16
Isopropanol	Different	Merck, 100995
Ketamin 10%	Mouse anaesthesia	Dr. Thilo Spruss, head of aninal care, Regensburg University
M-CSF	Cultivation of ex-vivo Microglia cells	R & D, 216-MC/CF
MgCl	15x Puffer	Merck, 1.05833
Na_2HPO	10x PBS buffer	Merck, 106566
NaCl	Different	VWR, REF 27810.364
NaN3	Immunohistochemistry, flat mounts	Sigma; S-2002
NaOH	Different	Merck; 1064981
Nuclease Free water	Different	Promega; Cat. P1193
Paraformaldehyde	Immunohistochemistry, flat mounts	Applichem; A3813
Powdered skimmed milk	Immunohistochemistry, flat mounts	Roth, T145.3
RNAse ZAP	RNA-isolation	Sigma; R-2020
SDS	Different	Roth, CN30.3
Sodium Acetate	10x DNA loading buffer	
Sodium Citrate	TUNEL assay	Merck, 1.06448
Sucrose	Kyro-embedding	Merck; 1.07651
Tris-HCl	Different	USB,123008
Triton X-100	Flat mounts	Sigma; X100
Tween 20	Flat mounts	Sigma; P1379
Xylazin 2%	Mouse anaesthesia	Dr. Thilo Spruss, head of aninal care, Regensburg University
Xylencyanol	10x DNA loading buffer	Sigma; X-4126
Xylol	HE stain	Roth, 9713.1
β-mercaptoethanol	RNA-isolation	Merck; 1.07209

Table 7. Chemicals: use and firm of purchase

Kit-system	Use	Firm, Article #
BigDye Terminator Sequencing Kit	Sequencing	Applied Biosystems
In Situ Cell Death Detection Kit, POD	TUNEL assay	Roche; 11684817910
RevertAidTM H Minus First Strand cDNA Synthesis Kit	Reverse transcription	Fermentas; K1632
RNeasy Mini Kit	RNA isolation	Qiagen; 74104
TaqPCR Core Kit	PCR	Qiagen; 201225
RNA 6000 Nano LabChip Kit	RNA quality control	Agilent Technologies; 5067-1511

Table 8. Kit system: use and firm of purchase

2.5 Dietary Supplementation

Table 9: Diet and supplements used for supplementation study

Supplementation	Purity %	Firm
EF-M diet (Control)		SSNIFF Spezialdiäten GmbH
Curcumin	99	ChemHome, Shanghai Honghao Chemicals Co.,Ltd., Shanghai, China
Luteolin	98	Hangzhou Skyherb Technologies. Co., Ltd., Zhejiang, China
DHA (DHASCO-T)		Martek Biosciences Corporation, Columbia, MD, USA

Table 9. Diet, supplements and firm of purchase

2.6 Electroretinograms

Table 10: Special materials needed for ERGs

Material	Firm
Tropicamide eyedrops	Mydriaticum Stulln Pharma
Corneregel	Bausch & Lomb
Ganzfeld bowl	Roland Consult, Ganzfeld QC450 SCX,
Amplifier and recording unit	Roland Consult, RETI-Port,

Table 10: ERG materials and firm of purchase

2.7 Buffers and Solutions

Table 11: Lists of buffers and solution used

Buffer/Solutions	Composition	Use	Firm, Article #
1 kb DNA ladder		Agarose gel	Fermentas; SM0332
10x Buffer S	15 mM MgCl2	Mouse genotyping	Genaxxon; M3454
10x DNA loading bubber	10 mM Tris-HCl (pH 7,5) 5 mM Sodium Acetate 2 mM EDTA 10% Glycerin 0,001% (w/v) Bromphenol blue 0,001% (w/v) Xylencyanol	Agarose gel	
10x PBS	1,5 M NaCl 83 mM Na2HPO4 17 mM H2PO4 (pH 7,4)	Different	
10x TBE Buffer	1 M Tris 1 M Boric Acid 20mM EDTA (pH 7.5)	Gel electrophoresis	
18% Sucrose	18% (w/v) Sucrose in sterile dH2O	Cryo-preservation	

Buffer/Solutions	Composition	Use	Firm, Article #
20% SDS Buffer	20 g SDS in 100 ml H2O	Different	
2x TaqMan® MasterMix		TaqMan assay	Applied Biosystems, 4370074
3% H_2O_2 Solution	3% (v/v) H2O2 in 1x PBS	TUNEL assay	
4% PFA-Lösung	4% (w/v) PFA in 1x PBS (pH 7,0	Immunohistochemistry, flat mounts	
Agarose Gel	0,75-2% (w/v) Agarose in 1x TBE-Buffer	Agarose gel	
Alkaline lysis buffer	25mM NaOH 0.2mM EDTA	DNA isolation	
Antibody solution	2% BSA, 0,02% NaN3 0,1% Triton X-100 in 1x PBS	Immunohistochemistry, flat mounts	
BLOTTO	1% Skimmed powdered milk 0,01% Tween 20 in 1x PBS	Immunohistochemistry, flat mounts	
DAB substrate		TUNNEL assay	Roche,1718096
Dako mounting medium		Immunohistochemistry, flat mounts	Dako, S3023
DAPI solution	0,1 µg/ml DAPI in 1x PBS	Immunohistochemistry	
Neutralizing buffer	40mM Tris-HCl (pH 5)	DNA isolation	
Permeabilization buffer	25% Triton X-100 25% Tween 20 in 1x PBS	Flat mounts	
Permeabilization buffer	0,1% Triton X-100 0,1% Natriumcitrat in 1x PBS	TUNEL assay	
RNA Later		RNA isolation	Ambion; AM7020
Tissue-Tek OCT Compound		Tissue embedding	Hartenstein, TTEK

Table 11. Buffers and solutions: composition, use and firm of purchase

2.8 Basic Materials

Table 12: All basic materials needed for experiments

Material	Use	Firm, Article #
1 ml tips	RNA isolation	B & D Systems; REF 300013
1,5 ml Cups	Different	Sarstedt; REF 72.706.400
10 µl Filter tips	Different	Biozym; 770020

Material	Use	Firm, Article #
10 µl Pipette tips	Different	VWR; 613-1068
100 µl Filter tips	Different	Biozym; 770100
100 µl Filter tips	Different	Biozym; 770100
100 µl Pipette tips	Different	VWR; 613-1066
100 µl Pipette tips	Different	VWR; 613-1066
1000 µl Filter tips	Different	Biozym; 770600
1000 µl Pipette tips	Different	VWR; 613-1062
15 ml Falcon tubes	Different	Sarstedt; REF 62.554.502
2 ml Cups	Different	Sarstedt; REF 72.695.400
30 µl Pipette tips	TaqMan	Matrix; 7432
50 ml Falcon tubes	Different	Sarstedt; REF 62.547.254
96-well Microplates	Function assays	Greiner bio-one; REF 655101
Disposable gloves	Different	Roth; L949.1
Disposable scalpal	Different	Feather, No. 11
Glass cover slips (10 mm Ø)	Immunohistochemistry, flat mounts	VWR; 631-1576
MicroAmp Optical 384-well Plat	TaqMan	Applied Biosystems; 4326270
MicroAmp Optical adhesive films	TaqMan	Applied Biosystems; 4311971
Needle 20G Nr.1	RNA isolation	B & D Systems; REF 301300
Pasteurpipetten	Different	VWR; 612-3752
PCR Cups	PCR	Biozym; 711030 / 711040
PCR Tube stripes	PCR	Biozym; 711030 / 711040
Peel-Away® Molds	Embedding	Polysciences, INC.
Polysine objective slides	Different	VWR; 631-1349

Table 12. Basic materials, use and firm of purchase

2.9 Machines and Software

Tables 13 and 14: List of machines and software used for experiments

Machine	Use	Firm
3130xl Genetic Analyzer	Sequencing	Applied Biosystems
7900 HT Fast real time PCR System	TaqMan	Applied Biosystems
Agilent 2100 Bioanalyzer	RNA Quality Control	Agilent Technologies
Axioimager Z1 Apotome Microscope	Fluorescent Microscope	Zeiss
Axioimager Z2 Apotome Microscope	Fluorescent Microscope	Zeiss
Axioskop 2 MOT Plus	Fluorescent Microscope	Zeiss
Cold microtome	Cryosections	Leica

Machine	Use	Firm
Dark Hood DH 30/32	Gel documentation	Biostep
Distille 2012 GFL	Different	GFL Burgwedel
Gel chamber Blue Marine 200	Gel electrophoresis	Blue Power
Microcentrifuge	Different	Labnet
Microscope DMIL HC kpl. inverse	Different	Leica
Microscope Leica DM IL	Different	Leica
Microwave Kor-6D07	Different	Daewoo
Multifuge 3L	Different	Heraeus
Multipipette	TaqMan	Matrix
NanoDrop	RNA and DNA concentration	PeqLab
Optomotry©	Optokinetic tracking	Cerebral Mechanics
Rotarod (4-40rpm)	Rotarod	PanLab/Harvard Apparatus
T3000 Thermocycler	PCR	Whatman Biometra
Table centrifuge Biofuge fresco	Different	Heraeus
Thermomixer compact 5436	Different	Eppendorf
Thermoprinter P93D	Gel documentation	Mitsubishi
Tissue Lyser	RNA isolation	Qiagen

Table 13. Machines: use and firm of purchase

Software	Use	Firm
Agilent 2100 BioAnalyzer	RNA Quality control	Agilent Technologies
Argus 3.0	Gel documentation	Argus
Axiovision 4.8	Fluorescent microscope	Zeiss
AxioVision LE 4.5	Fluorescent microscope	Zeiss
Corel Draw X4	Figures	Corel
Edit Seq 5.05	Sequence analysis	DNASTAR
Graphpad prism	Graph plots	Graphpad software
Microsoft Office	Different	Microsoft
RQ Manager 1.2	TaqMan	Applied Biosystems
SDS 2.3	TaqMan	Applied Biosystems
SeqMan	Sequence analysis	DNASTAR
Zen 2012	Fluorescent microscope	Zeiss

Table 14. Software: use and firm of purchase

3 Methods

3.1 Mouse Lines and Husbandry

The animals used in this study were housed in an air-conditioned environment at 20°C – 22°C and were subject to a constant 12 hours light-dark cycle with free access to water and standard mouse diet. Light intensity during light phase was 15 lux. Animal health status was regularly controlled and all experimental protocols were approved by the Committee of Animal Health and Care of the local government and conformed to international guidelines on the ethical use of animals. All efforts were made to minimize the number of animals used and their suffering. The required animals were killed, depending on their age, by either direct decapitation or by CO_2 asphyxiation with subsequent cervical dislocation. Mice were either genotyped using PCR or sequencing.

3.2 Mouse Genotyping

3.2.1 DNA Extractions

Mouse tail tips were cut using a sharp blade and the DNA extracted by incubating tails for 20 min in 75µl Alkaline Extraction Solution at 95°C, chilling samples on ice and then adding 75µl Neutralizing solution.

3.2.2 Photometric determination of DNA concentration

A spectrophotometer (Nanodrop ND-1000) was used to determine the concentration and purity of the DNA samples. Absorbance was measured at 260 nm and 280 nm and was calculated using the Lambert-Beer law: $E = \varepsilon \cdot d \cdot c$; with E being the extinction, ε the molar extinction coefficient, d the thickness of the sample and c the concentration of the sample. An extinction factor of 1 represents 50 µg/ml of double-stranded DNA. DNA was considered pure between $A_{260/280}$ of 1.8 to 2.2 using nuclease-free water as a reference.

3.2.3. DNA amplification with PCR

Polymerase chain reaction (PCR) is the standard methods used for amplifying small quantities of template DNA within a short time. DNA is mixed with forward and reverse primers, taq-

polymerase, deoxynucleotide triphosphates (dNTPs) and buffer. During the first step, template DNA is denatured at 95°C. Here, the sense and antisense strand are separated from each other. During the annealing-phase, primers bind to the single stranded DNA. The annealing temperature is dependent on every single pair of oligonucleotide (primer-pair). In the last step, taq-polymerase elongates the primers according to the template DNA. The temperature used in the elongation-phase (72°C) is optimal for the hyperthermophyl bacteria *Thermus aquaticus* activity, from which the *taq*-polymerase enzyme is isolated. CLN3 DNA were amplified using primer pairs (Table 16), PCR cocktail mix (Table 15) and PCR program (Table 17).

Mouse line	Composition	1x dilution (µl)	c (Stocks)	c (Dilution)
Cln3	dNTP-mix	4.00	1.25mM	0.2mM
	Primer Forward	0.625	10µM	0.25µM
	Primer Reverse	0.625	10µM	0.25µM
	15x Buffer (25mM $MgCl_2$)	2.5	25mM	2mM
	House *Taq* polymerase	0.625	2U/µl	0.05U/µl
	Nuclease-free water	14.625		
	gDNA	2		

Table 15: PCR solution for *Cln3* mouse genotyping

Primer name	Sequence	Product (bp)	Genotyping/Sequencing
CLN3-WT-F	CAGCATCTCCTCAGGGCTA	250	$Cln3^{+/+}$
CLN3-WT-R	CCAACATAGAAAGTAGGGTGTGC		$Cln3^{+/+}$
CLN3-552 F	GAGCTTTGTTCTGGTTGCCTTC	500	$Cln3^{\Delta ex7\text{-}8}$
CLN3-Ex9RA R	GCAGTCTCTGCCTCGTTTTCT		$Cln3^{\Delta ex7\text{-}8}$
CLN6 F	GGTGCTGGTACCCACTGAAG		
CLN6 R	TGCCCTGCTAAGGAACTCAC		

Table 16: Primer pair for Cln3 genotyping and Cln6 sequencing

Mouse line	Step	Temperature (°C), time	Cycle
Cln3	Pre-denaturing	95, 2 min	
	Denaturing	95, 30 sec	
	Annealing	58, 30 sec	
	Elongation	72, 30 sec	34
	Final Elongation	72, 5 min	

Table 17: PCR program for *CLN3* genotyping

3.2.4 DNA amplification for Sequencing

DNA from $CLN6^{nclf}$ mice was sequenced for an additional cystein insertiona in a six cystein sequence found the normal CLN6 amino acid sequence (Table 16, 18). This method first requires the amplification of total DNA using a Qiagen Taq Core kit, followed by digestion of DNA to separate the strands, then amplification of one of the strands using one of the primer pairs and a

fluorescent dye. Once the dye is incorporated into the elongating strand, it causes the polymerase to fall off, resulting in different lengths of DNA. Extensive washing steps are done to ensure all the unused dye is removed leaving behind pure DNA. DNA is then diluted in formamide, placed in a 96-well plate and sequenced using the automated capillary electrophoresis 3130xl Genetic Analyzer from ABI. Heated formamide causes DNA to denature allowing DNA strands to separate by size and migrate down the capillary at different speeds. The analyzer then uses a laser to excite the fluorescent material found at the end of the strand causing the DNA to be colored. The computer is then able to read the colors and determine the order of the bases in the sample. The Genetic Analyzer is operated by the Diagnostic Department at the Institute of Human Genetics at the University Clinic Regensburg.

Step	Solution composition	PCR	PCR temperature (°C), time	PCR cycle
Amplification	DNA (25ng/µl)- 2 µl 10x Buffer- 2.5 µl LsgQ- 5 µl PF (10µM)-0.5 µl PR (10µM)-0.5 µl dNTPs-0.5 µl Taq-0.25 µl H_2O-13.75 µl	Pre-denaturing Denaturing Annealing Elongation Final Elongation	94, 3 min 94, 30 sec 58, 30 sec 72, 1 min 72, 10 min	34
Digestion	Exol- 0.1 µl AAP (10µM) - 0.25 µl H_2O- 3.65 µl PCR product- 1 µl Done in double		37, 15 min 80, 15 min	
Cycle Sequencing	5x Buffer- 2 µl B.D. 1.1- 0.3 µl H_2O- 1.7 µl Directly into the digestion Primer F/R- 1 µl	Pre-denaturing Denaturing Annealing Elongation Final Elongation	96, 3 min 96, 30 sec 55, 30 sec 60, 3 min 60, 5 min	
Precipitation and washing	NaAC (3M, pH 4.9)- 2 µl 100% EtOH - 25 µl Spin 20 min 4300 U/min Dry pellet 70% EtOH- 100 µl Spin 15 min 4300 U/min Dry pellet HiDi 15 µl Plat			

Table 18. Method for DNA sequencing

3.2.5 DNA Separation and Analysis

Quantitative and qualitative DNA analysis were done via agarose gel electrophoresis. Agarose gel electrophoresis is a standard method to separate DNA fragments according to their molecular weight. The phosphate backbone of nucleic acids is ionized, thus deoxynucleotides are present as

anions and migrate from the cathode to the anode in an electric field. Depending on the size of the fragments, 1.5 % (w/v) or 2 % (w/v), agarose gel was prepared by dissolving agarose in an appropriate amount of TBE buffer and adding a few drops of ethidium bromide. The solution was transferred into a gel casting tray and a removable comb was added. DNA samples were mixed with 10x DNA loading buffer and 1x TBE buffer. After polymerization the comb was removed and the samples were loaded. For size determination, a 1 kb DNA ladder was used. Separation occurred at 120 to 150V and took 30 to 45 minutes. ethidium bromide is a DNA intercalating agent allowing DNA fragments to be visualized using UV irradiation (dark hood). The agarose gel was documented using the Argus 3.0 software.

3.2.6 Sequence Analysis

Sequences obtained from the Genetic Analyzer were viewed using Sequence Scanner 1.0 and compared to a reference sequence using Tools ClustalW2 software.

3.3 Retinal Preparations for Experiments

3.3.1 Cryo-embedding and Sections

Enucleated eyes were embedded in TissueTek O.C.T Compound after a short washing step in 1x PBS, flash-frozen with dry ice and stored at - 80°C. For permanent fixation of the tissue, the eyes were fixed in 4 % PFA for 2 hours and incubated in 18 % sucrose overnight followed by TissueTek embedding. 10 µm cryosections were prepared with a CryoMicrotome and mounted onto a Polysin-slide. Cryosections were stored at - 80°C for further experiments.

3.3.2 Whole Retinal Flat Mounts

Eyes were enucleated and fixed in 4 % PFA (4 h/4°C). Using a standard light microscope, a hole was made in the cornea and the lens removed. The retina was carefully separated from the RPE and stored in 1x PBS for further experiments.

3.3.3 Morphometry Experiments

Before enucleation, eyes were branded on the superiour limbus. Eyes were fixed for 24h in Ito's fixative (Karnovsky, 1965) and embedded in Epon. Sections 1 µm in thickness were cut along the nasal-temporal plane and stained with fuchsin/methylene blue. Branded enucleated eyes were further handled by Prof. Dr. Ernst Tamm's laboratory until eyes were sectioned and ready for analysis.

3.4 Morphological and Immunohistological Analyses of Prepared Retinae

3.4.1 Hematoxylin and Eosin Stain

Hematoxylin and eosin (HE) stain allows for a quick overview of the tissue morphology. This method stains the cell bodies blue and the tissue around the cell bodies with a red-ish color. Non-fixed retinal sections were fixed in 100% ethanol (ETOH) for 20 min at -20°C followed with a 5 min washing step in PBS and hematoxylin stain for 5 min. Hematoxylin was washed out with gentle running water for 15 min, stained with 1% Eosin Y diluted in water for 3 min , washed for 10 sec in water and dehydrated in increasing amount of ETOH (70% 5 sec, 80% 5 sec, 90% 5 sec and 100% 4 min). Samples were then incubated with 100% Xylol for 3 min and embedded with Xylol-soluble Entellan and cover slip.

3.4.2 Immunohistochemical Stain of Retinal Sections

Cryosections were thawed and air dried at room temperature (RT). Samples which required Iba1 staining required fixed sections which were first boarded with liquid barrier and further fixed with 4% PFA for 6 min. After fixation, cryosections were washed 3 times with 1x PBS for 5 minutes followed by a 10 min re-hydrating step. Sections were then blocked with BLOTTO 30 min at RT and incubated with primary antibody overnight. Samples were then washed with 1x PBS and incubated with fluorescently labelled secondary antibody for 1 hour at RT, diluted in 1x PBS (dilutions in table 5 and 6). During the incubation and all the following steps, the slides were covered to avoid bleaching from light. The nuclei were counterstained with 0.1 µg/ml DAPI (10 min/RT). Cryosections were embedded with Dako fluorescent mounting medium.

3.4.3 Immunohistochemical Stain of Retinal Flat Mounts

Prepared retinae were incubated with 25% Triton-X/ 25% Tween-20 on a shaker (4°C/ON) to ensure full permeability of the tissue. Tissues were then washed extensively with 1x PBS and followed the same staining procedure as above. Flat mounts were not counter stained with DAPI. Stained flat mounts were cut at four different sections to eliminate the natural rounding of the retina and were then embedded with DAKO fluorescent mounting medium.

3.4.4 TUNEL Assay

Cleavage of genomic DNA during apoptosis causes 'nicks' or breaks in the DNA strand(s). These breaks can be visualized by labeling the free 3'-OH end with modified nucleotides in an enzymatic reaction (terminal deoxynucleotidyl transferase dUTP nick end labeling, TUNEL). The first step is to mark the broken strand with deoxynucleotidyl transferase using terminal transferase (TdT), which catalyzes the polymerization of labeled nucleotides to free 3'-OH DNA ends (TUNEL reaction). Coupled to an anti-fluorescein antibody, 3'-OH attached fluorescein, also known as the peroxidase, can be detected. After subsequent substrate reaction, stained cryosections can be analyzed.

Cryosections were fixed in 4% PFA solution (20 min, RT) for 30 min and rehydrated in 1x PBS. Endogenous peroxidase activity was saturated with 3% H2O2 solution (10 min / RT), followed by tissue permeabilization (2 min, 4°C). The cryosections were treated with 50 µl TUNEL reaction mix from the In Situ Cell Death Detection Kit , which was freshly prepared by diluting enzyme solution with label solution 1:10 (37°C, 5% CO2, 60 min). As a negative control, label solution without enzyme solution was used. For a positive control, cryosections treated with recombinant DNase I solution (3,000 U/ul) prior to incubation with TUNEL reaction mix was used (10 min / RT). The TUNEL stained DNA fragments were detected using green fluorescence. Nuclei were counter-stained with DAPI and mounted using DAKO mounting media.

3.4.5 Microscopy

CLN3 samples and TUNEL stains were viewed using Zeiss Axioskop2 MOT Plus fluorescence microscope at 40x magnification. The appropriate filters were used to look at antibodies (488nm), auto-fluorescence (594nm) and DAPI stain (405nm). This microscope also allowed for bright field

analysis of HE stained tissues. All pictures were processed using Zeiss AxioVision LE 4.5. CLN6^{nclf} retinal sections were studied and imaged using Axioimager Z1 Apotome Microscope at 100x magnification. Flat mounts were mounted and view with Axioimager Z2 Apotome Microscope at 100x magnification using z-stacks of inner and outer plexiform layers as indicated by fluorescent sidebars. CLN6^{nclf} retinal sections were further processed using AxioVision LE 4.5 whilst flat mounts were processes using Zen 2012.

3.4.6 Retinal Morphometry Analysis

Eyes prepared for morphometry experiments were viewed using Axioimager Z1 Apotome Microscope under bright light settings. The entire retina was imaged using 63x magnification and stitched together using the fully licensed AxioVision software. The length of superior and anterior retina were measured using a curved line starting from the optic nerve head (ONH) to the end of the retina. The retinal segment was divided into ten equal parts where cross-length measurements of the whole retina and photoreceptor were measured. All measurements were exported into Microsoft Excel and analyzed.

3.5 Behaviour and Retinal Function Studies

3.5.1 Optomotry

The virtual optomotor system allows for rapid quantification of mouse visual acuity as previously described (Prusky et al., 2004; Douglas et al., 2005). Freely moving mice were place on a platform in the middle of a virtual cylinder made of four computer monitors projecting moving sine wave gratings of various spatial frequencies. The mice were visualized using a video camera found on the lid of the optomotor system which was connected to computer program OptoMotry. This enable the experimenter to track the behavior of the mice without interference. Mice were placed on the platform one at a time, and acclimated to their environment by keeping the monitors dim and gray. At all times, the mouse's head was tracked using a crosshair cursor superimposed in the video image. The coordinates of the crosshair cursor are used as to center the rotation of cylinder thus maintaining the virtual walls of the cylinder at a constant distance from the animal and effectively maintaining the spatial frequency of the grating. Once the mouse had settled and stopped moving, the gray monitors were replaced with a low-spatial-frequency sine wave grating

projected on the monitors. If the mouse was able to perceive the grating, it would move its head and neck in concert with the rotation. This was repeated a few times with short dim pauses in between to ensure accurate readings. The spatial frequency of the grating was increased until the mouse no longer responded. The software controlled the speed of rotation, geometry of the cylinder, the spatial frequency and contrast of the stimuli and enabled live video feedback of the testing arena. The experiment ended when the software had enough data to correctly assess the visual acuity of the animal. Experiments lasted between 10-30 minutes. If, during the experiment, the mouse fell off the platform, it was simply placed on the platform the experiments continued.

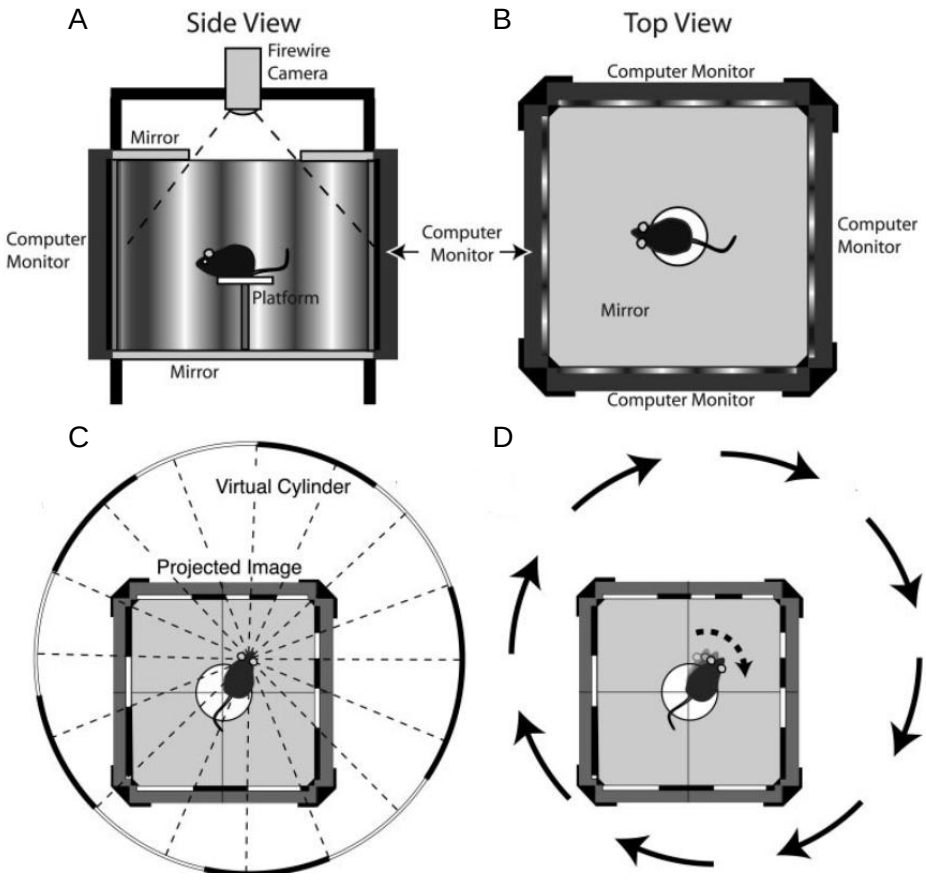

Figure 3. Schematic representation of the Optomotor machine. A. Side view. The mouse is placed on the platform and the sine wave grating rotate on the screen surrounding the mouse. B. Top view as seen by video camera. C. The mouse head is the center of the rotation of the cylinder. D. When the cylinder is rotating, the mouse tracks the movement with its head and neck. These images were adapted from Prusky et al., 2004.

3.5.1 Rotarod

Rotarod experiments to assess motor or cognitive difficulties were done on two subsequent days on an accelerating Rotarod which accelerated 4-40 rpm in one minute. The speed and time at which the mouse fell off the rotarod was recorded. Rotarod apparatus was cleaned after every experiment. Experiments were performed three times with 15 minute resting time in between.

3.5.2 Electroretinograms

All electroretinograms (ERGs) were performed by Prof. Dr. med. Herbert Jägle and Dr. med. Cornelia Volz from the University Eye Clinic in Regensburg. A brief method outline was provided by Prof. Jägle. Mice were dark adapted for at least 12 hours before the experiments and subsequently anesthetized by subcutaneous injection of ketamine and xylazine. Pupils were dilated with tropicamide eyedrops. Silver needle electrodes served as reference (fore-head) and ground (tail) and gold wire ring electrodes as active electrodes. Corneregel was applied to keep the eye hydrated and maintain good electrical contact. ERGs were recorded using a Ganzfeld bowl and an amplifier & recording unit. ERGs were recorded from both eyes simultaneously, band-pass filtered (1 to 300 Hz) and averaged. Single flash scotopic (dark adapted) responses to a series of ten LED-flash intensities ranging from -3.5 to 1.0 log cds/m2 with an inter stimulus interval of 2 s up to 20 s for the highest intensity were recorded. Response waveforms were analyzed by means of through and peak amplitude and implicit time measurement. All analysis and plotting was carried out with R 2.14.2 and gplot 0.9.

3.6 RNA Gene Expression Analysis

Total RNA was isolated from the retina of wild type and mutant mice. All conditions corresponded to those recommended for the RNAeasy Kits from Qiagen. All experiments were carried out in nuclease free environment and samples were always kept on ice. The yield of the RNA isolation depends on the amount of retina removed and the state of the tissue upon removal as well as handling during the experiment.

3.6.1 RNA Isolation

RNA isolation from retinal tissue was carried out using the RNeasy Kit from Qiagen. This method allows purification of total RNA on hydrophilic silicone gel columns using the appropriate buffer systems. First, tissues were homogenized in a buffer containing guanidinium isothiocyanate and lysed (RLT buffer). This chaotropic salt denatures all proteins, including RNases and thus preserves the RNA from degradation. Tissues were then homogenized using a tissue lyzer (2 x 30 sec, 30 Hz). 70% ethanol was added to the supernatant of the homogenate, allowing binding to the columns. During subsequent centrifugation (13,000 rpm, 1 min, RT), RNA molecules of 200 nucleotides bound to the silicon based column whilst the rest of the solution was removed. Subsequent washing and centrifugation with RW1 and RPE buffer resulted in pure RNA which was eluted with a corresponding volume of nuclease water by centrifugation (13,000 rpm, 1 min, RT). RNA was kept at -80 °C until further use

3.6.2 Photometric determination of RNA concentration

RNA concentrations were measured the same was as DNA samples (see above). A wavelength of 280 nm provided an indication of possible contamination of the RNA sample with proteins, a wavelength of 260 nm corresponds to the absorption maximum of the RNA bases. An extinction factor of 1 represents 40 µg/ml RNA. Pure RNA has an absorbance ratio A260/280 of 2.0. Nuclease-free water was used as reference.

3.6.3 Reverse Transcription

Isolated RNA cannot be used as a template in subsequent PCRs, therefore it has to be rewritten (reverse transcription) into a complementary DNA strand (cDNA). First-strand complementary DNA was carried out using the RevertAidTM H Minus First Strand cDNA Synthesis Kit from Fermentas. This includes the RevertAid™ H Minus M-MuLV reverse transcriptase from Moloney murine leukemia virus. This enzyme has an optimum temperature of 42-45°C and can synthesis cDNA up to 13 kb in length.

The reaction takes place as follows:

1. 1-3 µg of RNA are diluted into a total volume of 11 µl of nuclease-free water
2. 1 µl of hexamer primer is added

3. The reaction is incubated at 70°C for 5 min
4. 4 µl of Reaction Buffer + 1 µl of nuclease-free water + 2 µl of 10nM dNTP mix is added
5. The reaction is incubated at 25°C for 5 min
6. 1 µl M-MuLV Reverse Transcriptase (200 U/µl) is added
7. The reaction is incubated at 25°C for 10 min
8. The reaction is incubated at 42°C for 60 min
9. The reaction is incubated at 70°C for 10 min (denaturing of the transcriptase)
10. The reaction is diluted with the appropriate amount of nuclease- free water and store at -20°C until needed.

3.6.4 TaqMan technology

TaqMan PCR uses cyclic amplification of specific PCR product along with fluorescently labeled probes (Universal sample Library Probes), which target the desired sequence. The advantages of the TaqMan technology are its high sensitivity (<5 ng template sufficient) and specificity, good reproducibility and accurate quantification of mRNA. Each probe consists of eight or nine nucleotides attached to a fluorophore linked reporter (5 'end) and a quencher (3' end) which is complementary to the target sequence. The quencher dye suppresses the fluorescence of the reporter by means of fluorescence resonance energy transfer (FRET). As long as the reporter and the quencher are in proximity, quenching inhibits any fluorescent signals (Fig. 4).

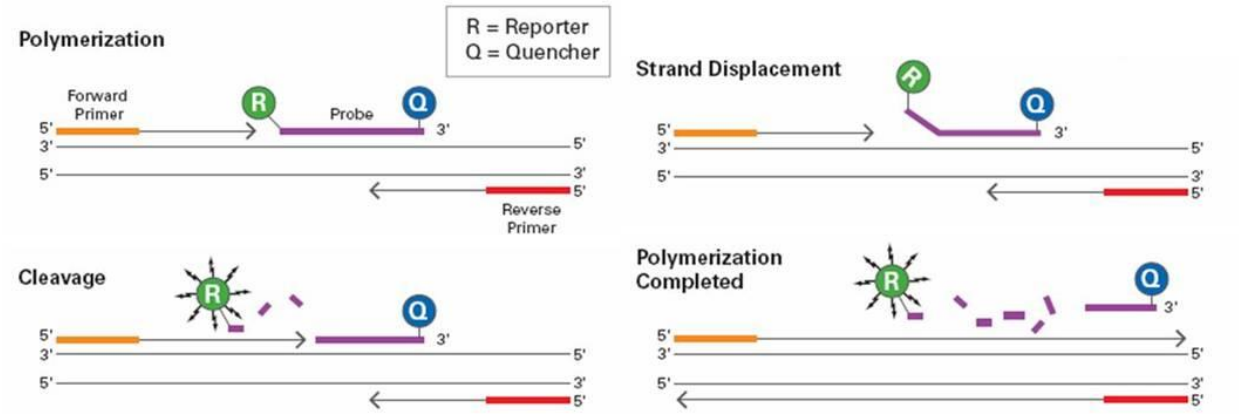

Figure 4. The principle of TaqMan technology. The probe (in purple) is attached to the fluorophore linked reporter (R) and fluorophore quencher (Q). The forward primer is in yellow and the reverse primer in red. Image adapted from http://www.asuragen.com/Services/services/gene_expression/ab_taqman.aspx

The probes first anneal to a specific region on single-stranded DNA which is amplified by designated primers. As the taq polymerase extends the primer and synthesizes nascent DNA, the 5' to 3' exonuclease activity of the polymerase cleaves the probe which is annealed to the DNA. This cleavage causes the fluorophore to be released from the reporter which breaks its close proximity to the quencher molecule allowing fluorescence of the fluorophore. With every PCR cycle, the fluorescence intensity increases and is directly dependent on the amount of DNA template present in the PCR (Fig. 6 D). The Universal Library sample uses probes made of locked nucleic acids (LNA). LNAs are modified nucleotides which have increased affinity for hybridization with complementary nucleotides whilst maintaining specificity and melting temperature. The real time RT-PCR reactions were performed on 384-well microtiter plates which were scanned after every cycle with a laser. The fluorescence intensity was calculated by the SDS 2.3 software program connected to the real time PCR system. For the quantification of 50 ng cDNA, a PCR protocol of 40 cycles was used (denaturation 95 ° C, 40 sec, annealing 60 ° C, 60 sec, elongation, 72 ° C, 2 min). The real time RT-PCR analysis was performed in duplicates. PCR solution composition is found in Table 19

Compostion	1x dilution (µl)	[ ]Stocks	[ ]Dilution
2x TaqMan Gene Expression Mastermix	5	2x	1x
Primer (forward)	1	10 µM	1 µM
Primer (reverse)	1	10 µM	1 µM
Universal ProbeLibrary Probe	0.125	10 µM	0.125 µM
Nuclease free water	0.375		
cDNA (0,02 µg/µl)	2.5		

Table 19. 10 µl TaqMan solution

3.6.5 Relative Quantification

The raw data from the real time RT-PCR experiments can be analyzed using either absolute or relative quantification. This work only required relative quantification, which will be described in detail. Replication of the cDNA during the PCR reaction increases exponentially. This can be represented in a diagram, plotting the fluorescence measured after each cycle to the number of cycles. As the amount of fluorescence depends directly on the amount of DNA template initially provided, the comparison of gene expression from different samples requires analysis of the CT values of each individual reaction. The CT-value (Cycle Threshold) is a threshold value that is placed in the linear region of the amplification curve where there is a statistically significant increase in gene expression. The CT value is where the threshold line intersects the amplification

curve. Therefore, greater initial DNA template have a lower gene expression where as less DNA template will have more. Relative quantification is based on a calibrator, a wild type sample, which is set to one. In addition, the measured gene expression values are normalized to a reference, or housekeeping, gene. A good housekeeping is characterized by a constant gene expression in the desired tissue. Normalizing a sample to a reference gene within that sample eliminates human experimental error and ensures accurate comparisons of the gene expression with other samples. The housekeeping gene used in all experiments was murine ATPase. CT values and relative quantification with the ΔΔCT method was done using the RQ Manager 2.1 software:

1. Calculation of average CT value --> CT Avg
2. Normalization to average CT value of reference gene ATPase:
   CT Avg (Gene)- CT Avg (Atpase) --> ΔCT Avg
3. In reference to the caibrator
   ΔCT Avg (Probe) - ΔCT Avg (calibrator) --> ΔΔCT Avg
4. Relative difference in gene expression --> $2^{-\Delta\Delta CT\ Avg}$

3.7 Food Supplementation Study

Experimental mouse diets were produced at SSNIFF Spezialdiäten GmbH (Soest, Germany) consisting of standard mouse diet EF-M (control) supplemented with either 0.6% Curcumin , 0.6% Luteolin or 5% DHA. Mice received supplement diets as soon as they were weaned (post natal day 21-23) and were the fed for 30 weeks. Body weight were measured on a weekly basis for the duration of the study.

3.8 Statistics

real time RT-PCR data from different mouse ages were analyzed using a two-way ANOVA with Bonferroni post-test. real time RT-PCR data from the food supplementation study were analyzed with a Kruskal-Wallis ANOVA. Rotarod and ERG experiments were analyzed using a one-way ANOVA with Bonferroni post-test. $P \leq 0.05$ was considered as statistically significant.

4. Results

4.1 Characterization of the *Cln3*$^{\Delta ex7-8}$ Retina

Previous studies done on *Cln3*$^{\Delta ex7-8}$ mice showed localized glial activation and inflammation preceding and during neuronal degeneration in the brain (Pontikis et al., 2004; Pontikis et al., 2005). However, little is known about retinal degeneration in this mouse model and whether reactive glia and inflammation play a role. One of the objectives of this thesis was to characterize the morphological and functional degeneration in the *Cln3*$^{\Delta ex7-8}$ retina and determine if Müller cells and microglia, in particular, play an active role in degeneration.

4.1.1 Histological Characterization of the *Cln3*$^{\Delta ex7-8}$ Retina and Immunohistological Evaluation of Müller and Microglia Cells.

In order to determine the severity and/or presence of retinal degeneration in the *Cln3*$^{\Delta ex7-8}$ model, mice were studied starting at 18 months of age. This time point would ensure detection of retinal degeneration, if present. Retinal sections of 18 month old *Cln3*$^{\Delta ex7-8}$ and wild type mice were first stained with hemotoxylin-eosin (HE) for morphological comparison (Fig. 6 A). Both retinas appeared to have identical striated retinal morphology with no observable change in the photoreceptor or inner and outer nuclear layers (PR, INL and ONL, respectively). These results point towards no obvious morphological degeneration in the *Cln3*$^{\Delta ex7-8}$ retina.

The presence and morphology of glial cells was determined as well. Retinal sections of 18 month old *Cln3*$^{\Delta ex7-8}$ and wild type were stained with GFAP and Iba1, markers for Müller cells and microglia, respectively. *Cln3*$^{\Delta ex7-8}$ retinas show up-regulated GFAP expression seen as fluorescent columns spanning the retina, indicative of reactive Müller cells (Fig. 6 B). In contrast, wild type retinas showed mostly end-feet signalling in the ganglion cell layer (GCL) with few retinal spanning strands normally associated with healthy aging retina.

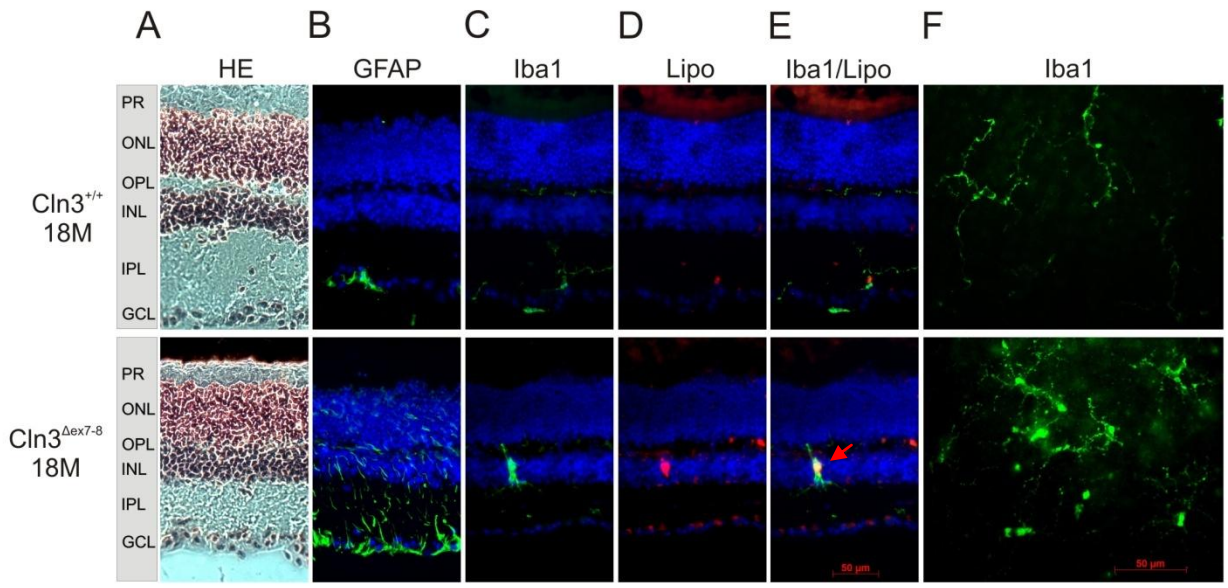

Figure 5. Histological and immunohistological evaluation of 18 month old *Cln3*$^{\Delta ex7-8}$ retina, Müller cells and microglia. A. Histological comparison of retinal layers in 18 month old (M) wild type (*Cln3*$^{+/+}$) and *Cln3*$^{\Delta ex7-8}$ retina with hemotoxylin-eosin (HE) stain. B. Immunolabelling of reactive Müller cells with GFAP antibody. C. Immunolabelling of microglia cells with Iba1 antibody. D. Auto-fluorescent accumulation of lipofuscin deposits in wild type and Cln3$^{\Delta ex7-8}$ retinas. E. Merged images of Iba1-labeled microglia with auto-fluorescent lipofuscin deposits. Arrow indicates co-localization of lipofuscin and microglial cell. E. Iba1-labeled flat-mounts, encompassing the plexiform layers, reveal different microglia morphology in wild type and Cln3$^{\Delta ex7-8}$ retinas. PR, photoreceptors; ONL, outer nuclear layer; OPL, outer plexiform layer; INL, inner nuclear layer; IPL, inner plexiform layer; GCL, ganglion cell layer. Scale bar, 50µM.

Iba1 staining of microglia revealed morphologically ramified cells in the inner and outer plexiform layers (IPL and OPL, respectively) of wild type retinas, where resting retinal microglia are normally found (Fig. 6 C). In contrast, Cln3$^{\Delta ex7-8}$ retinas showed migrating amoeboid microglia with little ramifications normally associated active microglia. Auto-fluorescent ceroid lipofuscin deposit were detected as bright roundish signals found throughout the *Cln3*$^{\Delta ex7-8}$ retina (Fig. 6 D). Wild type retinas had little or no storage material in comparison. Microglia were also observed engulfing lipofuscin deposits as shown by co-localization of Iba1 signal with auto-fluorescent signal (Fig. 6 E). Furthermore, flat mount stainings of microglia with Iba1 as a method of better assessing microglia morphology (Fig 6 F), showed long ramified microglia in wild type retinas, compared to rounder, more alert microglia seen in the Cln3$^{\Delta ex7-8}$ retinas.

As Müller cells and microglia appear to be active in 18 month old *Cln3*$^{\Delta ex7-8}$ retinas, 12 month old mutant retinas were also studied (Fig. 7). HE stains showed no morphological differences to age-matched wild type retinas (Fig. 7 A) . GFAP stains showed the presence of active Müller cells (Fig. 7 B). Sections stained with Iba1 showed ramified microglia in the IPL and OPL as did flat mounts (Fig. 7 C, F). Auto-fluorescent lipofuscin deposits could be seen throughout the retina (Fig. 7 D).

These data indicate microglia activation occurs at a later time point in the *Cln3*$^{\Delta ex7-8}$ retina contrary to reactive Müller cells which are first seen starting at 6 months (data not shown).

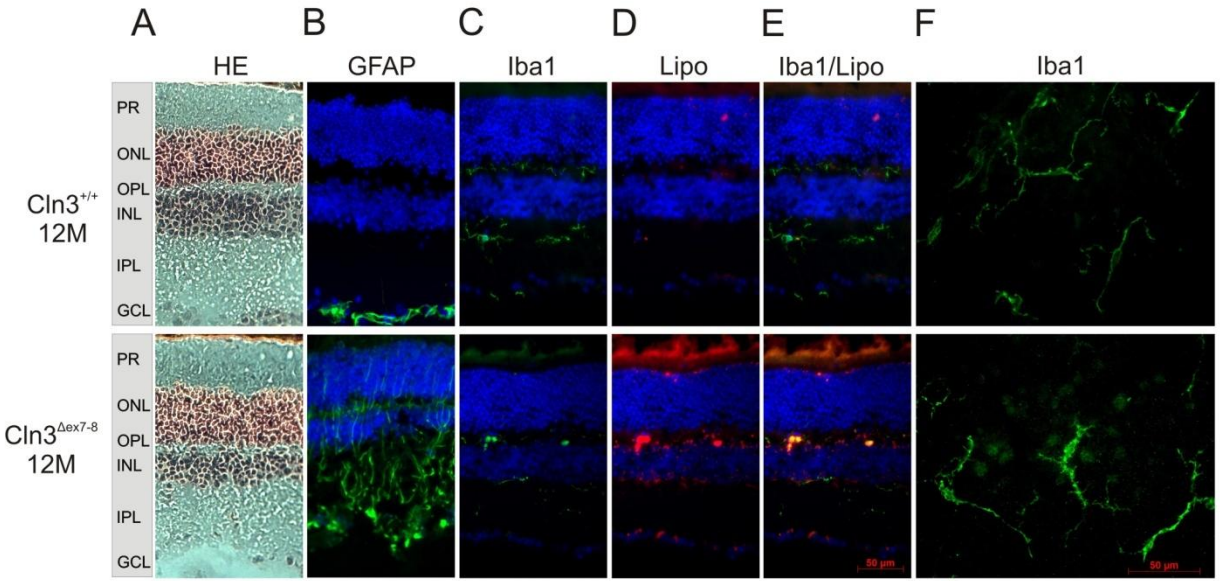

Figure 6. Histological and immunohistological evaluation of 12 months old *Cln3*$^{\Delta ex7-8}$ retina, Müller cells and microglia. A. Histological comparison of retinal layers in 12 month old wild type and *Cln3*$^{\Delta ex7-8}$ retina with HE stain. B. Immunolabelling of reactive Müller cells with GFAP antibody. C. Immunolabelling of microglia cells with Iba1 antibody. D. Auto-fluorescent accumulation of lipofuscin deposits in retinas. E. Merged images of Iba1-labeled microglia with auto-fluorescent lipofuscin deposits/ E. Iba1-labeled flat-mounts, reveal similar microglia morphology in wild type and Cln3$^{\Delta ex7-8}$ retinas. M, months; HE, hemotoxylin-eosin; PR, photoreceptors; ONL, outer nuclear layer; OPL, outer plexiform layer; INL, inner nuclear layer; IPL, inner plexiform layer; GCL, ganglion cell layer. Scale bar, 50µM

4.1.2 Functional Characterization of the *Cln3*$^{\Delta ex7-8}$ Retina

To assess changes in visual acuity or retinal function in the *Cln3*$^{\Delta ex7-8}$ mouse, optokinetic tracking (OKT) and electroretinogram (ERG) measurements were performed. These experiments indicate if any kind of retinal degeneration exist in this mouse model which is not obvious using morphological studies. Wild type and *Cln3*$^{\Delta ex7-8}$ mice were tested at different ages in order to temporally assess degeneration.

4.1.2.1 Optomotry Assessment of Visual Acuity

Visual acuity of *Cln3*$^{\Delta ex7-8}$ and wild type mice was studied using OKT measurements in an OptoMotry system. OKT is a reliable method for measuring mouse visual acuity by tracking head and neck movements in response to gratings projected on a virtual cylinder. Acuity is quantified by increasing the spatial frequency of the grating until a tracking response can no longer be elicited. OKT measurements of aging *Cln3*$^{\Delta ex7-8}$ and age-matched wild type mice were done every two

months starting at one month of age until 18 months. (Fig. 8) Wild type mice maintained normal OKT thresholds between 0.27 and 0.3 c/d (cycles per degree) at all ages measured. *Cln3*$^{\Delta ex7-8}$ mice had relatively normal OKT thresholds until 12 months of age, with slight decline starting at nine months of age. Past 12 months, OKT thresholds declined faster until 0.4 c/d at 18 months of age, indicating almost complete loss of vision. Due to the individual nature of the disease, the standard deviation was variable at each measured time point. These results indicate *Cln3*$^{\Delta ex7-8}$ mice suffer from progressive visual failure which is accelerated past 12 months of age.

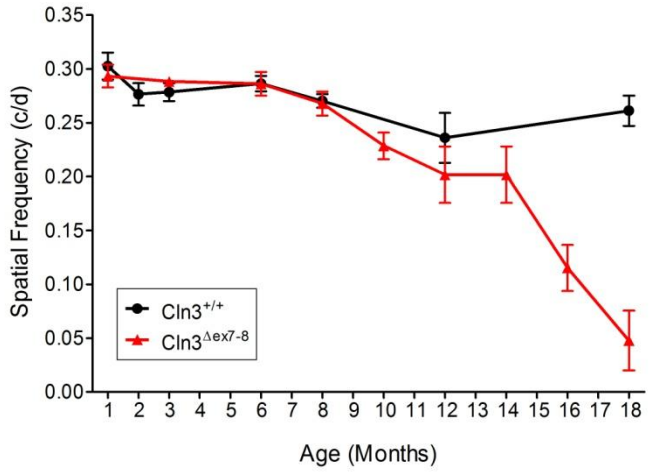

Figure 7. Optokinetic tracking measurement of visual acuity using the OptoMotor system in *Cln3*$^{\Delta ex7-8}$ and wild type mice. Changes in optokinetic tracking thresholds (cycles/degree) is plotted against age in months representing temporal change in visual acuity for both wild type and *Cln3*$^{\Delta ex7-8}$ mice. Mean value ± SD is shown. n= 5-9

4.1.2.2 Electroretinograms Measurements of Photoreceptors and Inner Retina

ERG experiments and data analysis were performed by Dr. med Cornelia Volz and Prof Dr. med. Herbert Jägle from the University Eye Clinic Regensburg. ERG measurements were performed on dark adapted (scoptopic) *Cln3*$^{\Delta ex7-8}$ and wild type mice at 6, 12 and 18 months of age (Fig. 9). Rod photoreceptor function was measured by the amplitude and implicit time of the leading trough of the response wave (a-wave) whereas the inner retinal function was measured by amplitude and implicit time of the positive peak wave (b-wave). At 6 months of age, both wild type and *Cln3*$^{\Delta ex7-8}$ mice had relatively similar a- and b-wave measurements (Fig. 9 A). At 12 months, the a-wave of the *Cln3*$^{\Delta ex7-8}$ mice had a lower negative drop compared to age-matched wild types, indicating decreased photoreceptor function. The b-wave in these mice also had a decreased positive amplitude, indicating a degeneration in the inner retinal cells. These differences were most striking at high flash intensities. Noteworthy, the decreased measurements of the b-wave was greater than the a-wave indicating a larger change in the inner retina compared to photoreceptors. 18 month

Cln3$^{\Delta ex7-8}$ mice showed further degeneration of the a-wave which became obvious at high flash intensity. In contrast, the b-wave of these mice was severely decrease in amplitude at all flash intensities, indicating severe degeneration of the inner retinal function. There was no difference in implicit time between wild type and *Cln3*$^{\Delta ex7-8}$ mice at 6 and 12 months of age (Fig. 9 B). At 18 month, the *Cln3*$^{\Delta ex7-8}$ a-wave implicit time was longer at most flash intensities compared to wild type. A graph plotting the b-/a-wave ratio (Fig. 9 C) highlights the lowered b-/a-wave ratio of *Cln3*$^{\Delta ex7-8}$ mice compared to wild type starting at 12 months of age, indicative of greater degeneration in the b-wave compared a-wave.

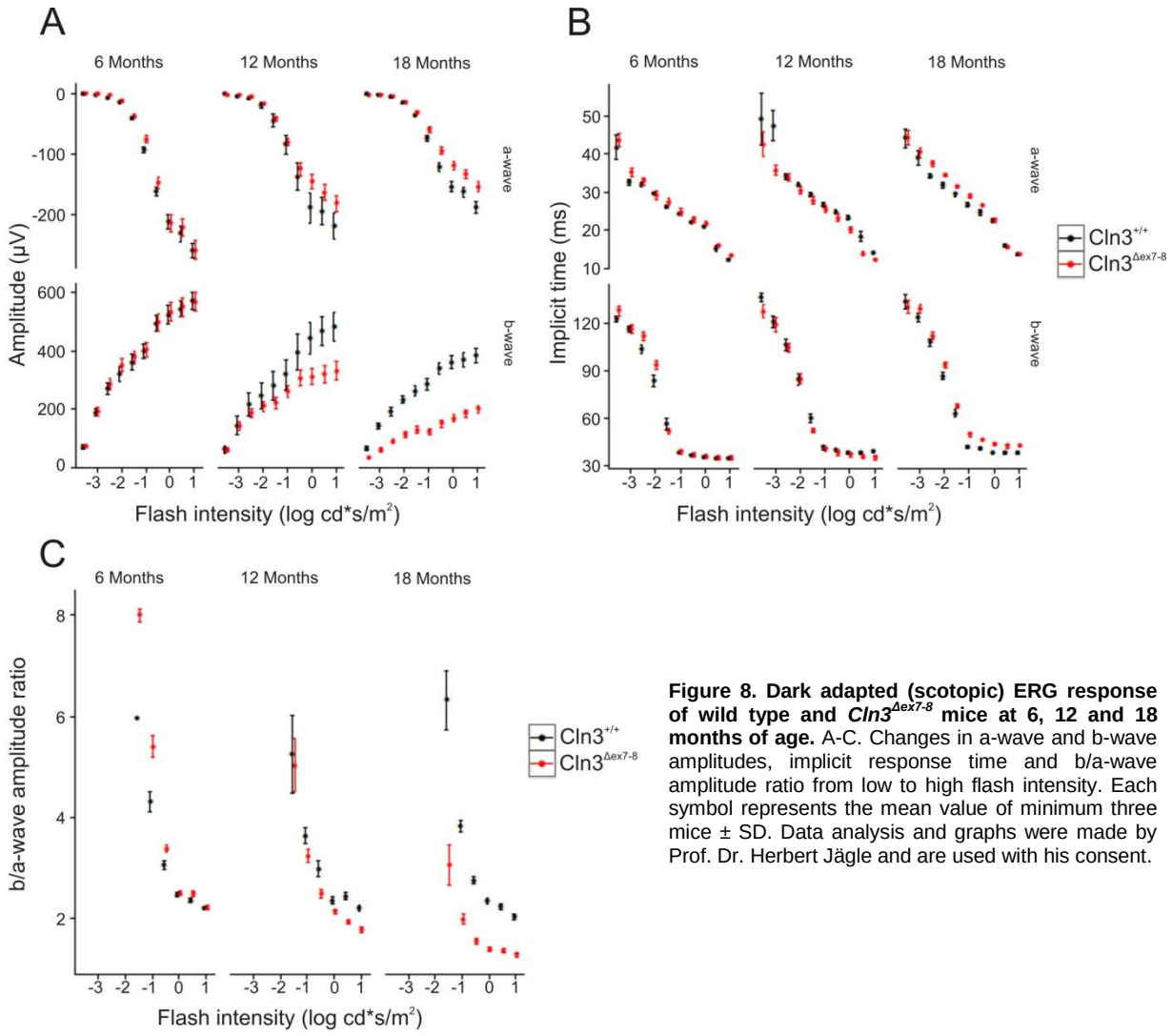

Figure 8. Dark adapted (scotopic) ERG response of wild type and *Cln3*$^{\Delta ex7-8}$ mice at 6, 12 and 18 months of age. A-C. Changes in a-wave and b-wave amplitudes, implicit response time and b/a-wave amplitude ratio from low to high flash intensity. Each symbol represents the mean value of minimum three mice ± SD. Data analysis and graphs were made by Prof. Dr. Herbert Jägle and are used with his consent.

Interestingly, the aging wild type also show a change in a- and b-wave amplitude as they age. Amplitudes decrease by one third from 6 months to 18 months, which is too high to be attributed to aging. Upon further speculation, this decrease was attributed to the presence of the *Crb1*^{rd8} mutation (section 4.1.3).

4.1.3 *CRB*^{rd8} Mutation present in the *Cln3*$^{\Delta ex7-8}$ and Wild Type Background

Mattapallil et al. reported the existence of the *Crb1*^{rd8} mutation in the C57BL/6N genetic background, which could confound retinal function studies in transgenic mouse models established on that background (Mattapallil et al., 2012). The *Cln3*$^{\Delta ex7-8}$ and corresponding wild types were all of the C57BL/6N background and all tested positive for the *Crb1*^{rd8} mutation via sequencing.

4.1.4 End of *Cln3*$^{\Delta ex7-8}$ Study

Due to the presence of the *Crb1*^{rd8} mutation as well as the lack of morphological degeneration and early microglia activation, further studies on the *Cln3*$^{\Delta ex7-8}$ mouse model were discontinued.

4.2 Characterization of the *Cln6*^{nclf} Retina

The second NCL model studied was the *Cln6*^{nclf} mouse model. Localized microglia and astrocyte activation were previously reported in brain studies done on CLN6 mutant sheep model (Oswald et al., 2005) and *Cln6*^{nclf} mouse model (Bronson et al., 1998; Thelen et al., 2012). Initial studies done by Bronson et al. also showed severe retinal degeneration in the *Cln6*^{nclf} mouse model starting at four months with complete loss of retina by nine months (Bronson et al., 1998). The role microglia, Müller cells and inflammation play in this degeneration have not previously been studied. Of note, *Cln6*^{nclf} and corresponding wild types were tested negative for *Crb1*^{rd8} mutation.

4.2.1 Morphological Characterization of the *Cln6*^{nclf} Retina

Temporal retinal degeneration and glial activation in *Cln6*^{nclf} mice was studied at different ages, starting at one month and ending at eight months of age. Histological changes in retina were analyzed using a fuchsin/methylene blue dye on 1 µm thick sections (Fig. 10). Retinal sections showed a progressive degeneration of all retinal layers in *Cln6*^{nclf} mice compared to wild-type

controls starting at four months (Fig. 10 A). At eight months of age, the photoreceptor cell layer in particular was heavily compromised in *Cln6*^{nclf} retinas with only a few rows of cell nuclei remaining.

Next, the glial status in the retina was assessed. Müller glia cells were detected using GFAP as a marker (Fig. 10 B). Wild type eight month old mice had some filamentous but mostly end-feet GFAP staining associated with normal aging retinas. One month old *Cln6*^{nclf} mice showed increase GFAP staining which became more intense by four months onwards . Increased GFAP expression at early ages in *Cln6*^{nclf} mice indicates reactive Müller cell gliosis as a prominent early event in retinal degeneration.

Retinal sections were also stained with the microglia marker Iba1 to assess changes in microglial morphology and migration into different layers (Fig. 10 C). Wild type microglial cells were seen in a non-alert ramified form in the IPL and OPL. In contrast, one month old *Cln6*^{nclf} retinas already had amoeboid microglia cells with protrusions reaching into the nuclear cell layers. At four, six and eight months of age, bloated microglia infiltrating the nuclear layers could be detected, indicating fully alert and active microglia. Lipofuscin deposits were seen in photoreceptor and inner-retinal layers as early as one month in *Cln6*^{nclf} mice and increased in number with age (Fig. 10 D). Alert phagocytic microglial cells often co-localized with auto-fluorescent lipofuscin deposits suggesting phagocytoses of large amounts of auto-fluorescent material (Fig. 10 E, arrowheads). To further confirm the morphological transition of ramified microglia cells into large phagocytes, retinal flat-mounts were stained with Iba1 (Fig 10 F). Retinal flat-mounts from wild-type mice displayed a highly ramified microglia network. In contrast, one month old *Cln6*^{nclf} retinas already showed a mixed population of ramified and phagocytic microglia. As the mice aged, the cells became rounder in shape with shorter protrusions, indicating a loss of the ramified network structure and an alerted state.

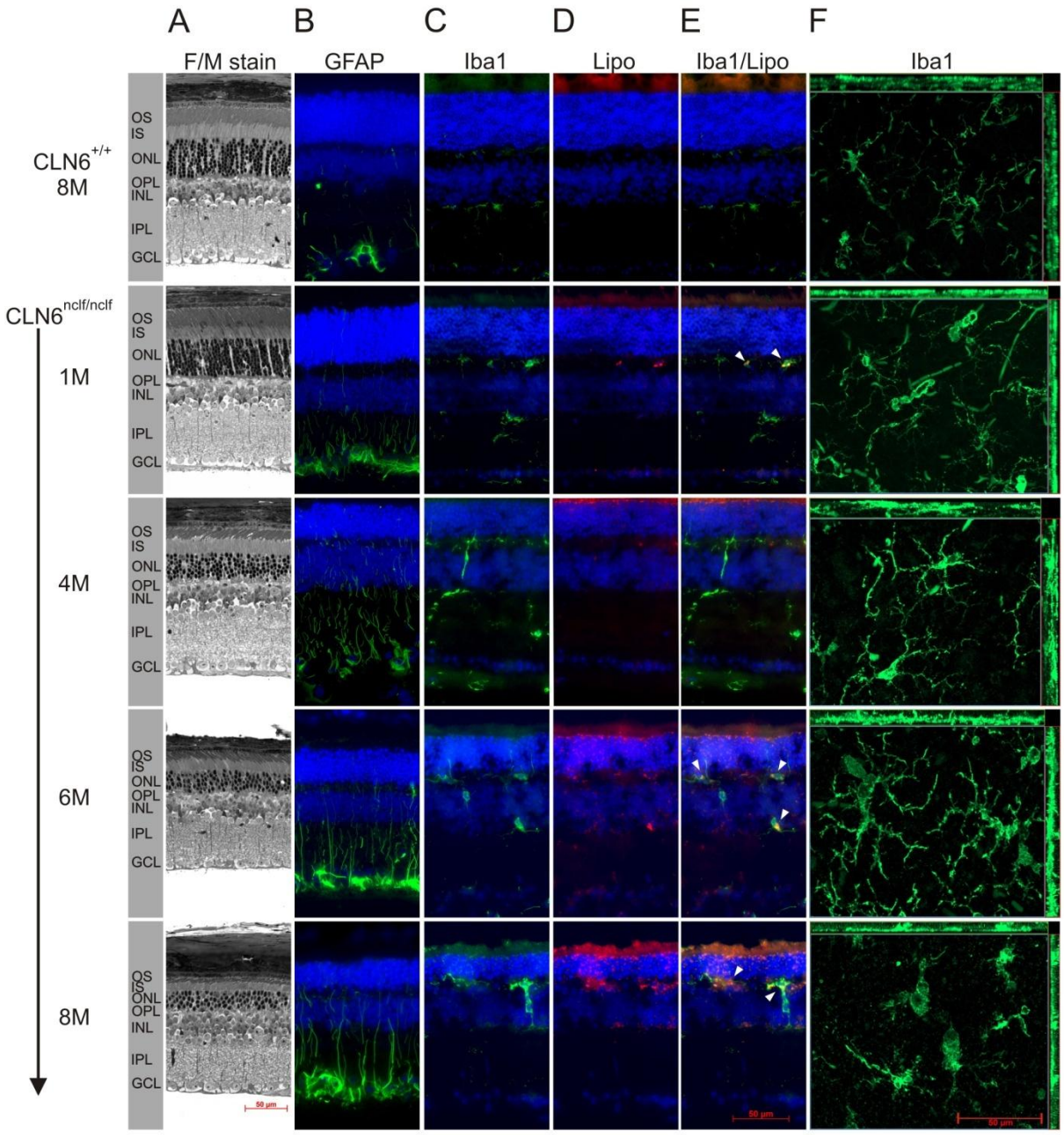

Figure 9. Histological and immunohistological characterization of wild type and aging *Cln6*^{nclf} mouse retina. A. Histological changes in retina sections from 8 month old wild type mice compared to 1,4,6 and 8 month old *Cln6*^{nclf} mice using fuchsin/methylene (F/M) blue staining. B. Immunolabelling of reactive Müller cells in wild type and aging *Cln6*^{nclf} retinas using anti-GFAP antibody. C. Staining of microglial cells in anti-Iba1 antibody. D. Auto-Fluorescent lipofuscin accumulation in wild type and *Cln6*^{nclf} retinas. E. Merged images of anti-Iba immunolabelling with auto-fluorescent lipofuscin deposits. White arrowheads indicate co-localization of lipofuscin with microglial cells. F. Anti-Iba1 labelled retinal flat-mount reveal different microglial morphologies in wild type and *Cln6*^{nclf} retinas. The thickness of the flat-mount is indicated on the sides of the images. OS, outer segments; IS, inner segments; OPL, outer plexiform layer; INL, inner nuclear layer; IPL, inner plexiform layer; GCL, ganglion cell layer. Scale bar, 50 µm.

4.2.2 Quantification of Retinal Degeneration

Histological experiments done on *Cln6*^{nclf} retinas showed progressive degeneration of cell layers, however the rate of cell death and which layers (if any) were more affected was unclear. TUNEL assays were performed to assess and quantify in which layers cell death was occurring. Retinal morphometry experiments were done to quantify shrinking of total retinal and photoreceptor thickness.

4.2.2.1 TUNEL Assay

TUNEL assays identify which cells are undergoing apoptosis by labeling fragmented DNA strands. Cross-sections from six month old wild type as well as one and six month old *Cln6*^{nclf} retinas underwent TUNEL reaction and the labeled cells visualized (Fig. 11). Wild type retinas had only a few TUNEL positive cells. One and six month *Cln6*^{nclf} retinas, showed numerous but equal number of TUNEL positive cells located mostly in the ONL. Since *Cln6*^{nclf} retinal degeneration is progressive, cells are constantly undergoing apoptosis, which is why approximately the same number of cells can be identified by TUNEL assay at any given time. For this reason, TUNEL positive cells were not quantified.

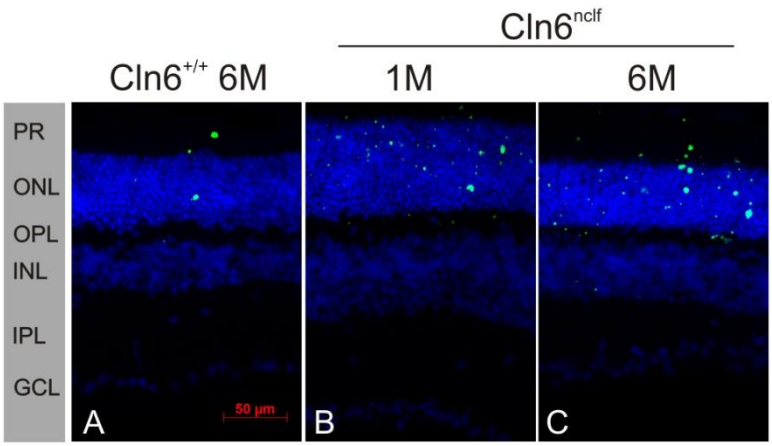

Figure 10. TUNEL stains of *Cln6*$^{+/+}$ and *Cln6*^{nclf} retinas. Apoptotic cells in the retina were detected using *in situ* detection of fragmented DNA strands (TUNEL assay). A-C. TUNNEL stain of 6 month old wild type retinas were compared to 1 and 6 month old *Cln6*^{nclf} retinas. PR, photoreceptors; ONL, outer nuclear layer; OPL, outer plexiform layer; INL, inner nuclear layer; IPL, inner plexiform layer; GCL, ganglion cell layer. Scale bar, 50µM

4.2.2.2 Retinal Morphometry

As an alternative method of quantifying progressive cell death, retinal morphometric analyses was performed. This method allows measurement of total or specific cell layers of the retina making it possible to evaluate the progression of cell death as well shrinking of specific layers. Morphometric analysis were performed on 1 µm thick retinal sections previously embedded in Epon. Whole retina and photoreceptor membrane thickness of one, four, six and eight month old *Cln6*^{nclf} and wild type mice were measured (Fig 12). Whole retinal measurements indicated changes already occurred in the central retina of one month old *Cln6*^{nclf} mice and this effect steadily increased with disease progression throughout the whole retina (Fig. 12 A). Measuring the Outer and Inner Segment (OS and IS, respectively) of the photoreceptors showed a drastic decrease in thickness between four and six months, contrary to the steady decrease seen in total retinal thickness (Fig. 12 B). This marked decrease in photoreceptor membrane thickness coincides with the time point when microglia markedly changed their phenotype.

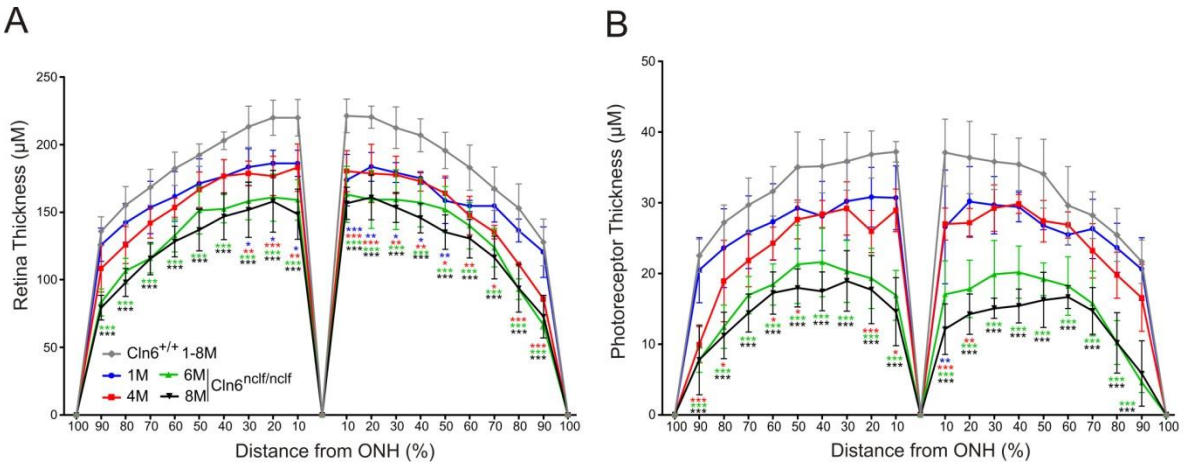

Figure 11. Retinal morphometry measurements of *Cln6*$^{+/+}$ and *Cln6*^{nclf} whole retina and photoreceptor membrane. Anterior and posterior retinal areas were divided into ten sections using the optic nerve head as a central reference. The thickness of total retina and outer/inner segment of photoreceptors was measured and plotted. A. Quantification of whole retinal thickness of *Cln6*^{nclf} retinas compared to wild type controls. B. Quantification of photoreceptor layer thickness compared to wild type control. The mean value ± SD is plotted. n=4 animals per age group. *Cln6*^{nclf} measurements were statistically compared to age-matched controls using two-way ANOVA followed by Bonferroni post-test. *$p < 0.05$; **$p < 0.01$; ***$p < 0.001$.

4.2.3 Behavioural and Functional Characterization of the *Cln6^{nclf}* Retina and Mouse Model

Functional retinal studies to understand the depth of retinal degeneration in the *Cln6^{nclf}* model were done using OKT and ERGs. Furthermore, possible motor problems exhibited by the *Cln6^{nclf}* mice which could interfere with OKT measurements were also assessed using Rotarod measurements.

4.2.3.1 Optokinetic Tracking

OKT measurements using an OptoMotor system were done on wild type and *Cln6^{nclf}* mice monthly, starting at one month of age and ending at eight months of age (Fig. 13). Wild-type mice had a relatively stable maximal OKT threshold at 0.3 c/d. *Cln6^{nclf}* mice also showed normal OKT thresholds up to four months of age which declined slowly, but not significantly. However, starting at five months of age, *Cln6^{nclf}* mice appeared to have a significant and rapid decline in OKT thresholds with 0.05 c/d by eight months of age. The large variability of OKT thresholds in older animals most likely reflects variable disease progression in *Cln6^{nclf}* mice.

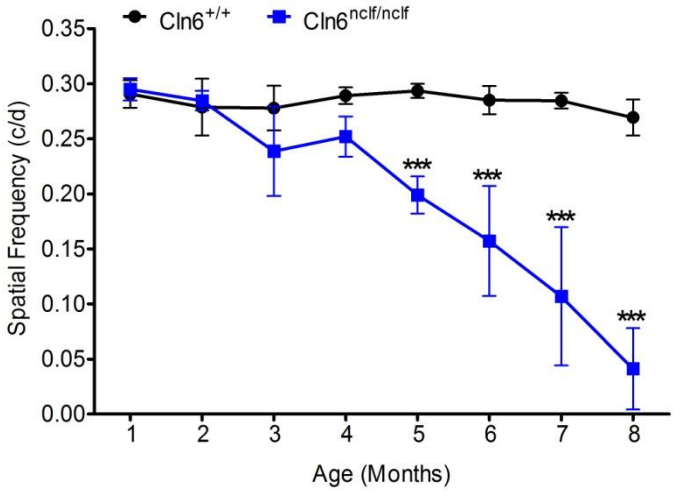

Figure 12. Optokinetic tracking measurement of aging wild type and *Cln6^{nclf}* mice. Mouse visual acuity was measured via OKT in an OptoMotor system. Changes in OKT threshold (cycle/degree) is plotted against age in months. Mean value ± SD is shown. n= 12 animals per age group. *Cln6^{nclf}* measurements were statistically compared to age-matched controls using two-way ANOVA followed by Bonferroni post-test. ****p* <0.001.

4.2.3.2 Rotarod Performance

To clarify if the progressive decline in visual acuity was indeed due to vision loss and not motor-neuron deficits, which could also influence OKT readings, rotarod experiments were performed

(Fig. 14). Mice were subjected to rotarod experiments with three trials per day for two consecutive days. The performances from both days were compared to determine if mice had improved rotarod performance. All mice tested showed a significant improvement on the second day of rotarod testing indicating that they had normal learning abilities. However, contrary to four and six month old mice which all show approximately the same rate of improvement, eight month old *Cln6*^{nclf} mice had a significantly reduced improvement rate compared to age-matched wild type mice. This indicates that older *Cln6*^{nclf} mice have a reduced cognitive function and/or motor impairment. It has been previously reported that these mice start having motor problems at approximately eight months of age (Bronson et al., 1998). These results indicate that the decrease in OKT measurements from four to six months seen in the *Cln6*^{nclf} mice is indeed due to a loss of visual acuity and is most likely not affected by motor problems.

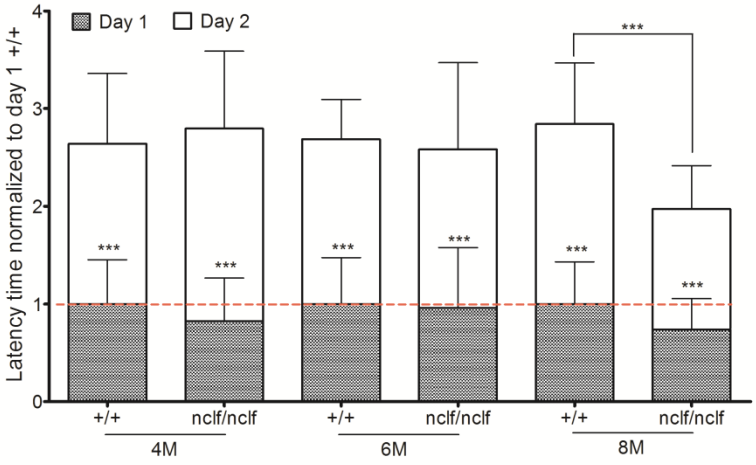

Figure 13. Rotarod performance of wild type and *Cln6*^{nclf} mice aged 4, 6 and 8 months. Mouse rotarod performance was tested three times on two subsequent days (Day 1 and 2). The average performance of wild type mice on day 2 along with *Cln6*^{nclf} performance on both days were normalized to wild type performance on day 1. Statistical changes in performance from day 1 to 2 for each group along with day dependent differences between control and *Cln6*^{nclf} was calculated using Kruskal-Wallis ANOVA. n=6-15 animals per age group. ***p <0.001.

4.2.3.3 ERG Measurements of Retinal Function

ERG experiments were done as mentioned above (section 4.1.2.2) on dark adapted aging CLN6^{nclf} and age-matched wild types (Fig. 15). The a-wave amplitude was significantly decreased in one month *Cln6*^{nclf} mice at most flash intensities and progressively decreased until eight months where almost no response is recorded (Fig. 15 A). B-wave amplitudes significantly differ from age-matched controls starting at three months with very little response present at eight months. Wild type mice showed a normal mild decrease in both a- and b-wave amplitudes with age. The implicit time was not significantly different at most ages compared to controls and was slightly higher in eight month old *Cln6*^{nclf} mice in both the a- and b-wave (Fig. 15 B). Lastly, the b-/a-wave amplitude

ratio was higher for *Cln6*^{nclf} mice starting at one month of age, indicating an early photoreceptor-dominated degeneration followed by an inner retinal degeneration (Fig. 15 C).

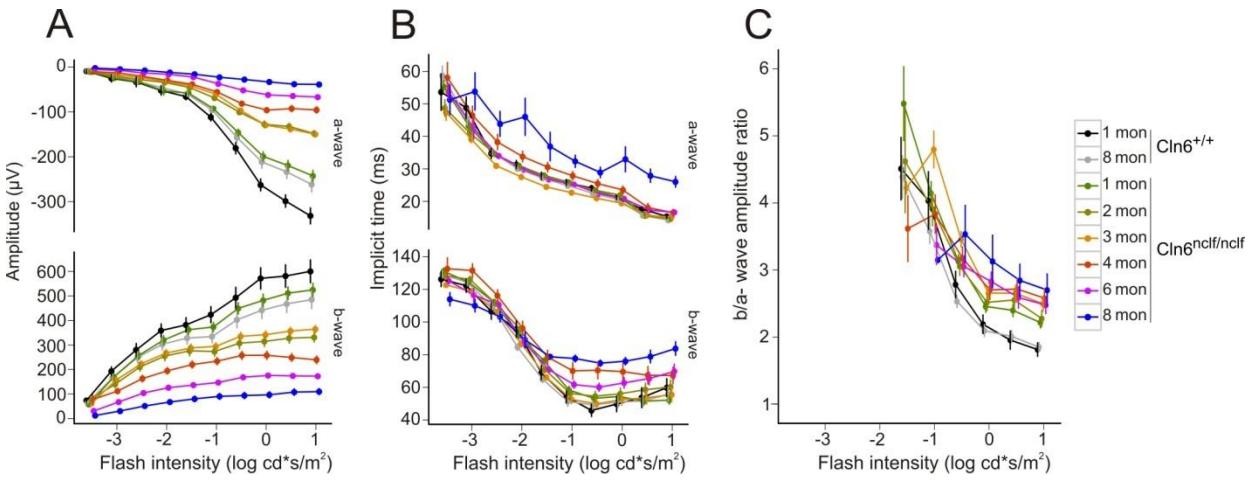

Figure 14. Dark adapted (scotopic) ERG response amplitudes, implicit times and b/a-wave amplitude ratios of age-matched wild type and *Cln6*^{nclf} mice. A-C. Response amplitude of a- and b-wave, implicit response time of a- and b- wave as well as b/a-wave ratio were plotted from low to high intensity for 1 and 8 month old wild type, and *Cln6*^{nclf} mice aged 1 to 8 months. Each symbol represents the mean of three animals ± SEM. For the brightest flash intensity, mean amplitude values of *Cln6*^{nclf} mice and age-matched controls were compared with ANOVA. a-wave: 1 month: p=0.0048, 2 months: p=0.0005, 3 to 8 months: p<0.0001. b-wave: 1 month: p=0.245, 2 months: p=0.059, 3 to 8 months: p<0.0001. Data analysis and graphs were made by Prof. Dr. Herbert Jägle and are used with his consent.

4.2.4 Transcriptional Changes in Stress and Inflammatory Gene Markers in the *Cln6*^{nclf} Retina

Quantitative real-time RT-PCR was used to identify whether progressive retinal degeneration in *Cln6*^{nclf} mice is connected with cell death, stress response and inflammation. Whole retina from aging *Cln6*^{nclf} mice and age-matched wild types (ages one to eight months) were examined for transcriptional marker expression changes (Fig 16). Experiments were carried out in duplicates and analyzed using ΔΔCT relative quantification. Age-matched wild types were used as calibrators and adenosine triphosphatase (ATPase) as a reference.

First, NCLF mRNA levels were determined to study a potential nonsense-mediated decay of mutant mRNA. At all analyzed time points, NCLF transcript levels were significantly reduced in *Cln6*^{nclf} retinas (Fig. 16 A), indicating that ER-stress pathways could be active in mutant cells. At all ages tested, *Cln6*^{nclf} retinas had half the amount of NCLF mRNA compared to wild type. Next, apoptotic and inflammatory markers were studied via CD95 and tumor necrosis factor-alpha (TNFα),

respectively. CD95 expression (also known as Fas receptor) was increased six to seven fold at one and six months in *Cln6*^{nclf} retinas (Fig. 16 B). At other ages, CD95 expression was on average two fold higher in *Cln6*^{nclf} retinas but was not determined to be significant. TNFα had increased expression at all aged test but was significantly increased at eight months (Fig. 16 C). GFAP mRNA levels, expressed by reactive Müller cells, were increased five to ten fold in *Cln6*^{nclf} mice at all ages, correlating to the immunohistochemical experiments shown above (Fig. 16 D). Photoreceptor stress marker, endothelin 2 (EDN2) was strongly up-regulated in *Cln6*^{nclf} retinas at all ages, indicating a prominent stress response at all ages (Fig 16 E). Next, classical microglia markers: CD68, early growth response 1 (EGR1) and complement C1q subunit a (C1qa) were assessed. CD68 expression was significantly higher in one and six month old *Cln6*^{nclf} with approximately two-fold increased expression at other ages (Fig. 16 F). EGR1 transcript levels were increase four to five fold between one and three month of age with expression levels increasing to 12-fold and higher starting at four months in *Cln6*^{nclf} retinas (Fig. 16 G). Finally, C1qa expression levels were significantly increased at all ages (Fig. 16 H). These experiments suggest that retinal degeneration in *Cln6*^{nclf} retinas follows a temporally ordered sequence of very early cell stress associated with increased immune response.

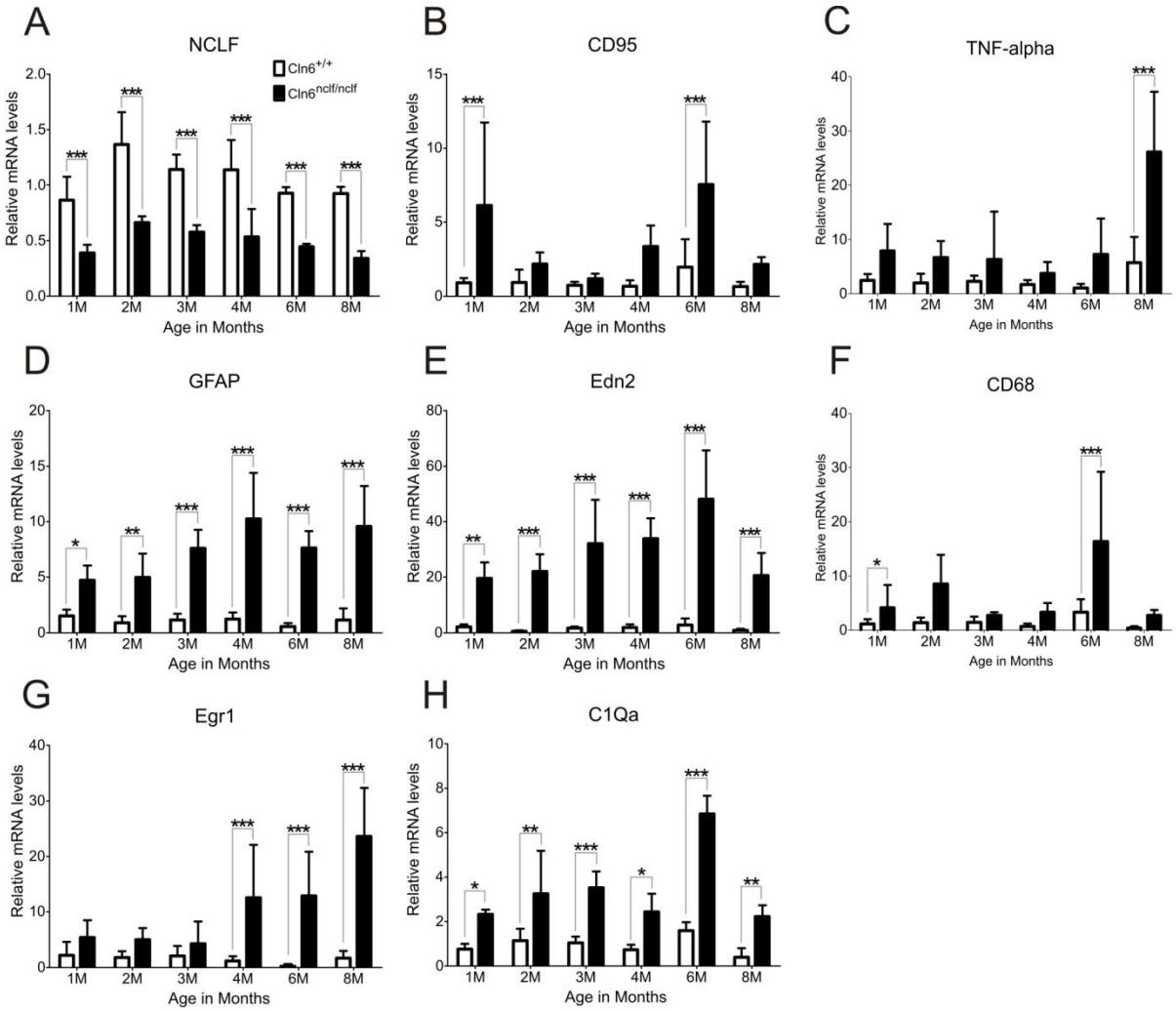

Figure 15. Quantitative real-time RT-PCR expression analysis of *Cln6*^{nclf} retinas compared to age-matched wild type controls. Relative mRNA levels were analyzed for NCLF (A), CD95 (B), TNFα (C), GFAP (D), EDN2 (E), CD68 (F), EGR1 (G) and C1Qa (H). mRNA expression was normalized to the reference gene Atp5b and graphed relative to age-matched wild-type (± SD). n=7-10 animals per age. Age-matched expression was compared using two-way ANOVA followed by Bonferroni post test. *$p < 0.05$; **$p < 0.01$; ***$p < 0.001$.

4.3 CLN6^{nclf} Dietary Supplementation Study

Numerous studies show natural dietary compounds are able to target microglial pathways reducing inflammatory processes whilst simultaneously supporting neuronal survival. Based on *in vivo* and *in vitro* studies which showed significant changes in microglia transcription profile, attenuation of activated microglia and decreased neuronal degeneration, three natural compounds were selected for this supplementation study: curcumin, luteolin and docosahexaenoic acid (DHA). *Cln6*^{nclf} mice received standard chow or chow supplemented with 0.6% curcumin, 0.6% luteolin or 5% DHA for thirty weeks directly after weaning (post natal day 21-23). The study ended when the

mice were seven months old. Mice were weighed weekly to ensure proper and comparable development (Fig. 17).

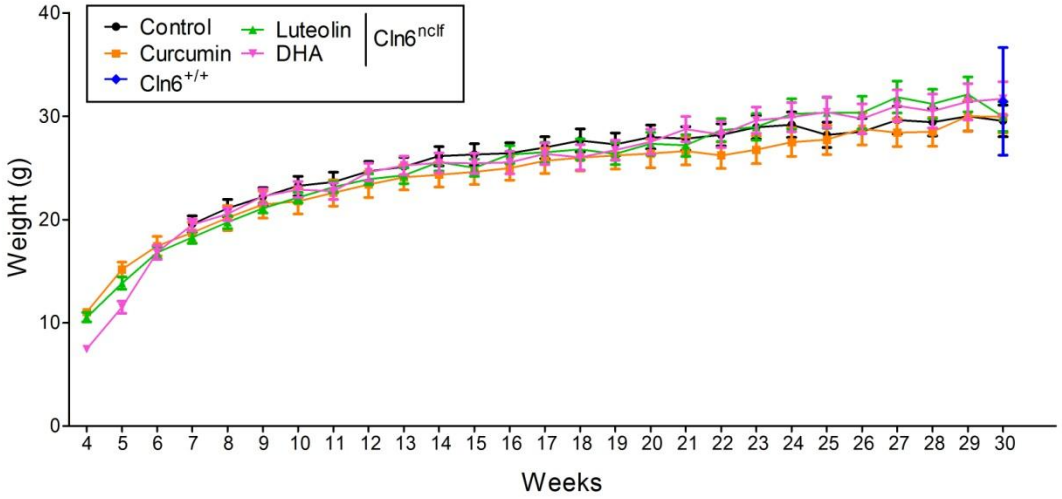

Figure 16. Weekly body weight of control-fed and supplemented mice. Wild type body weight is plotted only at 30 weeks. n=12 animals per group.

4.3.1 Supplementation effect on *Cln6*^{nclf} Retinal Histology and Microglia

Histological comparison of control-fed and supplemented retinas were done as previously described (section 4.2.1) (Fig. 18). Supplemented retinas had generally better preserved photoreceptor and ONL thickness (Fig. 18 A). The OS of the photoreceptor layers appeared to be thicker compared to control retinas, particularly in DHA supplemented retinas. The ONL of control retinas comprised of 4 cell layers compared to the 5-6 layers found in curcumin and luteolin supplemented retinas and 7-8 layers in DHA supplemented retinas. GFAP staining revealed the presence of reactive Müller cells in all retinas (Fig. 18 B). The shape and location of microglia as seen by Iba1 staining as well as auto-fluorescent lipofuscin deposits were also comparable in control-fed and supplemented mice (Fig. 18 C, D). Retinal flat-mounts stained with Iba1 as a method for analyzing microglial morphology revealed different microglial phenotype between control and supplemented retinas (Fig. 18 F). Amoeboid microglia with almost not ramifications were observed in control retinas, whilst curcumin, luteolin and DHA supplemented retinas had highly ramified microglia within an intact network.

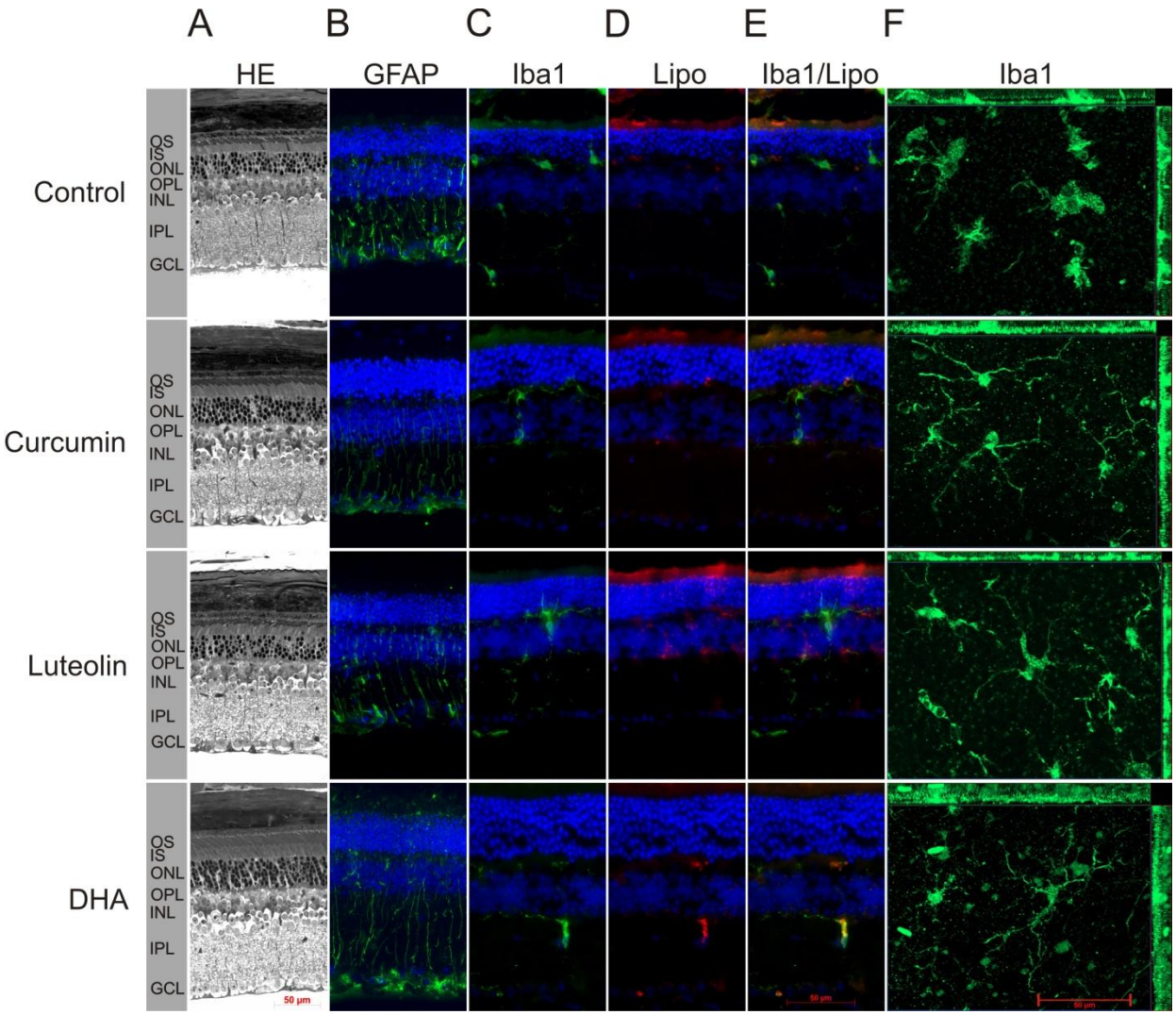

Figure 17. Histological and immunohistological comparison of control-fed mice supplemented with 0.6% curcumin, 0.6% luteolin and 5% DHA. A. Histological comparison of control animals and supplemented retinas using fuchsin/methylene blue stain. B. Immunolabelling of Müller cells with anti-GFAP antibody C. Staining of microglial cells with anti-Iba1 antibody. D. Auto-fluorescent lipofuscin accumulation in wild type and *Cln6*^{nclf} retinas. E. Merged images of anti-Iba1 immunolabelling with auto-fluorescent lipofuscin deposits. F. Anti-Iba1 labeled retinal flat mounts reveal ramified microglia compared to control retinas. The thickness of the flat-mount is indicated on the sides of the image. OS, outer segments; IS, inner segments; OPL, outer plexiform layer; INL, inner nuclear layer; IPL, inner plexiform layer; GCL, ganglion cell layer. Scale bar, 50 µm.

4.3.2 Retinal Morphometry of Supplemented Retinas

Histological analysis revealed a better preserved retinal morphology in supplemented retinas compared to control. These findings were verified by quantifying the OS and IS length of photoreceptors and total retinal thickness using morphometric analysis (Fig. 19). Both curcumin and luteolin supplemented retinas had approximately the same total retinal thickness and slightly increase photoreceptor thickness which was not significant compared to controls. In contrast, DHA

supplemented mice had non-significant increase in total retinal thickness and a significant increase in photoreceptor thickness.

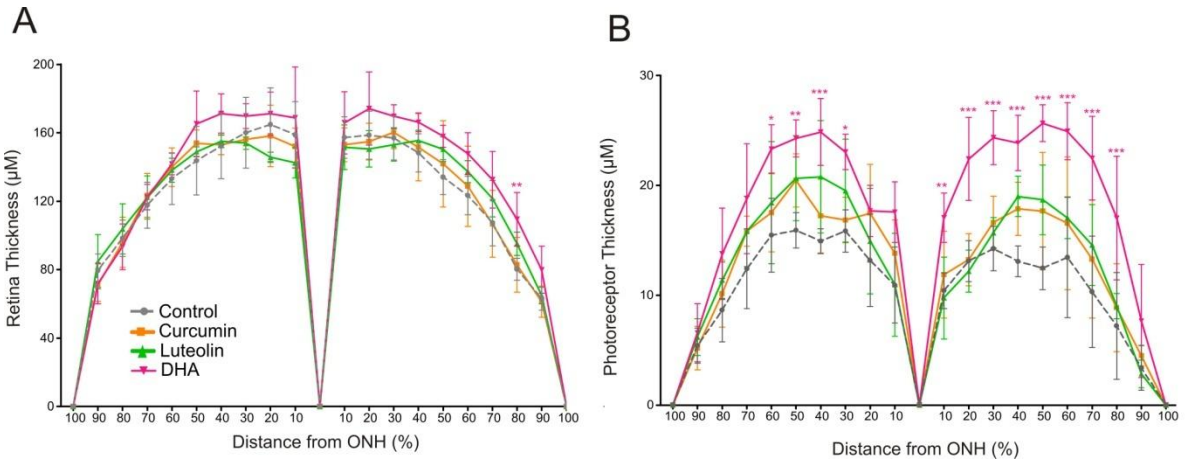

Figure 18. Retinal morphometry measurements of total retina and photoreceptor membrane layer. Anterior and posterior retinal areas were divided into ten sections using the optic nerve head as a central reference. The thickness of total retina and outer/inner segment of photoreceptors was measured and plotted. A. Quantification of whole retinal thickness of curcumin, luteolin and DHA-supplemented versus control retinas. B. Quantification of the photoreceptor layer. Mean value ± SD is plotted. Supplemented groups were compared to control using two-way ANOVA followed by Bonferroni post-test. n= 5 animals per group. **p*< 0.05; ***p*< 0.01; ****p*< 0.001

4.3.3 Retinal Function of Supplemented Retinas

Although supplementation was shown to have some effects on preserving retinal morphology as well as attenuating microglial morphology, whether these effects translated to better vision remained unclear. Thus, OKT and ERG measurements were performed.

4.3.3.1 OKT Measurements of Supplemented Retinas

OKT measurements of both control and supplemented *Cln6*^{nclf} mice were done monthly (Fig. 20). As seen previously, non-supplemented *Cln6*^{nclf} mice had slight decrease in visual acuity up to four months of age after which decline became more rapid. By seven months, control mice have an OKT threshold of 0.06 c/d. Mice supplemented with curcumin and DHA both had higher visual acuity compared to control mice starting at three months of age onwards. At seven months, curcumin supplemented mice had an OKT threshold of 0.156 c/d whereas DHA had an OKT threshold of 0.139 c/d. Luteolin supplemented mice had uneven OKT measurements until four months of age after which thresholds became significantly better than controls. At seven month, mice had an average OKT threshold of 0.19 c/d.

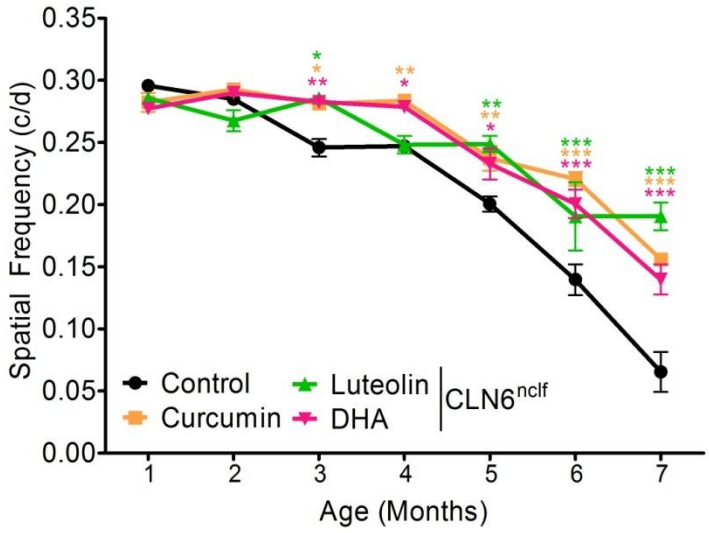

Figure 19. Optokinetic tracking of control and supplemented mice. Visual acuity of control and supplemented mice was measured monthly. Changes in OKT threshold (cycle/degree) is plotted against age in months Mean value ± SD is shown. n= 12 animals per age group. Supplemented measurements were statistically compared to controls using two-way ANOVA followed by Bonferroni post-test. **p*< 0.05; ***p*< 0.01; ****p*< 0.001

4.3.3.2 ERGs of Supplemented Retinas

ERGs were done on dark adapted seven month old control and supplemented mice (Fig. 21). A-wave amplitudes were increased in all supplemented retinas at higher flash intensities compared to control. Amplitudes difference were significant in curcumin and DHA supplemented retinas at highest flash intensity. B-wave amplitudes were also increased for all supplemented retinas compared to control and were also considered significant at highest flash intensity. These data indicate a preservation of both the photoreceptor and inner-retinal function. Curcumin and luteolin supplemented retinas had similar a- and b-wave implicit time compared to control retinas. In contrast, DHA supplemented retinas had shorter implicit time for both a-and b-wave at higher flash intensities, which is consist with less severe retinal degeneration. The b/a-wave ratio of both luteolin and curcumin supplemented retinas was similar to control retinas. DHA supplemented retinas had lower b/a-wave ratio at higher flash intensities, indicating a stronger change in the a-wave compared to b-wave.

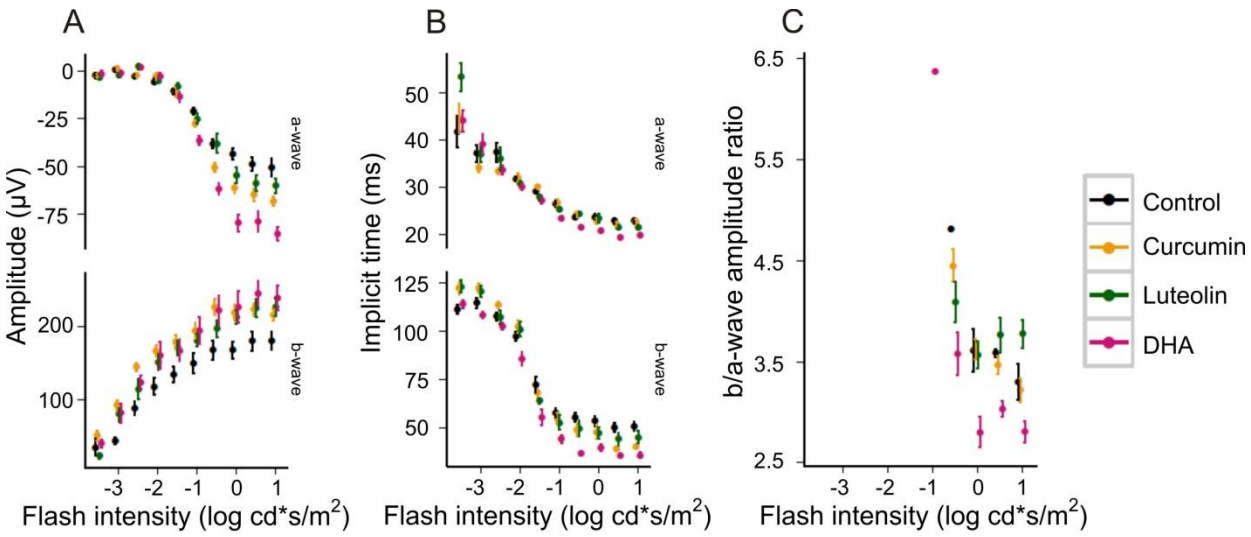

Figure 20. Dark adapted ERG response amplitude, implicit time and b/a-wave amplitude ratio of age-matched *Cln6*^{nclf} control and supplemented mice. A-C. Response amplitude of a- and b-wave, implicit response time of a- and b- wave as well as b/a-wave ratio were plotted from low to high intensity for control and curcumin, luteolin, DHA-supplemented mice at seven months of age. Each symbol represents the mean of 6 animals ± SEM. Statistical comparison of supplemented response vs. control response was done using two-way ANOVA for the amplitudes of the highest flash intensity. Amplitude: a-wave: p=0.002, p= 0.128 and p<0.0001, b-wave: p=0.028, p=0.0147 p=0.009 for curcumin, luteolin and DHA, respectively. Implicit time: a-wave: p=0.77, p=0.0983 and p=0.0002, b-wave: p=0.0004, p=0.159 and p<0.0001 for curcumin, luteolin and DHA, respectively. Data analysis and graphs were made by Prof. Dr. Herbert Jägle and are used with his consent.

4.3.4 Transcriptional changes affected by Supplementation

Quantitative real-time RT-PCR comparing whole supplemented retinas to non-fed retinas were done as previously described (section 4.2.4) (Fig. 22). Seven month wild type retinas were also included and compared to non-fed retinas as an additional experimental control. Markers related to stress, inflammation and apoptosis were analyzed.

First, mRNA levels of NCLF were analyzed to see if supplementation effected non-sense mediated decay (Fig. 22 A). Supplemented retinas had approximately the same level of NCLF expression as control retinas. Wild types retinas had approximately two-fold NCLF expression, in concordance to experiments done in section 4.2.4. Apoptosis marker, caspase 8 was significantly reduced in DHA supplemented and wild type retinas compared to non-fed retinas (Fig. 22 B). A similar profile was also seen for CD95 (Fig. 22 C). Reactive Müller cell marker, GFAP, was also significantly reduced in DHA supplemented and wild type retinas (Fig. 22 D). This is in contrast to the immunohistochemical staining seen above (Fig. 18 B). However, it is possible that the GFAP antibody is sensitive enough to detect slightest increase in GFAP expression. END2 expression remained the same for supplemented retinas and control with significantly lowered expression in wild type retinas (Fig. 22 E).

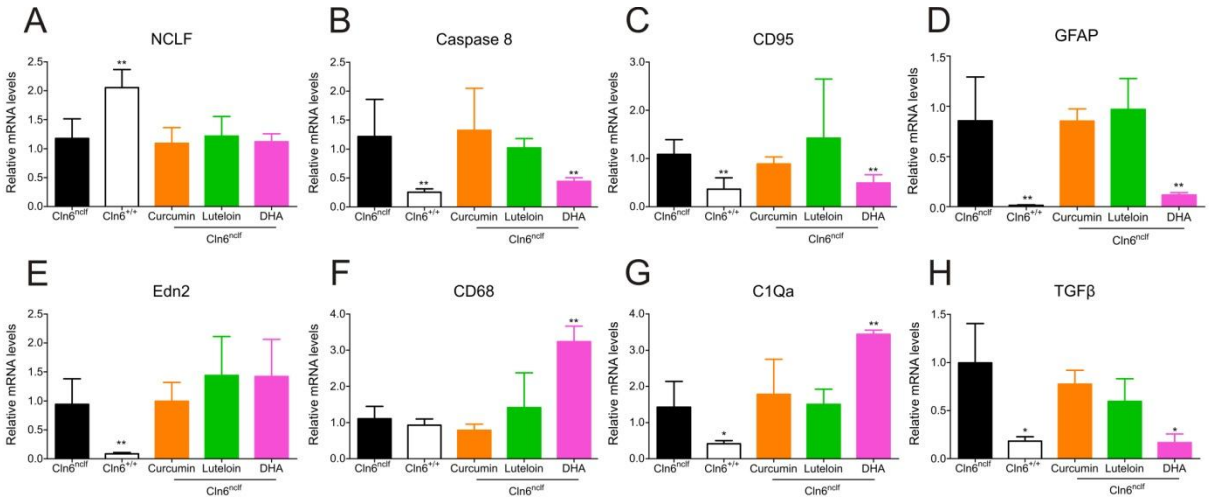

Figure 21. Quantitative real-time RT-PCR expression analysis of curcumin, luteolin, DHA-supplemented retinas compared to control. Relative mRNA levels were analyzed for NCLF (A), Caspase 8 (B), CD95 (C), GFAP (D), EDN2 (E), CD68 (F), C1Qa (G) and TGFβ (H). Supplemented and wild type mRNA expression was normalized to the reference gene Atp5b and graphed relative to control expression (± SD). n= 5 animals per age. Age-matched expression was compared using one-way ANOVA followed by Bonferroni post test. *$p < 0.05$; **$p < 0.01$; ***$p < 0.001$.

Classical microglia marker CD68 was significantly increased in DHA supplemented retinas, as was as C1qa (Fig. 22 F, G). As shown before, C1qa levels were significantly decreased in wild type retinas. Finally, Tgfβ1 (Transforming growth factor beta), a marker for alternatively activated microglia associated with tissue repair and neuroprotection was significantly decreased in wild type retinas, as expected, as well as DHA supplemented retinas (Fig. 22 H). These data imply curcumin and luteolin had very little effect at the transcriptional level, whereas DHA supplementation had positive effects on apoptotic markers and mixed effects on microglia marker expression.

5. Discussion

5.1 Comparison of retinal Degeneration in NCL Models

Loss of vision is an early symptom in most forms of human NCL, indicating the retina is highly vulnerable to NCL pathologies (Haltia and Goebel, 2012) However, since patients present vision problems long before neurological symptoms emerge, they are often misdiagnosed with maculopathies (Birch, 1999) leading to a lack of information of how retinal degeneration in NCL progresses or if specific biomarkers are present. As such, naturally occurring and genetically modified animal models of NCL have greatly improved understanding of early disease pathology in patients. In many instances, NCL mice recapitulate typical clinical and histopathological features of patients including vision loss, neuro-motor deficits and storage of ceroid lipofuscin material in lysosomes (Shacka, 2012). Unfortunately, the little research which has been dedicated to studying retinal degeneration in NCL models has led to a large gap in the knowledge of retinal phenotype.

The first part of this thesis focused on characterizing retinal degeneration in two mouse models of NCL: *Cln3*$^{\Delta ex7\text{-}8}$, a model for juvenile NCL, and *Cln6*^{nclf}, a model for late-infantile NCL. Upon initial comparison of both models, it becomes obvious that *Cln6*^{nclf} mice have a far more severe retinal phenotype starting at four months of age compared to the *Cln3*$^{\Delta ex7\text{-}8}$ model which is relatively normal until nine months of age. Histology and morphometry data showed thinning of the nuclear layers in *Cln6*^{nclf} retinas already started at one month of age and progressed until only a few cell layers were present in the ONL. This course of retinal degeneration is principally consistent with preliminary observations of the initial report describing the *nclf* phenotype in the Jackson lab (Bronson et al., 1998). However, data from this study showed degeneration of the outer retina clearly preceded cell death in the inner retina, implicating that photoreceptor cells are very early affected during disease progression. In contrast, *Cln3*$^{\Delta ex7\text{-}8}$ retinas retained cell layers, even at 18 months of age, with no obvious inner or outer retinal degeneration.

Both retinas did show a large accumulation of auto-fluorescent deposits with age. Accumulation of fluorescent storage material has been also reported in the visual cortex and retina of CLN6 mutant sheep and other animal models (Oswald et al., 2005; Katz et al., 2011). In mice, retinal auto-fluorescence has been shown for Ppt1$^{-/-}$ (Lei et al., 2006) and the spontaneous Cln8^{mnd} (*motor neuron degeneration*) mouse model (Seigel et al., 2005). Ppt1$^{-/-}$, a CLN1 mutant mouse model of

infantile NCL, present large amounts of yellow-emitting auto-fluorescent storage bodies from four to eight months of age with mild changes in retinal morphology (Lei et al., 2006). In contrast, retinal auto-fluorescence in Cln8^{mnd} animals is already evident at birth and photoreceptor loss begins at postnatal day 15 (Messer et al., 1993; Seigel et al., 2005). In this regard, Cln8^{mnd} and *Cln6*^{nclf} mice are similar. Accumulation of lipofuscin deposits have also been reported *abcr-/-* mice, a mouse model for Stargardt's disease, a juvenile form of maculopathy (Weng et al., 1999). In this model, the outer segments of the photoreceptor are shortened, as seen in the *Cln6*^{nclf} retina, indicating that accumulation of lipofuscin may cause impairment in the RPE resulting in inability to properly maintain photoreceptor membrane homeostasis (Mata et al., 2001).

OKT measurements of *Cln3*$^{\Delta ex7\text{-}8}$ mice showed slow decline in visual acuity starting at nine months with rapid decline occurring past 12 months of age resulting in severe vision impairment at 18 months. Electroretinogram measurements at six months were normal, at 12 months there was a mild decrease in b-wave response, and at 18 months a significant reduction was seen in both a- and b-wave (photoreceptors and inner retina, respectively). These data are concurrent with OKT measurements. ERG investigations by Staropoli et al. on *Cln3*$^{\Delta ex7\text{-}8}$ mice up to 16 months of age yielded similar results (Staropoli et al., 2012). However, they report virtual no change in a-wave response in 16 month old mice. It is possible a marked drop in the a-wave amplitude occurs between the 16th and 18th month. Similar ERG measurements were also reported in *Cln3*$^{-/-}$ mice (Katz et al., 2008).

In contrast, OKT thresholds and ERGs measurements of *Cln6*^{nclf} mice showed a markedly early impaired retinal function. The ERGs indicated an early photoreceptor-dominated degeneration followed by inner retinal degeneration. Interestingly, ERG responses were already impaired at one month of age, whereas OKT threshold changes were only significant from five months of age onwards. Thus, there was a close concordance of early diminished ERG response with retinal thinning and quantitative cell loss. Of note, the phenomenon of disconcordant electrophysiological and visual behavioral profiles has been recently described in mutant rhodopsin transgenic rats (McGill et al., 2012). Similar to the present study, OKT threshold in rhodopsin transgenic rats did not decline until months after significant photoreceptor loss.

The ERG data obtained from *Cln6*^{nclf} mice is again. similar of the phenotype described in Cln8^{mnd} mice (Chang et al., 1994). The amplitudes of the a- and the b-wave rapidly declined with age and

the ERG was nearly undetectable at six months in *Cln8*^{mnd} mice (Chang et al., 1994). The Ppt1$^{-/-}$ model shows mild reductions in both a- and b-wave at four months but has dramatic changes in ERGs at eight months (Lei et al., 2006). Overall, *Cln3*$^{\Delta ex7-8}$ mice have the latest and mildest form of retinal degeneration when compared to other NCL models studied.

Comparative analysis of retinal degeneration in the NCL models is, however, confounded with the recent discovery of the *Crb1*^{rd8} mutation in the C57BL/6N genetic background (Mattapallil et al., 2012). *Cln3*$^{\Delta ex7-8}$ and relevant *Cln3*$^{+/+}$ mice were found to be positive for the *Crb1*^{rd8} mutation, which explains why ERG response amplitudes decreased for *Cln3*$^{+/+}$ mice by one/third between 6 and 18 months. It also makes it difficult to assess how much of the *Cln3*$^{\Delta ex7-8}$ retinal degeneration observed via OKT and ERGs is really due to the CLN3 mutation. Whether the *rd8* mutation influences CLN3 and to which extent is unknown. Furthermore, ERGs published by Staropoli et al. were also conducted on animals with a the C57BL/6N genetic background (Staropoli et al., 2012). Further studies on *Cln3*$^{\Delta ex7-8}$ mice crossed onto another background, such as C57BL/6J, will elucidate the severity of retinal degeneration in these mice. On the other hand, *Cln6*^{nclf}, *Cln8*^{mnd}, *Ppt1*$^{-/-}$ and *Cln3*$^{-/-}$ mice mentioned in the above studies were done on mice with C57BL/6J background, where the *rd8* mutation has not been reported. Furthermore, the *Cln6*^{nclf} mice used in this study all test negative for the mutation. It is safer to assume that retinal phenotypes reported in these mouse models is correct.

5.2 Microglia and Müller Cells in NCL Retinal Degeneration

There is a growing consensus that microglia and astrocytes contribute significantly or even trigger apoptosis in several diseases including retinal dystrophies (Schuetz and Thanos, 2004; Maragakis and Rothstein, 2006). Microglia and Müller cells are usually the first cells which respond to distress signals in the retinal and brain by altering morphology, up/down regulating protein and mRNA marker expression in addition to migrating to distressed sites. It is not surprising that activation of these cell types have been found in neurodegenerative diseases such as Alzheimer's, multiple sclerosis and Parkinson's (Boillee et al., 2006; Kim and Joh, 2006). Furthermore, brain studies on NCL animal models as well as patients have also revealed the presence of activated microglia cells and astrocytes, often in localized area where significant cell death occurs (Kohlschutter et al., 1993a; Thelen et al., 2012). However, the presence and contribution of glia cells in NCL retinal degeneration is unknown. The second part of this thesis aimed to characterize microglial and

Müller cell phenotype in the retina and study whether these cells cause and/or contribute to cell death.

5.2.1 Glial Activation in *Cln3*$^{\Delta ex7-8}$ Retina

Cln3$^{\Delta ex7-8}$ retinas showed up-regulated GFAP expression, a Müller cell marker, as early as six months of age. However, microglia morphology was comparable to wild type even at 12 months of age and active microglia were seen at 18 months. Since microglia respond to dysfunction of photoreceptors or changes in microenvironment, it is possible that these changes are too subtle for the microglia to pick up or there are sufficient signals from other cells blocking the microglial activation pathway. Since Müller cells span the entire retina and help regulate homeostasis, these cells would be more prone to detecting subtle changes in the retina environment. It is also possible that the pathways in the Müller cells themselves is affected by the *Cln3*$^{\Delta ex7-8}$ mutation causing stress and impaired cell function. Intriguingly, Katz et al. only detected CLN3 protein expression in the mitochondria of Müller cells and inner retinal cells in wild type mice (Katz et al., 1997). This would also explain why the inner retinal cells of *Cln3*$^{\Delta ex7-8}$ mice are more affected in the ERGs than photoreceptors. Similarly, low grad activation of astrocytes has also been reported in brains of both the *Cln3*$^{-/-}$ and Cln3$^{\Delta ex7-8}$ mice with little macrophage morphology of microglia. Taken together, the Cln3$^{\Delta ex7-8}$ retinal phenotype is most likely caused by stressed Müller cells and inner retinal cells due to dysfunctional mitochondria. It is also likely Müller cells are unable to maintain their regulatory functions at later stages in the CLN3 disease resulting in decreased maintenance of photoreceptors cells which in turn send out stress signals to the microglia.

The importance astrocytes play in NCL has also been demonstrated in the Ppt1$^{-/-}$ mice. Reactive astrocytes were attenuated in these mice by cross breeding with GFAP$^{-/-}$ Vimentin$^{-/-}$ mice resulting in an earlier and faster degenerative phenotype with profound neuroinflammatory response (Macauley et al., 2011). However, the up-regulation GFAP expression is normally the first pathological changes observed in the Ppt1$^{-/-}$ brains (Kielar et al., 2007; Macauley et al., 2009). The exact role these glial cells play in NCL pathology is not yet clear. It would be interesting to study if *Cln3*$^{\Delta ex7-8}$ mice would also have an accelerated phenotype when astrocytes/Müller cells were attenuated. This may help elucidate if astrocytes play a more neuroprotective or deleterious role.

5.2.2 Glial Activation in *Cln6*^{nclf} Retina

Müller cell analysis using GFAP staining and mRNA expression showed early activation already present in one month *Cln6*^{nclf} mice which progressively increased with age. This is considerably earlier than GFAP staining of astrocytes in *Cln6*^{nclf} cerebral cortices, which appear between five to six months of age (Bronson et al., 1998; Thelen et al., 2012). Therefore, gliosis associated with neuronal degeneration in the *Cln6*^{nclf} mouse seems to occur in the eye before the brain. Iba1 detection of microglial cells in retinal sections and flat-mounts demonstrated a mixed population of alerted microglia at one month of age which became a homogenous group of amoeboid microglia by four months. Amoeboid microglia were seen migrating into nuclear and photoreceptor layers coinciding with a loss of microglial network. The presence of amoeboid microglia was followed by rapid decrease in OKT measurements, as well as accelerated thinning of the photoreceptor layer. This suggests that microglia actively contribute to accelerating retinal degeneration once fully active. The presence of active microglia before massive cell death has also been reported in the retinoschisis Rs1h-/Y mouse. In this model, microglia activating transcripts precede gene expression patterns related to apoptosis and microglial transformation from ramified to an amoeboid phagoctyic morphology coincided with cell death (Gehrig et al., 2007; Ebert et al., 2009). Furthermore, highly activated microglia which transformed to a phagocytic shape was seen past one year of age in the *Cln6*^{nclf} mouse brain (Thelen et al., 2012). Similar to induction of reactive astrocytes, microglia activation occurs much later in the brain compared to retina.

Alerted microglial cells also contained auto-fluorescent granules at all ages examined, which could reflect phagocytic processes of dying neurons affected by lysosomal storage of ceroid lipofuscin. In Ppt1$^{-/-}$ mice, F4/80 stained mostly microglia in brain regions with prominent neuro-pathological changes (Bible et al., 2004). However, storage body accumulation was evenly spread in the brain, indicating that lipofuscin deposits per se may not be the trigger for microglial activation (Bible et al., 2004). Conversely, in the *Cln6*^{nclf} brain, widespread microglial activation closely resembling that of lipopigment storage was seen along with localized clusters of activated microglia and astrocytes (Thelen et al., 2012). This data suggests that lipofuscin may trigger activation of microglia cells, however the presence of localized clusters indicate that other signals are also present. These signals may come from stressed neurons and astrocytes/Müller cells.

A deeper analysis of inflammation and glial cell activation in the *Cln6*^{nclf} mouse retina was done via temporal mRNA expression profiling. TUNEL assays of *Cln6*^{nclf} retinas revealed the constant presence of apoptosis which is also seen with apoptosis transcript marker CD95. However, highest CD95 expression was seen at one and six months, which is also when TUNEL assays were done. At other ages, CD95 expression is higher than wild type, but not significantly, indicating the presence of constant low level apoptosis. It is likely the number of TUNEL stained cells would have also been lower at other ages tested. Inflammatory marker expression, TNFα, was also increased in *Cln6*^{nclf} mice at all ages, but never significantly, indicating the presence of low-grade inflammation.

Strong and early induction of EDN2 and C1qa were also present in *Cln6*^{nclf} retinas. EDN2 was initially described as a secreted factor of stressed photoreceptors that binds to its receptor EDNRB on Müller cells (Rattner and Nathans, 2005). In turn, Müller cells produce leukemia inhibitory factor, which triggers release of the survival factor FGF2 in Müller cells and/or photoreceptors to protect neurons from further damage (Joly et al., 2008). However, studies on glaucomatous DBA/2J show EDN2 is very early up-regulated in retinal microglia and blocking EDN2 with antagonist bosentan reduced the incidence of glaucoma development in these mice (Howell et al., 2011). The authors speculate since EDN2 is a potent vasoactive peptide, it induces vasoconstriction in the ONH and retina during glaucoma causing degeneration. It is unclear whether EDN2 in the *Cln6*^{nclf} retina is neuroprotective or a microglia-specific signal that triggers photoreceptor degeneration. A very similar temporal expression profile was also detected for C1qa. C1qa is subunit of the macromolecular C1q complex exclusively synthesized by monocytes, macrophages, and microglial cells (Muller et al., 1978; Schafer et al., 2000). As part of the classical complement activation pathway, C1qa is a reliable marker of pro-inflammatory non-ramified microglial cells (Farber et al., 2009). The high expression of C1qa in *Cln6*^{nclf} retinas at all analyzed time points could suggest that alerted microglial cells are present at the very initial stages of NCL disease progression. Since C1qa triggers pro-inflammatory cytokine release, phagocytosis and oxidative burst in an autocrine and paracrine way (Farber et al., 2009), a constant high level of C1qa in *Cln6*^{nclf} retinas may reflect chronic inflammatory events in NCL.

Activated phagocytic microglia marker CD68 was strongly increased at one and six month in *Cln6*^{nclf} retinas with increased expression at other ages. This expression profile is similar to that of CD95, suggesting a co-incident of increase phagocytosis and apoptosis. EGR1 transcript levels were also strongly increased in *Cln6*^{nclf} retinas from four months onwards, with increased expression

from one to three months. EGR1 up-regulation is commonly associated with microglial activation and their migration into the nuclear layers (Langmann, 2007b; Langmann et al., 2009). Interestingly, in the retinal degeneration slow (*rds*) mouse, the EGR1 response was accompanied by induction of neurotrophic factors (Sharma et al., 2012). These authors therefore hypothesized that activation of EGR1 and neurotrophic factors could represent a protective immune mechanism contributing to the characteristically slow retinal degeneration of *rds* mice (Sharma et al., 2012). The exact function of EGR1 in *Cln6^{nclf}* microglial cells is unknown and needs further exploration.

Overall, *Cln6^{nclf}* retinas have an early induction of glial and inflammatory response which coincides with accelerated cell death. However, whether microglial activation is the main cause of cell death is unclear. Since morphometric and ERG analysis show retinal degeneration already occurs in one month old *Cln6^{nclf}* mice, and no studies have been done prior that that age, it is difficult to assess if the retinas of these mice simply never fully develop, or if cell death is occurring independent or dependent on microglial activation. Studies on CLN6 sheep have shown activated glial cells present in embryo 40 days before animals were born (Oswald et al., 2005). It is possible that enough microglia cell are active before the one month time point to cause significant degeneration to the retina and that this activation only gets worse as the mice age.

5.3 Immuno-modulation and Neuronal Degeneration Rescue via Dietary Supplements

With the increasing evidence that activated microglial cells release neurotoxic molecules including pro-inflammatory cytokines and reactive oxygen species which contribute to neurodegenerative processes, heightened effort are being made in finding neuroinflammation-targeting therapeutics. This includes screening approved CNS drugs, developing novel synthetic compounds which selectively down-regulate neuroinflammation and isolating active compounds from natural products (Choi et al., 2011). In fact, several natural compounds exist which can target microglial pathways whilst supporting neuronal survival. Curcumin is a herbal medicine which has been used for centuries in India and China (Ammon and Wahl, 1991). Curcumin has been shown to reduce toxic microglial secretions and protect neurons and photoreceptors (Jin et al., 2007; Jung et al., 2006; He et al., 2010; Mandal et al., 2009). Luteolin, a flavonoid abundant in leafy greens (Lopez-Lazaro 2009), has been shown to reduce microglia reactivity *in vivo* and induce neuroprotective phenotype *in vitro* (Jang et al., 2008; Dirscherl et al., 2012). DHA is highly enriched in the retina

and is a precursor for neuroprotectin D1, promoting the survival of photoreceptors and RPE cells (Mukherjee et al., 2007). It has also been shown to inhibit microglial synthesis of pro-inflammatory cytokines (Antonietta Ajmone-Cat et al., 2012). Furthermore, reports on patients with juvenile NCL have found reduced DHA levels in the plasma and cerebral cortex, which may contribute to retinal and brain degeneration (Kohlschutter et al., 1993b). On the same note, other hereditary forms of retinal degeneration have also been described to have low DHA levels and have used dietary supplementation as a therapeutic option (Schaefer et al., 1995; Ebert et al., 2009).

Targeting the immune system in NCL is not a novel idea. Studies done by Groh et al, in which lymphocytes were inactivated in Ppt1$^{-/-}$ mice, showed substantial disease attenuation (Groh et al., 2013). Pharmacological and genetic suppression of the immune system in the *Cln3*$^{-/-}$ mouse resulted in improved motor performance (Seehafer et al., 2011). Since reactive microglia have also been identified in CLN3 patients (Haltia, 2003), targeting the immune system and by extension, inflammation, has now become an option for therapeutic intervention. The third part of this thesis was to select the NCL mouse model with the most prominent glial activation and supplement these mice with anti-inflammatory diets in order to reduce glial reactivity and promote neuronal survival. As the *Cln6*^{nclf} mice were found have early Müller and microglial induction which correlates with cell death, mice were supplemented with 0.6% curcumin, 0.6% luteolin or 5% DHA for thirty weeks directly after weaning.

With all three dietary regimens, OKT measurements were significantly higher compared to non-supplemented control mice starting at three months for curcumin and DHA and five months for luteolin-supplemented mice. Luteolin-supplemented mice had uneven OKT measurements which showed initial improvement at three months but drastic decrease in thresholds at four months and improvement again thereafter. This puzzling "roller-coaster" effect may be due to an infection these particular mice got during the experiment or potential toxic effects of the compound. However, no verifications were made. ERG analysis also showed improvements in b-wave for all three regimens with DHA having the greatest preservation of the a-wave. The preservation of the photoreceptor layer and particularly the outer segments in DHA-treated mice was also highlighted in morphometric and histological analyses. A beneficial effect on photoreceptor outer segments has also been seen in DHA supplementation of rhodopsin mutant rats, although no alteration in the rate of retinal degeneration was detected (Martin et al., 2004). Surprisingly, curcumin did not have a larger effect on retinal preservation. Previous studies on rats with light induce retinal

degeneration which were supplemented with 0.2% curcumin diet were able to show significant decrease in ONL degeneration (Mandal et al., 2009). However, the improvement in ERG measurements of these curcumin-supplemented rats is similar to that of the curcumin-supplemented *Cln6*^{nclf} mice. Moreover, mice with type 2 diabetes which were given a 2% DHA diet also had similar improvements in retinal function as DHA-supplemented *Cln6*^{nclf} mice (Sapieha et al., 2012).

Immunohistochemical analysis of microglia with Iba1 showed mainly ramified cells in all supplemented *Cln6*^{nclf} retinas compared to the amoeboid microglia in controls. However, cross sections did show amoeboid microglia migrated into cells layers. Nevertheless, these amoeboid microglia did retain extended ramifications, which was not seen in the controls. With these somewhat contradictory results, it is important to note that microglia morphology is not always equivalent to inflammation state (Graeber et al., 2011). The microglia morphology identified in the supplemented *Cln6*^{nclf} retinas look similar to those found in DHA-supplemented retinoschisis-deficient mice (Ebert et al., 2009). In this retinal degeneration model, the ramified microglial population produced less pro-inflammatory cytokines and the retinal morphology was improved upon DHA-treatment (Ebert et al., 2009). Furthermore, BV2 microglia cells treated with LPS (lipopolysaccharide) and luteolin also had somewhat amoeboid microglia with long ramified protrusions (Dirscherl et al., 2010). These *in vitro* studies also showed that luteolin was able alter microglia transcriptom making it a potent modulator of microglial activation by inducing an anti-inflammatory, anti-oxidative, neuroprotective phenotype. With this in mind, it is tempting to speculate that DHA- and in part curcumin and luteolin-supplemented *Cln6*^{nclf} retinas display less microglial reactivity. Accumulation of lipofuscin deposits for control and supplemented retinas appeared to be similar in all cases.

Both luteolin and curcumin did not significantly alter mRNA expression of inflammatory or microglial markers. This is quite surprising since *in vivo* studies of mice supplemented with luteolin and curcumin have shown decreased expression of pro-inflammatory cytokines such as IL-6 and IL-1β (Jang et al., 2008; He et al., 2010). Furthermore, *in vitro* studies done with both compounds on LPS-activated BV2 cells induced the expression of distinct anti-inflammatory gene clusters (Dirscherl et al., 2010; Karlstetter et al., 2011).

DHA-supplementation also had surprising effects on the retinal mRNA marker expression. Along with the expected decrease in apoptosis and inflammatory marker expression of caspase 8 and CD95, retinas had an unexpected up-regulation of "classical" activated microglia markers: C1qa, CD68 and EGR1 (data not shown). In addition, these eyes also had decreased expression of Tgfβ, a marker for 'alternatively' activated microglia associated with neuroprotection. These data suggest that DHA-supplementation in *Cln6*^{nclf} mice pushes for a more activate microglial phenotype, however morphology studies suggest the microglia are not completely active. This expression profile is in contrast to other studies done concerning microglia and DHA, which report a decrease in similar markers (Ebert et al., 2009). Furthermore, studies done on DHA-supplemented type 2 diabetes mice, showed no change in expression of similar markers, despite improvement in retinal function (Sapieha et al., 2012). It is possible that DHA supplementation in CLN6^{nclf} retina push microglia to better clear debris and dead cells without letting microglia reach fully alerted states. This would also explain how apoptosis markers are significantly decreased in these retinas. Decrease in apoptosis can also be attributed to preservation of the photoreceptor outer membranes (German et al., 2006). Although, DHA levels in the *Cln6*^{nclf} mouse have not been verified. it is likely these mice, similar to JNCL patients, have low concentrations of DHA in neural tissues (Kohlschutter et al., 1993b).

Nonetheless, these studies are not without limitations. Luteolin and curcumin supplementation were expected to yield better preservation of the *Cln6*^{nclf} retina. As both substances are hormetic (Mattson and Cheng, 2006; Son et al., 2008), and no previous study has supplemented mice for the length of this study, it is possible that curcumin and luteolin had some toxic effects. Furthermore, curcumin supplementation studies done on Neimann-Pick disease type C (NPC) mice did lead to toxic effects as these mice have innate low levels of cytochrome P450, an important enzyme which catalyzes the metabolism of organic products and drugs (this work is not yet published and is in review). Curcumin has also been shown to decrease cytochrome P450 levels in rat liver (Oetari et al., 1996). This combined effect led to toxic build up of curcumin in NPC mice. Cytochrome P450 levels have not verified in NCL patients or mice, but since both NPC and NCL are neurodegenerative lysosomal storage diseases, it may be an explanation as to why curcumin supplementation did not yield better results. Supplementation studies would have to be tested on wild type mice and new studies would have to be done with lower doses.

mRNA marker expression data may have also been influenced by the low number of mice dedicated to those experiment (n=5). Since NCL is an individual disease, it is also expected that treatment would have individual results. A larger number of mice would have compensated for this variability. Finally, the amount of dietary substance which was reabsorbed and cross the blood brain/retinal barrier is unknown. There is evidence that flavonoids Naringenin and Quercetin are able to penetrate into the brain (Youdim et al., 2004) but this has not been determined for luteolin. Furthermore, curcumin has been detected in the forebrain of mice after systemic injection (Purkayastha et al., 2009) and bioactive levels have been shown in the retina after dietary supplementation, however curcumin accumulation has not been experimental proven in the retina (Mandal et al., 2009). DHA accumulation in the retina has been reported in the rod outer segment in mice supplemented with flaxseed oil (Martin et al., 2004). On the other hand, the effect these supplements had on the retina could be seen by the positive results in ERG and OKT measurements implying that these supplements did have some influence on visual function.

5.4 Perspective

5.4.1 Cln3 and Cln6: Different but Similar?

Comparison of retinal degeneration of *Cln3*$^{\Delta ex7\text{-}8}$ and *Cln6*^{nclf} were confounded by the presence of the *Crb1*^{rd8} mutation. Nonetheless, this raises the question of how dis/similar CLN3 and CLN6 are to each other, and how similarities and difference might be helpful in better understand NCL Although, the CLN6 protein is localized on the ER membrane and CLN3 protein on lysosomal membrane, both have been implicated in autophagy mechanisms (Cao et al., 2006; Thelen et al., 2012). The *nclf* mutation in CLN6 has been suggested to inhibit fusion between autophagosomes and lysosomes whereas the 1-kb mutation in CLN3 delays the maturation of autophagic vacuoles (Cao et al., 2006; Thelen et al., 2012). Moreover, studies undertaken by Cao et al. compared gene expression via microarray of primary cerebellar neuronal precursor cells from *Cln6*^{nclf} and *Cln3*$^{\Delta ex7\text{-}8}$ mice revealed 36 shared probes (out of 1,662 total probes found to be different from wild type) with only 8 concordant in their direction of change (Cao et al., 2011). These experiments, as well as the ones done in this current study, reveal distinct patho-mechanism exist at least between CLN3 and CLN6 disease. This suggests that perhaps treatments which may work for one disease would not be so effective in the other. However, better understanding of one of these proteins would help elucidate what the function of other NCL proteins may be. Also, the protein expression

pattern of CLN6 and most of the other NCLs (such as in Müller cells or certain neurons) would also help elucidate which cell types are more affected by the mutation.

Finally, studies in this thesis have shown that the ocular phenotype in NCL is helpful to understand molecular mechanisms and could also be useful to develop diagnostic tools for experimental therapies. Since vision loss is relatively easier to quantify than motor and behavioral deterioration in NCL mouse models, preclinical therapies which ameliorate the retinal phenotype could be an effective means to monitor effects on the brain. However, this could only apply to mouse model which exhibit a retinal phenotype.

5.4.2 Müller Cells, Microglia and Modulation via Natural Compounds

In both *Cln3*$^{\Delta ex7\text{-}8}$ and *Cln6*^{nclf} retina, Müller cells were found to be reactive. Whether this is because of dysfunctional mitochondria, photoreceptor cell death, both or other mechanisms remains to be elucidated. Similarly, the balance between neuroprotective and neurodegenerative microglia as well as their role in *Cln6*^{nclf} retinas needs to be further explored. From these studies, the blurred lines between what defines "classically" and "alternatively" activated microglia make it difficult to assess how much damage microglia cause. This study also highlights the importance of comparing microglia morphology and marker expression to get a better understanding of microglial reactivity.

As a final point, there is a lot of promise for using natural immuno-modulating compounds as a treatment option of neurodegenerative disease. As the knowledge of microglial behavior and function in the retina and brain increases, microglia themselves have become a target for therapeutic intervention. Clinical trials studying the positive effect of curcumin on Alzheimer's disease are underway (clinicaltrials.gov). Furthermore, curcumin is also being used as a non-invasive biomarker for detecting β-amyloid plaques in the eyes of AD patients via retinal imaging. Beneficial effects of reservatrol, *ginseng* and green tea, amongst a growing number of compounds, have all been shown to have positive effects in disease and reduce microglia activating pathways (Choi et al., 2011).

Unfortunately there is no widely accepted treatment that can cure, slow down, or stop the symptoms of NCL, although phase I clinical trial of neural stem cells for INCL and

immunosurpressants for JNCL can slow disease progression for a limited time (clinicaltrials.gov; http://www.bdsra.org/ research/Pearce-trial.htm). There is still a lot of work which needs to be done in the NCL field towards understanding CLN protein mechanisms, all the key players in NCL pathology, and treatment development. Based on the studies done in this thesis, increase in dietary anti-inflammatory compounds starting at an early enough time point would help reduce inflammation and slow disease progression. However, this type of intervention is by no means a cure and would be most beneficial if paired with another treatment option.

6. Summary

Microglia are specialized macrophages of the central nervous system involved in immune regulation, tissue development, homeostasis and wound repair. In healthy tissue, microglia are found in a ramified state which is tightly controlled by neurons. Upon insult, microglia undergo morphological changes, resembling active phagocytic macrophages and are highly motile. In neurodegenerative diseases, such are Alzheimer's or multiple sclerosis and in most inherited retinal dystrophies, microglia cells are found in a permanent pro-inflammatory active state which exacerbates cell death and disease progression. Similarly, astrocytes in the brain or Müller cells in the retina, also become reactive in diseased tissue and may contribute to disease progression through overshoot release of protective factors such as VEGF (vascular endothelial growth factor), massive proliferation and release of inflammatory intermediates which recruit microglia to site of injury. Along with active microglia, reactive astrocytes/Müller cells are also found in virtually all neurodegenerative and retinal dystrophies.

Microglia and Müller cell status has not been well defined in retinal degeneration of neurodegenerative disease neuronal ceroid lipofuscinosis (NCL). The NCLs are early onset lysosomal storage disorders characterized by vision loss, mental and motor deficits, and spontaneous seizures. Massive accumulation of auto-fluorescent material in neurons lead to progressive neuronal degeneration and cell death Furthermore, neuropathological analyses of autopsy material from NCL patients and animal models revealed brain atrophy closely associated with microglial and astrocyte activity. However, it is unclear whether this phenomenon is mainly confined to the brain or also occurs in the retina

Two mouse models of NCL, *Cln3*$^{\Delta ex7\text{-}8}$ and *Cln6*^{nclf}, were selected for detailed characterization of retinal degeneration with focus on microglia and Müller cell activity. Studies showed that *Cln3*$^{\Delta ex7\text{-}8}$ mice had a late onset of retinal degeneration which started at 9 months and progressed until severe retinal impairment at 18 months. Reactive Müller cells were present starting at six months with no significant microglial activation until late disease stage. Furthermore, degeneration originated from inner retinal cells as seen through electroretinograms with little photoreceptor death. In contrast, temporal studies on *Cln6*^{nclf} mice showed an early progressive retinal degenerative phenotype which started before one month of age resulting in loss of vision and

retinal function by eight months. Full retinal degeneration was accompanied by reactive Müller cells already present at one month of age and fully active microglia at four months. Mixed population of ramified and active microglia were seen at one month. Transcript profiling of the *Cln6*^{ncl} mouse retina also showed up-regulated expression of apoptotic, inflammatory and active microglia markers.

Based on the strong reactivity of microglia, *Cln6*^{nclf} mice were supplemented with immuno-modulatory compounds curcumin, luteolin or DHA in order to ameliorate microgliosis and reduce retinal degeneration. Studies showed *Cln6*^{nclf} mice supplemented with 0.6% curcumin, 0.6% luteolin or 5% DHA had improved retinal function, better visual acuity and DHA-supplementation had the greatest preservation of photoreceptors. All supplements were able to attenuate microglia activation as seen by the presence of microglial ramification and intact network. However, curcumin and luteolin supplementation did not have any effect on retinal transcriptom whilst DHA-supplementation reduced expression of inflammatory and apoptotic markers.

Taken together, microglial reactivity accompanies disease progression in the *Cln6*^{nclf} retina but not *Cln3*$^{\Delta ex7\text{-}8}$. Immuno-modulating compounds were able to attenuate disease progression and reactive microglia to a certain extent in *Cln6*^{nclf} mice, indicating modulation of microglial activity could be helpful in preserving vision and may ameliorate neuronal degeneration in NCL. Finally, inspection of the retinal function may also allow to monitor general disease progression and could be used to assess the efficacy of therapeutic interventions for NCL patients.

7. Zusammenfassung

Mikrogliazellen sind spezialisierte Makrophagen des zentralen Nervensystems, die an der Immunoregulation, Gewebeentwicklung und Wungheilung beteiligt sind. Im gesunden Gewebe liegen Mikrogliazellen in einer verzweigten Form vor, welche von Neuronen kontrolliert wird. Nach einer Schädigung ändert sich die Morphologie der Mikrogliazellen und ähnelt dann der von aktivierten, phagozytischen Makrophagen. Außerdem werden die Mikroglia dadurch sehr beweglich. In neurodegenerativen Erkrankungen, wie Alzheimer oder multiple Sklerose, und in den meisten erblichen Netzhautdystrophien befinden sich Mikrogliazellen dauerhaft in diesem proinflammatorischen Zustand, welcher den Zelltod und die Progression der Erkrankung beschleunigt. In ähnlicher Weise werden Astrozyten im Gehirn oder Müllerzellen in der Netzhaut im erkrankten Gewebe aktiviert und können den weiteren Verlauf der Erkrankung negativ beeinflussen. Neben aktiven Mikrogliazellen kommen auch reaktive Astrozyten/Müllerzellen in praktisch allen neurodegenerativen und retinalen Dystrophien vor.

Die neuronalen Ceroid-Lipofuszinosen (NCL) sind neurodegenerative Erkrankungen, welche mit einer Netzhautdegeneration einhergehen. Hier ist der Einfluss von Mikroglia und Müllerzellen noch nicht genau bekannt. Die NCL-Erkrankungen sind lysosomale Speicherkrankheiten, die im frühen Lebensalter beginnen und durch Sehverlust, mentale und motorische Defizite und spontane epileptische Anfälle charakterisiert sind. Eine massive Anreicherung von autofluoreszentem Material in den Nervenzellen führt zu fortschreitender Neurodegeneration und zum Zelluntegang. Außerdem zeigen neuropathologische Untersuchungen an Autopsiematerial von NCL-Patienten und an Tiermodellen eine Hirnatrophie, die eng mit der Aktivität der Mirkoglia und Asztozyten assoziiert ist. Es bleibt jedoch unklar, ob sich dieses Phänomen nur im Gehirn abspielt, oder ob es auch in der Netzhaut auftritt.

Zwei Mausmodelle für NCL, Cln3$^{\Delta ex7\text{-}8}$ und Cln6^{nclfb}, wurden für eine detaillierte Charakterisierung der Netzhautdegeneration untersucht, wobei der Fokus auf die Aktivität der Mikroglia und der Müllerzellen gelegt wurde. Studien haben gezeigt, dass die Netzhautdegeneration bei Cln3$^{\Delta ex7\text{-}8}$-Mäusen erst spät einsetzt. Diese beginnt im neunten Lebensmonat und wird bis zum achtzehnten Lebensmonat progressiv schlechter. Das Endstadium der Erkrankung ist schließlich durch eine schwere Netzhautschädigung gekennzeichnet. Reaktive Müllerzellen konnten ab dem sechsten

Monate identifiziert werden. Eine Aktivierung von Mikrogliazellen hingegen wurde erst in einem späten Stadium der Krankheit beobachtet. Des Weiteren begann die Degeneration in den inneren Netzhautschichten, wie durch Elektroretinogramme gezeigt werden konnte, wobei die Photorezeptoren kaum von dem Zellsterben betroffen waren. Im Gegensatz dazu zeigten Studien an Cln6^{nclf}-Mäusen einen frühzeitigen, progressiv degenerativen Phänotyp der Retina, welcher vor dem ersten Lebensmonat begann und zum Verlust der Sehkraft und der Netzhautfunktion im achten Lebensmonat führte. Während des gesamten Prozesses konnten reaktive Müllerzellen beobachtet werden, welche schon im ersten Lebensmonat auftraten. Ferner wurden im ersten Monat gemischte Gruppen von verzweigten und aktivierten Mikroglia identifiziert, welche alle nach vier Monaten komplett aktiv waren. Expressionsprofile der Netzhaut von Cln6^{ncl}-Mäusen zeigten zudem eine erhöhte Expression von apoptotischen, inflammatorischen und aktiven Mikrogliamarkern.

Aufgrund der starken Aktivierung der Mikrogliazellen wurden Cln6^{nclf}-Mäuse mit den immunmodulatorischen Substanzen Curcumin, Luteolin oder DHA behandelt. Ziel war es, die Mikrogliose zu verbessern und die Netzhautdegeneration zu mildern. Studien zeigten, dass 0,6% Curcumin, 0,6%Luteolin oder 5% DHA zu einer verbesserten Netzhautfunktion und einer besseren Sehschärfe führten. Ferner wurde bei Behandlung mit DHA der größte Erhalt von Photorezeptoren beobachtet. Alle Substanzen konnten die Aktivierung der Mikroglia abmildern, was durch die Anwesenheit von verzweigten Mikroglia in einem intakten Netzwerk belegt werden konnte. Jedoch hatten Curcumin und Luteolin keine Wirkung auf das retinale Expressionsprofil, während DHA die Expression von inflammatorischen und apoptotischen Marker reduzierte, aber auch und die Expresion der Mikrogliamarker hochregulierte.

Zusammenfassend kann gesagt werden, dass der Phänotyp von Cln6^{nclf}-Mäusen mit einer Aktivierung von Mikroglia einhergeht. Diese konnte jedoch nicht bei *Cln3*$^{\Delta ex7\text{-}8}$-Mäusen beobachtet werden. Immunmodulatorische Substanzen waren bei Cln6^{nclf}-Mäusen innerhalb eines gewissen Rahmens in der Lage, das Fortschreiten der Erkrankung abzumildern und die Aktivierung der Mikroglia einzugrenzen. Dies deutet darauf hin, dass sich die Beeinflussung der Mikrogliaaktivität positiv auf den Erhalt der Sehkraft auswirkt und dass die Neurodegeneration bei NCL-Patienten abgeschwächt werden kann. Schlussendlich kann die Überprüfung der Netzhautfunktion auch dazu dienen, den Fortschritt der Erkrankung zu überwachen und die Wirkung einer Therapie für NCL-Patienten zu beurteilen.

8. References

Ammon HP, Wahl MA (1991) Pharmacology of Curcuma longa. Planta Med 57:1-7.

Antonietta Ajmone-Cat M, Lavinia Salvatori M, De Simone R, Mancini M, Biagioni S, Bernardo A, Cacci E, Minghetti L (2012) Docosahexaenoic acid modulates inflammatory and antineurogenic functions of activated microglial cells. J Neurosci Res 90:575-587.

Arsov T, Smith KR, Damiano J, Franceschetti S, Canafoglia L, Bromhead CJ, Andermann E, Vears DF, Cossette P, Rajagopalan S, McDougall A, Sofia V, Farrell M, Aguglia U, Zini A, Meletti S, Morbin M, Mullen S, Andermann F, Mole SE, Bahlo M, Berkovic SF (2011) Kufs disease, the major adult form of neuronal ceroid lipofuscinosis, caused by mutations in CLN6. Am J Hum Genet 88:566-573.

Ballabio A, Gieselmann V (2009) Lysosomal disorders: from storage to cellular damage. Biochim Biophys Acta 1793:684-696.

Banati RB, Gehrmann J, Schubert P, Kreutzberg GW (1993) Cytotoxicity of microglia. Glia 7:111-118.

Bauer J, Sminia T, Wouterlood FG, Dijkstra CD (1994) Phagocytic activity of macrophages and microglial cells during the course of acute and chronic relapsing experimental autoimmune encephalomyelitis. J Neurosci Res 38:365-375.

Benedict JW, Getty AL, Wishart TM, Gillingwater TH, Pearce DA (2009) Protein product of CLN6 gene responsible for variant late-onset infantile neuronal ceroid lipofuscinosis interacts with CRMP-2. J Neurosci Res 87:2157-2166.

Biber K, de Jong EK, van Weering HR, Boddeke HW (2006) Chemokines and their receptors in central nervous system disease. Curr Drug Targets 7:29-46.

Biber K, Neumann H, Inoue K, Boddeke HW (2007) Neuronal 'On' and 'Off' signals control microglia. Trends Neurosci 30:596-602.

Bible E, Gupta P, Hofmann SL, Cooper JD (2004) Regional and cellular neuropathology in the palmitoyl protein thioesterase-1 null mutant mouse model of infantile neuronal ceroid lipofuscinosis. Neurobiol Dis 16:346-359.

Bignami A, Dahl D (1979) The radial glia of Muller in the rat retina and their response to injury. An immunofluorescence study with antibodies to the glial fibrillary acidic (GFA) protein. Exp Eye Res 28:63-69.

Birch DG (1999) Retinal degeneration in retinitis pigmentosa and neuronal ceroid lipofuscinosis: An overview. Mol Genet Metab 66:356-366.

Block ML, Zecca L, Hong JS (2007) Microglia-mediated neurotoxicity: uncovering the molecular mechanisms. Nat Rev Neurosci 8:57-69.

Boillee S, Yamanaka K, Lobsiger CS, Copeland NG, Jenkins NA, Kassiotis G, Kollias G, Cleveland DW (2006) Onset and progression in inherited ALS determined by motor neurons and microglia. Science 312:1389-1392.

Bras J, Verloes A, Schneider SA, Mole SE, Guerreiro RJ (2012) Mutation of the parkinsonism gene ATP13A2 causes neuronal ceroid-lipofuscinosis. Hum Mol Genet 21:2646-2650.

Bringmann A, Pannicke T, Grosche J, Francke M, Wiedemann P, Skatchkov SN, Osborne NN, Reichenbach A (2006) Muller cells in the healthy and diseased retina. Prog Retin Eye Res 25:397-424.

Bringmann A, Pannicke T, Biedermann B, Francke M, Iandiev I, Grosche J, Wiedemann P, Albrecht J, Reichenbach A (2009) Role of retinal glial cells in neurotransmitter uptake and metabolism. Neurochem Int 54:143-160.

Bronson RT, Donahue LR, Johnson KR, Tanner A, Lane PW, Faust JR (1998) Neuronal ceroid lipofuscinosis (nclf), a new disorder of the mouse linked to chromosome 9. Am J Med Genet 77:289-297.

Cao Y, Espinola JA, Fossale E, Massey AC, Cuervo AM, MacDonald ME, Cotman SL (2006) Autophagy is disrupted in a knock-in mouse model of juvenile neuronal ceroid lipofuscinosis. J Biol Chem 281:20483-20493.

Cao Y, Staropoli JF, Biswas S, Espinola JA, MacDonald ME, Lee JM, Cotman SL (2011) Distinct early molecular responses to mutations causing vLINCL and JNCL presage ATP synthase subunit C accumulation in cerebellar cells. PLoS One 6:e17118.

Cardona AE, Pioro EP, Sasse ME, Kostenko V, Cardona SM, Dijkstra IM, Huang D, Kidd G, Dombrowski S, Dutta R, Lee JC, Cook DN, Jung S, Lira SA, Littman DR, Ransohoff RM (2006) Control of microglial neurotoxicity by the fractalkine receptor. Nat Neurosci 9:917-924.

Carter DA, Dick AD (2004) CD200 maintains microglial potential to migrate in adult human retinal explant model. Curr Eye Res 28:427-436.

Chang B, Hawes NL, Hurd RE, Davisson MT, Nusinowitz S, Heckenlively JR (2002) Retinal degeneration mutants in the mouse. Vision Res 42:517-525.

Chang B, Bronson RT, Hawes NL, Roderick TH, Peng C, Hageman GS, Heckenlively JR (1994) Retinal degeneration in motor neuron degeneration: a mouse model of ceroid lipofuscinosis. Invest Ophthalmol Vis Sci 35:1071-1076.

Chang GQ, Hao Y, Wong F (1993) Apoptosis: final common pathway of photoreceptor death in rd, rds, and rhodopsin mutant mice. Neuron 11:595-605.

Chattopadhyay S, Kingsley E, Serour A, Curran TM, Brooks AI, Pearce DA (2004) Altered gene expression in the eye of a mouse model for batten disease. Invest Ophthalmol Vis Sci 45:2893-2905.

Chen CY, Peng WH, Tsai KD, Hsu SL (2007) Luteolin suppresses inflammation-associated gene expression by blocking NF-kappaB and AP-1 activation pathway in mouse alveolar macrophages. Life Sci 81:1602-1614.

Chen HQ, Jin ZY, Wang XJ, Xu XM, Deng L, Zhao JW (2008) Luteolin protects dopaminergic neurons from inflammation-induced injury through inhibition of microglial activation. Neurosci Lett 448:175-179.

Choi DK, Koppula S, Suk K (2011) Inhibitors of microglial neurotoxicity: focus on natural products. Molecules 16:1021-1043.

Collins J, Holder GE, Herbert H, Adams GG (2006) Batten disease: features to facilitate early diagnosis. Br J Ophthalmol 90:1119-1124.

Consortium TIBD (1995) Isolation of a novel gene underlying Batten disease, CLN3. . Cell 82:949-957.

Cooper JD, Russell C, Mitchison HM (2006) Progress towards understanding disease mechanisms in small vertebrate models of neuronal ceroid lipofuscinosis. Biochim Biophys Acta 1762:873-889.

Cotman SL, Vrbanac V, Lebel LA, Lee RL, Johnson KA, Donahue LR, Teed AM, Antonellis K, Bronson RT, Lerner TJ, MacDonald ME (2002) Cln3(Deltaex7/8) knock-in mice with the common JNCL mutation exhibit progressive neurologic disease that begins before birth. Hum Mol Genet 11:2709-2721.

Coull JA, Beggs S, Boudreau D, Boivin D, Tsuda M, Inoue K, Gravel C, Salter MW, De Koninck Y (2005) BDNF from microglia causes the shift in neuronal anion gradient underlying neuropathic pain. Nature 438:1017-1021.

Creel DJ (2013) The Electroretinogram and Electro-oculogram: Clinical Applications. In: Webvision: The Organization of Retina and Visual System (Kolb H, Nelson, R., Fernandez, E., Jone, B., ed).

Curcio CA, Medeiros NE, Millican CL (1996) Photoreceptor loss in age-related macular degeneration. Invest Ophthalmol Vis Sci 37:1236-1249.

Davalos D, Grutzendler J, Yang G, Kim JV, Zuo Y, Jung S, Littman DR, Dustin ML, Gan WB (2005) ATP mediates rapid microglial response to local brain injury in vivo. Nat Neurosci 8:752-758.

Davoust N, Vuaillat C, Androdias G, Nataf S (2008) From bone marrow to microglia: barriers and avenues. Trends Immunol 29:227-234.

Del Rio Hortega P (1919) El tercer elemento de los centros nerviosis. Bol Soc Esp Biol 9:69–129.

Ding X, Patel M, Chan CC (2009) Molecular pathology of age-related macular degeneration. Prog Retin Eye Res 28:1-18.

Dirscherl K, Karlstetter M, Ebert S, Kraus D, Hlawatsch J, Walczak Y, Moehle C, Fuchshofer R, Langmann T (2010) Luteolin triggers global changes in the microglial transcriptome leading to a unique anti-inflammatory and neuroprotective phenotype. J Neuroinflammation 7:3.

Douglas RM, Alam NM, Silver BD, McGill TJ, Tschetter WW, Prusky GT (2005) Independent visual threshold measurements in the two eyes of freely moving rats and mice using a virtual-reality optokinetic system. Vis Neurosci 22:677-684.

Duffield JS (2003) The inflammatory macrophage: a story of Jekyll and Hyde. Clin Sci (Lond) 104:27-38.

Dunaief JL, Dentchev T, Ying GS, Milam AH (2002) The role of apoptosis in age-related macular degeneration. Arch Ophthalmol 120:1435-1442.

Dunn KC, Aotaki-Keen AE, Putkey FR, Hjelmeland LM (1996) ARPE-19, a human retinal pigment epithelial cell line with differentiated properties. Exp Eye Res 62:155-169.

Ebert S, Weigelt K, Walczak Y, Drobnik W, Mauerer R, Hume DA, Weber BH, Langmann T (2009) Docosahexaenoic acid attenuates microglial activation and delays early retinal degeneration. J Neurochem 110:1863-1875.

El Khoury J, Toft M, Hickman SE, Means TK, Terada K, Geula C, Luster AD (2007) Ccr2 deficiency impairs microglial accumulation and accelerates progression of Alzheimer-like disease. Nat Med 13:432-438.

Elkabes S, DiCicco-Bloom EM, Black IB (1996) Brain microglia/macrophages express neurotrophins that selectively regulate microglial proliferation and function. J Neurosci 16:2508-2521.

Elshatory Y, Brooks AI, Chattopadhyay S, Curran TM, Gupta P, Ramalingam V, Hofmann SL, Pearce DA (2003) Early changes in gene expression in two models of Batten disease. FEBS Lett 538:207-212.

Farber K, Cheung G, Mitchell D, Wallis R, Weihe E, Schwaeble W, Kettenmann H (2009) C1q, the recognition subcomponent of the classical pathway of complement, drives microglial activation. J Neurosci Res 87:644-652.

Fisher SK, Erickson PA, Lewis GP, Anderson DH (1991) Intraretinal proliferation induced by retinal detachment. Invest Ophthalmol Vis Sci 32:1739-1748.

Futerman AH, van Meer G (2004) The cell biology of lysosomal storage disorders. Nat Rev Mol Cell Biol 5:554-565.

Gachet Y, Codlin S, Hyams JS, Mole SE (2005) btn1, the Schizosaccharomyces pombe homologue of the human Batten disease gene CLN3, regulates vacuole homeostasis. J Cell Sci 118:5525-5536.

Gao H, Boustany RM, Espinola JA, Cotman SL, Srinidhi L, Antonellis KA, Gillis T, Qin X, Liu S, Donahue LR, Bronson RT, Faust JR, Stout D, Haines JL, Lerner TJ, MacDonald ME (2002) Mutations in a novel CLN6-encoded transmembrane protein cause variant neuronal ceroid lipofuscinosis in man and mouse. Am J Hum Genet 70:324-335.

Gehrig A, Langmann T, Horling F, Janssen A, Bonin M, Walter M, Poths S, Weber BH (2007) Genome-wide expression profiling of the retinoschisin-deficient retina in early postnatal mouse development. Invest Ophthalmol Vis Sci 48:891-900.

Gehrmann J, Matsumoto Y, Kreutzberg GW (1995) Microglia: intrinsic immuneffector cell of the brain. Brain Res Brain Res Rev 20:269-287.

German OL, Insua MF, Gentili C, Rotstein NP, Politi LE (2006) Docosahexaenoic acid prevents apoptosis of retina photoreceptors by activating the ERK/MAPK pathway. J Neurochem 98:1507-1520.

Ginhoux F, Greter M, Leboeuf M, Nandi S, See P, Gokhan S, Mehler MF, Conway SJ, Ng LG, Stanley ER, Samokhvalov IM, Merad M (2010) Fate mapping analysis reveals that adult microglia derive from primitive macrophages. Science 330:841-845.

Goebel HH (1992) Retina in various animal models of neuronal ceroid-lipofuscinosis. Am J Med Genet 42:605-608.

Gordon S, Perry VH, Rabinowitz S, Chung LP, Rosen H (1988) Plasma membrane receptors of the mononuclear phagocyte system. J Cell Sci Suppl 9:1-26.

Graeber MB (2010) Changing face of microglia. Science 330:783-788.

Graeber MB, Streit WJ (2001) Microglia: biology and pathology. Acta Neuropathol 119:89-105.

Graeber MB, Li W, Rodriguez ML (2011) Role of microglia in CNS inflammation. FEBS Lett 585:3798-3805.

Groh J, Kuhl TG, Ip CW, Nelvagal HR, Sri S, Duckett S, Mirza M, Langmann T, Cooper JD, Martini R (2013) Immune cells perturb axons and impair neuronal survival in a mouse model of infantile neuronal ceroid lipofuscinosis. Brain 136:1083-1101.

Gupta N, Brown KE, Milam AH (2003) Activated microglia in human retinitis pigmentosa, late-onset retinal degeneration, and age-related macular degeneration. Exp Eye Res 76:463-471.

Haltia M (2003) The neuronal ceroid-lipofuscinoses. J Neuropathol Exp Neurol 62:1-13.

Haltia M (2006) The neuronal ceroid-lipofuscinoses: from past to present. Biochim Biophys Acta 1762:850-856.

Haltia M, Goebel HH (2012) The neuronal ceroid-lipofuscinoses: A historical introduction. Biochim Biophys Acta.

He LF, Chen HJ, Qian LH, Chen GY, Buzby JS (2010) Curcumin protects pre-oligodendrocytes from activated microglia in vitro and in vivo. Brain Res 1339:60-69.

Hoek RM, Ruuls SR, Murphy CA, Wright GJ, Goddard R, Zurawski SM, Blom B, Homola ME, Streit WJ, Brown MH, Barclay AN, Sedgwick JD (2000) Down-regulation of the macrophage lineage through interaction with OX2 (CD200). Science 290:1768-1771.

Horst CJ, Johnson LV, Besharse JC (1990) Transmembrane assemblage of the photoreceptor connecting cilium and motile cilium transition zone contain a common immunologic epitope. Cell Motil Cytoskeleton 17:329-344.

Howell GR, Macalinao DG, Sousa GL, Walden M, Soto I, Kneeland SC, Barbay JM, King BL, Marchant JK, Hibbs M, Stevens B, Barres BA, Clark AF, Libby RT, John SW (2011) Molecular clustering identifies complement and endothelin induction as early events in a mouse model of glaucoma. J Clin Invest 121:1429-1444.

Hu C, Kitts DD (2004) Luteolin and luteolin-7-O-glucoside from dandelion flower suppress iNOS and COX-2 in RAW264.7 cells. Mol Cell Biochem 265:107-113.

Hume DA, Gordon S (1983) Mononuclear phagocyte system of the mouse defined by immunohistochemical localization of antigen F4/80. Identification of resident macrophages in renal medullary and cortical interstitium and the juxtaglomerular complex. J Exp Med 157:1704-1709.

Iandiev I, Wurm A, Hollborn M, Wiedemann P, Grimm C, Reme CE, Reichenbach A, Pannicke T, Bringmann A (2008) Muller cell response to blue light injury of the rat retina. Invest Ophthalmol Vis Sci 49:3559-3567.

Jalanko A, Braulke T (2009) Neuronal ceroid lipofuscinoses. Biochim Biophys Acta 1793:697-709.

Jalanko A, Tyynela J, Peltonen L (2006) From genes to systems: new global strategies for the characterization of NCL biology. Biochim Biophys Acta 1762:934-944.

Jalanko A, Vesa J, Manninen T, von Schantz C, Minye H, Fabritius AL, Salonen T, Rapola J, Gentile M, Kopra O, Peltonen L (2005) Mice with Ppt1Deltaex4 mutation replicate the INCL phenotype and show an inflammation-associated loss of interneurons. Neurobiol Dis 18:226-241.

Jin CY, Lee JD, Park C, Choi YH, Kim GY (2007) Curcumin attenuates the release of pro-inflammatory cytokines in lipopolysaccharide-stimulated BV2 microglia. Acta Pharmacol Sin 28:1645-1651.

Jolly RD, Shimada A, Dopfmer I, Slack PM, Birtles MJ, Palmer DN (1989) Ceroid-lipofuscinosis (Batten's disease): pathogenesis and sequential neuropathological changes in the ovine model. Neuropathol Appl Neurobiol 15:371-383.

Joly S, Lange C, Thiersch M, Samardzija M, Grimm C (2008) Leukemia inhibitory factor extends the lifespan of injured photoreceptors in vivo. J Neurosci 28:13765-13774.

Joly S, Francke M, Ulbricht E, Beck S, Seeliger M, Hirrlinger P, Hirrlinger J, Lang KS, Zinkernagel M, Odermatt B, Samardzija M, Reichenbach A, Grimm C, Reme CE (2009) Cooperative phagocytes: resident microglia and bone marrow immigrants remove dead photoreceptors in retinal lesions. Am J Pathol 174:2310-2323.

Jung KK, Lee HS, Cho JY, Shin WC, Rhee MH, Kim TG, Kang JH, Kim SH, Hong S, Kang SY (2006) Inhibitory effect of curcumin on nitric oxide production from lipopolysaccharide-activated primary microglia. Life Sci 79:2022-2031.

Kaneko H, Nishiguchi KM, Nakamura M, Kachi S, Terasaki H (2008) Characteristics of bone marrow-derived microglia in the normal and injured retina. Invest Ophthalmol Vis Sci 49:4162-4168.

Karlstetter M, Ebert S, Langmann T (2010) Microglia in the healthy and degenerating retina: insights from novel mouse models. Immunobiology 215:685-691.

Karlstetter M, Lippe E, Walczak Y, Moehle C, Aslanidis A, Mirza M, Langmann T (2011) Curcumin is a potent modulator of microglial gene expression and migration. J Neuroinflammation 8:125.

Karnovsky MJ (1965) A Formaldehyde-Glutaraldehyde Fixative of High Osmolarity for use Electron Microscopy. Journal of Cell Biology 27:137A-138A.

Katz ML, Johnson GS, Tullis GE, Lei B (2008) Phenotypic characterization of a mouse model of juvenile neuronal ceroid lipofuscinosis. Neurobiol Dis 29:242-253.

Katz ML, Gao CL, Prabhakaram M, Shibuya H, Liu PC, Johnson GS (1997) Immunochemical localization of the Batten disease (CLN3) protein in retina. Invest Ophthalmol Vis Sci 38:2375-2386.

Katz ML, Farias FH, Sanders DN, Zeng R, Khan S, Johnson GS, O'Brien DP (2011) A missense mutation in canine CLN6 in an Australian shepherd with neuronal ceroid lipofuscinosis. J Biomed Biotechnol 2011:198042.

Kettenmann H, Hoppe D, Gottmann K, Banati R, Kreutzberg G (1990) Cultured microglial cells have a distinct pattern of membrane channels different from peritoneal macrophages. J Neurosci Res 26:278-287.

Kielar C, Maddox L, Bible E, Pontikis CC, Macauley SL, Griffey MA, Wong M, Sands MS, Cooper JD (2007) Successive neuron loss in the thalamus and cortex in a mouse model of infantile neuronal ceroid lipofuscinosis. Neurobiol Dis 25:150-162.

Kim YS, Joh TH (2006) Microglia, major player in the brain inflammation: their roles in the pathogenesis of Parkinson's disease. Exp Mol Med 38:333-347.

Kitzmuller C, Haines RL, Codlin S, Cutler DF, Mole SE (2008) A function retained by the common mutant CLN3 protein is responsible for the late onset of juvenile neuronal ceroid lipofuscinosis. Hum Mol Genet 17:303-312.

Klinke J, Toth EL (2003) Preconception care for women with type 1 diabetes. Can Fam Physician 49:769-773.

Kohlschutter A, Gardiner RM, Goebel HH (1993a) Human forms of neuronal ceroid-lipofuscinosis (Batten disease): consensus on diagnostic criteria, Hamburg 1992. J Inherit Metab Dis 16:241-244.

Kohlschutter A, Schade B, Blomer B, Hubner C (1993b) Low erythrocyte plasmalogen and plasma docosahexaenoic acid (DHA) in juvenile neuronal ceroid-lipofuscinosis (JNCL). J Inherit Metab Dis 16:299-304.

Kollmann K, Uusi-Rauva K, Scifo E, Tyynela J, Jalanko A, Braulke T (2013) Cell biology and function of neuronal ceroid lipofuscinosis-related proteins. Biochim Biophys Acta.

Kopra O, Vesa J, von Schantz C, Manninen T, Minye H, Fabritius AL, Rapola J, van Diggelen OP, Saarela J, Jalanko A, Peltonen L (2004) A mouse model for Finnish variant late infantile neuronal

ceroid lipofuscinosis, CLN5, reveals neuropathology associated with early aging. Hum Mol Genet 13:2893-2906.

Kousi M, Lehesjoki AE, Mole SE (2012) Update of the mutation spectrum and clinical correlations of over 360 mutations in eight genes that underlie the neuronal ceroid lipofuscinoses. Hum Mutat 33:42-63.

Kreutzberg GW (1996) Microglia: a sensor for pathological events in the CNS. Trends Neurosci 19:312-318.

Kurze AK, Galliciotti G, Heine C, Mole SE, Quitsch A, Braulke T (2010) Pathogenic mutations cause rapid degradation of lysosomal storage disease-related membrane protein CLN6. Hum Mutat 31:E1163-1174.

Kyttala A, Ihrke G, Vesa J, Schell MJ, Luzio JP (2004) Two motifs target Batten disease protein CLN3 to lysosomes in transfected nonneuronal and neuronal cells. Mol Biol Cell 15:1313-1323.

Langmann T (2007a) Microglia activation in retinal degeneration. J Leukoc Biol 81:1345-1351.

Langmann T (2007b) Microglia activation in retinal degeneration. JLeukocBiol 81:1345-1351.

Langmann T, Ebert S, Walczak Y, Weigelt K, Ehrengruber MU, Stiewe T, Weber BH (2009) Induction of early growth response-1 mediates microglia activation in vitro but is dispensable in vivo. Neuromolecular Med 11:87-96.

Laskin DL (2009) Macrophages and inflammatory mediators in chemical toxicity: a battle of forces. Chem Res Toxicol 22:1376-1385.

Lei B, Tullis GE, Kirk MD, Zhang K, Katz ML (2006) Ocular phenotype in a mouse gene knockout model for infantile neuronal ceroid lipofuscinosis. J Neurosci Res 84:1139-1149.

Lewis GP, Fisher SK (2003) Up-regulation of glial fibrillary acidic protein in response to retinal injury: its potential role in glial remodeling and a comparison to vimentin expression. Int Rev Cytol 230:263-290.

Liu GJ, Nagarajah R, Banati RB, Bennett MR (2009) Glutamate induces directed chemotaxis of microglia. Eur J Neurosci 29:1108-1118.

Lopez-Lazaro M (2009) Distribution and biological activities of the flavonoid luteolin. Mini Rev Med Chem 9:31-59.

Lu YB, Franze K, Seifert G, Steinhauser C, Kirchhoff F, Wolburg H, Guck J, Janmey P, Wei EQ, Kas J, Reichenbach A (2006) Viscoelastic properties of individual glial cells and neurons in the CNS. Proc Natl Acad Sci U S A 103:17759-17764.

Lynch MA (2009) The multifaceted profile of activated microglia. Mol Neurobiol 40:139-156.

Macauley SL, Pekny M, Sands MS (2011) The role of attenuated astrocyte activation in infantile neuronal ceroid lipofuscinosis. J Neurosci 31:15575-15585.

Macauley SL, Wozniak DF, Kielar C, Tan Y, Cooper JD, Sands MS (2009) Cerebellar pathology and motor deficits in the palmitoyl protein thioesterase 1-deficient mouse. Exp Neurol 217:124-135.

Mandal MN, Patlolla JM, Zheng L, Agbaga MP, Tran JT, Wicker L, Kasus-Jacobi A, Elliott MH, Rao CV, Anderson RE (2009) Curcumin protects retinal cells from light-and oxidant stress-induced cell death. Free Radic Biol Med 46:672-679.

Maragakis NJ, Rothstein JD (2006) Mechanisms of Disease: astrocytes in neurodegenerative disease. Nat Clin Pract Neurol 2:679-689.

Marin-Teva JL, Dusart I, Colin C, Gervais A, van Rooijen N, Mallat M (2004) Microglia promote the death of developing Purkinje cells. Neuron 41:535-547.

Martin RE, Ranchon-Cole I, Brush RS, Williamson CR, Hopkins SA, Li F, Anderson RE (2004) P23H and S334ter opsin mutations: Increasing photoreceptor outer segment n-3 fatty acid content does not affect the course of retinal degeneration. Mol Vis 10:199-207.

Masland RH (1988) Amacrine cells. Trends Neurosci 11:405-410.

Mata NL, Tzekov RT, Liu X, Weng J, Birch DG, Travis GH (2001) Delayed dark-adaptation and lipofuscin accumulation in abcr+/- mice: implications for involvement of ABCR in age-related macular degeneration. Invest Ophthalmol Vis Sci 42:1685-1690.

Mattapallil MJ, Wawrousek EF, Chan CC, Zhao H, Roychoudhury J, Ferguson TA, Caspi RR (2012) The Rd8 mutation of the Crb1 gene is present in vendor lines of C57BL/6N mice and embryonic stem cells, and confounds ocular induced mutant phenotypes. Invest Ophthalmol Vis Sci 53:2921-2927.

Mattson MP, Cheng A (2006) Neurohormetic phytochemicals: Low-dose toxins that induce adaptive neuronal stress responses. Trends Neurosci 29:632-639.

McGill TJ, Prusky GT, Douglas RM, Yasumura D, Matthes MT, Lowe RJ, Duncan JL, Yang H, Ahern K, Daniello KM, Silver B, Lavail MM (2012) Discordant anatomical, electrophysiological, and visual behavioral profiles of retinal degeneration in rat models of retinal degenerative disease. Invest Ophthalmol Vis Sci.

Messer A, Plummer J, Wong V, Lavail MM (1993) Retinal degeneration in motor neuron degeneration (mnd) mutant mice. Exp Eye Res 57:637-641.

Miller JW, Adamis AP, Shima DT, D'Amore PA, Moulton RS, O'Reilly MS, Folkman J, Dvorak HF, Brown LF, Berse B, et al. (1994) Vascular endothelial growth factor/vascular permeability factor is temporally and spatially correlated with ocular angiogenesis in a primate model. Am J Pathol 145:574-584.

Minghetti L, Levi G (1998) Microglia as effector cells in brain damage and repair: focus on prostanoids and nitric oxide. Prog Neurobiol 54:99-125.

Mole SE, Williams RE, Goebel HH (2005) Correlations between genotype, ultrastructural morphology and clinical phenotype in the neuronal ceroid lipofuscinoses. Neurogenetics 6:107-126.

Mole SE, Michaux G, Codlin S, Wheeler RB, Sharp JD, Cutler DF (2004) CLN6, which is associated with a lysosomal storage disease, is an endoplasmic reticulum protein. Exp Cell Res 298:399-406.

Moore SJ, Buckley DJ, MacMillan A, Marshall HD, Steele L, Ray PN, Nawaz Z, Baskin B, Frecker M, Carr SM, Ives E, Parfrey PS (2008) The clinical and genetic epidemiology of neuronal ceroid lipofuscinosis in Newfoundland. Clin Genet 74:213-222.

Mukherjee PK, Marcheselli VL, Barreiro S, Hu J, Bok D, Bazan NG (2007) Neurotrophins enhance retinal pigment epithelial cell survival through neuroprotectin D1 signaling. Proc Natl Acad Sci U S A 104:13152-13157.

Muller W, Hanauske-Abel H, Loos M (1978) Biosynthesis of the first component of complement by human and guinea pig peritoneal macrophages: evidence for an independent production of the C1 subunits. J Immunol 121:1578-1584.

Nakazawa T, Takeda M, Lewis GP, Cho KS, Jiao J, Wilhelmsson U, Fisher SK, Pekny M, Chen DF, Miller JW (2007a) Attenuated glial reactions and photoreceptor degeneration after retinal detachment in mice deficient in glial fibrillary acidic protein and vimentin. Invest Ophthalmol Vis Sci 48:2760-2768.

Nakazawa T, Matsubara A, Noda K, Hisatomi T, She H, Skondra D, Miyahara S, Sobrin L, Thomas KL, Chen DF, Grosskreutz CL, Hafezi-Moghadam A, Miller JW (2006) Characterization of cytokine responses to retinal detachment in rats. Mol Vis 12:867-878.

Nakazawa T, Hisatomi T, Nakazawa C, Noda K, Maruyama K, She H, Matsubara A, Miyahara S, Nakao S, Yin Y, Benowitz L, Hafezi-Moghadam A, Miller JW (2007b) Monocyte chemoattractant protein 1 mediates retinal detachment-induced photoreceptor apoptosis. Proc Natl Acad Sci U S A 104:2425-2430.

Newman E, Reichenbach A (1996) The Muller cell: a functional element of the retina. Trends Neurosci 19:307-312.

Nimmerjahn A, Kirchhoff F, Helmchen F (2005) Resting microglial cells are highly dynamic surveillants of brain parenchyma in vivo. Science 308:1314-1318.

Noskova L, Stranecky V, Hartmannova H, Pristoupilova A, Baresova V, Ivanek R, Hulkova H, Jahnova H, van der Zee J, Staropoli JF, Sims KB, Tyynela J, Van Broeckhoven C, Nijssen PC, Mole SE, Elleder M, Kmoch S (2011) Mutations in DNAJC5, encoding cysteine-string protein alpha, cause autosomal-dominant adult-onset neuronal ceroid lipofuscinosis. Am J Hum Genet 89:241-252.

Oetari S, Sudibyo M, Commandeur JN, Samhoedi R, Vermeulen NP (1996) Effects of curcumin on cytochrome P450 and glutathione S-transferase activities in rat liver. Biochem Pharmacol 51:39-45.

Oswald MJ, Palmer DN, Kay GW, Shemilt SJ, Rezaie P, Cooper JD (2005) Glial activation spreads from specific cerebral foci and precedes neurodegeneration in presymptomatic ovine neuronal ceroid lipofuscinosis (CLN6). Neurobiol Dis 20:49-63.

Patel M, Chan CC (2008) Immunopathological aspects of age-related macular degeneration. Semin Immunopathol 30:97-110.

Pearce DA, Sherman F (1997) BTN1, a yeast gene corresponding to the human gene responsible for Batten's disease, is not essential for viability, mitochondrial function, or degradation of mitochondrial ATP synthase. Yeast 13:691-697.

Pena JA, Cardozo JJ, Montiel CM, Molina OM, Boustany R (2001) Serial MRI findings in the Costa Rican variant of neuronal ceroid-lipofuscinosis. Pediatr Neurol 25:78-80.

Perry VH (1998) A revised view of the central nervous system microenvironment and major histocompatibility complex class II antigen presentation. J Neuroimmunol 90:113-121.

Perry VH, Cunningham C, Holmes C (2007) Systemic infections and inflammation affect chronic neurodegeneration. Nat Rev Immunol 7:161-167.

Pocock JM, Kettenmann H (2007) Neurotransmitter receptors on microglia. Trends Neurosci 30:527-535.

Poitry-Yamate CL, Poitry S, Tsacopoulos M (1995) Lactate released by Muller glial cells is metabolized by photoreceptors from mammalian retina. J Neurosci 15:5179-5191.

Pontikis CC, Cotman SL, MacDonald ME, Cooper JD (2005) Thalamocortical neuron loss and localized astrocytosis in the Cln3Deltaex7/8 knock-in mouse model of Batten disease. Neurobiol Dis 20:823-836.

Pontikis CC, Cella CV, Parihar N, Lim MJ, Chakrabarti S, Mitchison HM, Mobley WC, Rezaie P, Pearce DA, Cooper JD (2004) Late onset neurodegeneration in the Cln3-/- mouse model of juvenile neuronal ceroid lipofuscinosis is preceded by low level glial activation. Brain Res 1023:231-242.

Portera-Cailliau C, Sung CH, Nathans J, Adler R (1994) Apoptotic photoreceptor cell death in mouse models of retinitis pigmentosa. Proc Natl Acad Sci U S A 91:974-978.

Prusky GT, Alam NM, Beekman S, Douglas RM (2004) Rapid quantification of adult and developing mouse spatial vision using a virtual optomotor system. Invest Ophthalmol Vis Sci 45:4611-4616.

Purkayastha S, Berliner A, Fernando SS, Ranasinghe B, Ray I, Tariq H, Banerjee P (2009) Curcumin Blocks Brain Tumor Formation. Brain Res.

Raivich G (2005) Like cops on the beat: the active role of resting microglia. Trends Neurosci 28:571-573.

Rakheja D, Narayan SB, Bennett MJ (2008) The function of CLN3P, the Batten disease protein. Mol Genet Metab 93:269-274.

Ransohoff RM, Perry VH (2009) Microglial physiology: unique stimuli, specialized responses. Annu Rev Immunol 27:119-145.

Ranta S, Zhang Y, Ross B, Lonka L, Takkunen E, Messer A, Sharp J, Wheeler R, Kusumi K, Mole S, Liu W, Soares MB, Bonaldo MF, Hirvasniemi A, de la Chapelle A, Gilliam TC, Lehesjoki AE (1999) The neuronal ceroid lipofuscinoses in human EPMR and mnd mutant mice are associated with mutations in CLN8. Nat Genet 23:233-236.

Rattner A, Nathans J (2005) The genomic response to retinal disease and injury: evidence for endothelin signaling from photoreceptors to glia. JNeurosci 25:4540-4549.

Reichenbach A, Bringmann A (2010) Mueller Cells in the Healthy and Diseased Retina: Springer New York.

Roumier A, Bechade C, Poncer JC, Smalla KH, Tomasello E, Vivier E, Gundelfinger ED, Triller A, Bessis A (2004) Impaired synaptic function in the microglial KARAP/DAP12-deficient mouse. J Neurosci 24:11421-11428.

Ruivo R, Anne C, Sagne C, Gasnier B (2009) Molecular and cellular basis of lysosomal transmembrane protein dysfunction. Biochim Biophys Acta 1793:636-649.

Sancho-Pelluz J, Arango-Gonzalez B, Kustermann S, Romero FJ, van Veen T, Zrenner E, Ekstrom P, Paquet-Durand F (2008) Photoreceptor cell death mechanisms in inherited retinal degeneration. Mol Neurobiol 38:253-269.

Sanz MM, Johnson LE, Ahuja S, Ekstrom PA, Romero J, van Veen T (2007) Significant photoreceptor rescue by treatment with a combination of antioxidants in an animal model for retinal degeneration. Neuroscience 145:1120-1129.

Sapieha P, Chen J, Stahl A, Seaward MR, Favazza TL, Juan AM, Hatton CJ, Joyal JS, Krah NM, Dennison RJ, Tang J, Kern TS, Akula JD, Smith LE (2012) Omega-3 polyunsaturated fatty acids preserve retinal function in type 2 diabetic mice. Nutr Diabetes 2:e36.

Savukoski M, Klockars T, Holmberg V, Santavuori P, Lander ES, Peltonen L (1998) CLN5, a novel gene encoding a putative transmembrane protein mutated in Finnish variant late infantile neuronal ceroid lipofuscinosis. Nat Genet 19:286-288.

Schaefer EJ, Robins SJ, Patton GM, Sandberg MA, Weigel-DiFranco CA, Rosner B, Berson EL (1995) Red blood cell membrane phosphatidylethanolamine fatty acid content in various forms of retinitis pigmentosa. J Lipid Res 36:1427-1433.

Schafer MK, Schwaeble WJ, Post C, Salvati P, Calabresi M, Sim RB, Petry F, Loos M, Weihe E (2000) Complement C1q is dramatically up-regulated in brain microglia in response to transient global cerebral ischemia. J Immunol 164:5446-5452.

Schuetz E, Thanos S (2004) Microglia-targeted pharmacotherapy in retinal neurodegenerative diseases. Curr Drug Targets 5:619-627.

Schutte M, Werner P (1998) Redistribution of glutathione in the ischemic rat retina. Neurosci Lett 246:53-56.

Schwartz M, Butovsky O, Bruck W, Hanisch UK (2006) Microglial phenotype: is the commitment reversible? Trends Neurosci 29:68-74.

Seehafer SS, Pearce DA (2006) You say lipofuscin, we say ceroid: defining autofluorescent storage material. Neurobiol Aging 27:576-588.

Seehafer SS, Ramirez-Montealegre D, Wong AM, Chan CH, Castaneda J, Horak M, Ahmadi SM, Lim MJ, Cooper JD, Pearce DA (2011) Immunosuppression alters disease severity in juvenile Batten disease mice. J Neuroimmunol 230:169-172.

Seigel GM, Wagner J, Wronska A, Campbell L, Ju W, Zhong N (2005) Progression of early postnatal retinal pathology in a mouse model of neuronal ceroid lipofuscinosis. Eye (Lond) 19:1306-1312.

Shacka JJ (2012) Mouse models of neuronal ceroid lipofuscinoses: useful pre-clinical tools to delineate disease pathophysiology and validate therapeutics. Brain Res Bull 88:43-57.

Sharma YV, Cojocaru RI, Ritter LM, Khattree N, Brooks M, Scott A, Swaroop A, Goldberg AF (2012) Protective gene expression changes elicited by an inherited defect in photoreceptor structure. PLoS One 7:e31371.

Sharp JD, Wheeler RB, Parker KA, Gardiner RM, Williams RE, Mole SE (2003) Spectrum of CLN6 mutations in variant late infantile neuronal ceroid lipofuscinosis. Hum Mutat 22:35-42.

Siintola E, Topcu M, Kohlschutter A, Salonen T, Joensuu T, Anttonen AK, Lehesjoki AE (2005) Two novel CLN6 mutations in variant late-infantile neuronal ceroid lipofuscinosis patients of Turkish origin. Clin Genet 68:167-173.

Siintola E, Partanen S, Stromme P, Haapanen A, Haltia M, Maehlen J, Lehesjoki AE, Tyynela J (2006) Cathepsin D deficiency underlies congenital human neuronal ceroid-lipofuscinosis. Brain 129:1438-1445.

Siintola E, Topcu M, Aula N, Lohi H, Minassian BA, Paterson AD, Liu XQ, Wilson C, Lahtinen U, Anttonen AK, Lehesjoki AE (2007) The novel neuronal ceroid lipofuscinosis gene MFSD8 encodes a putative lysosomal transporter. Am J Hum Genet 81:136-146.

Sleat DE, Donnelly RJ, Lackland H, Liu CG, Sohar I, Pullarkat RK, Lobel P (1997) Association of mutations in a lysosomal protein with classical late-infantile neuronal ceroid lipofuscinosis. Science 277:1802-1805.

Smith KR, Damiano J, Franceschetti S, Carpenter S, Canafoglia L, Morbin M, Rossi G, Pareyson D, Mole SE, Staropoli JF, Sims KB, Lewis J, Lin WL, Dickson DW, Dahl HH, Bahlo M, Berkovic SF (2012) Strikingly different clinicopathological phenotypes determined by progranulin-mutation dosage. Am J Hum Genet 90:1102-1107.

Smith KR, Dahl HH, Canafoglia L, Andermann E, Damiano J, Morbin M, Bruni AC, Giaccone G, Cossette P, Saftig P, Grotzinger J, Schwake M, Andermann F, Staropoli JF, Sims KB, Mole SE, Franceschetti S, Alexander NA, Cooper JD, Chapman HA, Carpenter S, Berkovic SF, Bahlo M (2013) Cathepsin F mutations cause Type B Kufs disease, an adult-onset neuronal ceroid lipofuscinosis. Hum Mol Genet 22:1417-1423.

Son TG, Camandola S, Mattson MP (2008) Hormetic dietary phytochemicals. Neuromolecular Med 10:236-246.

Soulet D, Rivest S (2008) Microglia. Curr Biol 18:R506-508.

Staropoli JF, Haliw L, Biswas S, Garrett L, Holter SM, Becker L, Skosyrski S, Da Silva-Buttkus P, Calzada-Wack J, Neff F, Rathkolb B, Rozman J, Schrewe A, Adler T, Puk O, Sun M, Favor J, Racz I, Bekeredjian R, Busch DH, Graw J, Klingenspor M, Klopstock T, Wolf E, Wurst W, Zimmer A, Lopez E, Harati H, Hill E, Krause DS, Guide J, Dragileva E, Gale E, Wheeler VC, Boustany RM, Brown DE, Breton S, Ruether K, Gailus-Durner V, Fuchs H, de Angelis MH, Cotman SL (2012) Large-scale phenotyping of an accurate genetic mouse model of JNCL identifies novel early pathology outside the central nervous system. PLoS One 7:e38310.

Steinfeld R, Fuhrmann JC, Gartner J (2006) Detection of tripeptidyl peptidase I activity in living cells by fluorogenic substrates. J Histochem Cytochem 54:991-996.

Streit WJ, Walter SA, Pennell NA (1999) Reactive microgliosis. Prog Neurobiol 57:563-581.

Sundaram V, Moore AT, Ali RR, Bainbridge JW (2012) Retinal dystrophies and gene therapy. Eur J Pediatr 171:757-765.

Sung CH, Chuang JZ (2010) The cell biology of vision. J Cell Biol 190:953-963.

Tammen I, Houweling PJ, Frugier T, Mitchell NL, Kay GW, Cavanagh JA, Cook RW, Raadsma HW, Palmer DN (2006) A missense mutation (c.184C>T) in ovine CLN6 causes neuronal ceroid lipofuscinosis in Merino sheep whereas affected South Hampshire sheep have reduced levels of CLN6 mRNA. Biochim Biophys Acta 1762:898-905.

Thanos S (1991) The Relationship of Microglial Cells to Dying Neurons During Natural Neuronal Cell Death and Axotomy-induced Degeneration of the Rat Retina. Eur J Neurosci 3:1189-1207.

Thelen M, Damme M, Schweizer M, Hagel C, Wong AM, Cooper JD, Braulke T, Galliciotti G (2012) Disruption of the autophagy-lysosome pathway is involved in neuropathology of the nclf mouse model of neuronal ceroid lipofuscinosis. PLoS One 7:e35493.

Tyynela J, Cooper JD, Khan MN, Shemilts SJ, Haltia M (2004) Hippocampal pathology in the human neuronal ceroid-lipofuscinoses: distinct patterns of storage deposition, neurodegeneration and glial activation. Brain Pathol 14:349-357.

Van Ginderachter JA, Meerschaut S, Liu Y, Brys L, De Groeve K, Hassanzadeh Ghassabeh G, Raes G, De Baetselier P (2006) Peroxisome proliferator-activated receptor gamma (PPARgamma) ligands reverse CTL suppression by alternatively activated (M2) macrophages in cancer. Blood 108:525-535.

Vaughan DW, Peters A (1974) Neuroglial cells in the cerebral cortex of rats from young adulthood to old age: an electron microscope study. J Neurocytol 3:405-429.

Veiga S, Carrero P, Pernia O, Azcoitia I, Garcia-Segura LM (2007) Translocator protein 18 kDa is involved in the regulation of reactive gliosis. Glia 55:1426-1436.

Vesa J, Hellsten E, Verkruyse LA, Camp LA, Rapola J, Santavuori P, Hofmann SL, Peltonen L (1995) Mutations in the palmitoyl protein thioesterase gene causing infantile neuronal ceroid lipofuscinosis. Nature 376:584-587.

Warrier V, Vieira M, Mole SE (2013) Genetic basis and phenotypic correlations of the neuronal ceroid lipofusinoses. Biochim Biophys Acta.

Weber BH, Schrewe H, Molday LL, Gehrig A, White KL, Seeliger MW, Jaissle GB, Friedburg C, Tamm E, Molday RS (2002) Inactivation of the murine X-linked juvenile retinoschisis gene, Rs1h, suggests a role of retinoschisin in retinal cell layer organization and synaptic structure. Proc Natl Acad Sci U S A 99:6222-6227.

Weng J, Mata NL, Azarian SM, Tzekov RT, Birch DG, Travis GH (1999) Insights into the function of Rim protein in photoreceptors and etiology of Stargardt's disease from the phenotype in abcr knockout mice. Cell 98:13-23.

Wheeler RB, Sharp JD, Schultz RA, Joslin JM, Williams RE, Mole SE (2002) The gene mutated in variant late-infantile neuronal ceroid lipofuscinosis (CLN6) and in nclf mutant mice encodes a novel predicted transmembrane protein. Am J Hum Genet 70:537-542.

Williams RE (2011) Appendix 1: NCL incidence and prevalence data. In: The Neuronal Ceroid Lipofuscinoses (Batten Disease), Second Edition (Mole SE, Williams, R.E., Goebel, H.H., ed), pp 361–365. Oxford: Oxford University Press.

Winkler BS, Boulton ME, Gottsch JD, Sternberg P (1999) Oxidative damage and age-related macular degeneration. Mol Vis 5:32.

Xu H, Chen M, Mayer EJ, Forrester JV, Dick AD (2007) Turnover of resident retinal microglia in the normal adult mouse. Glia 55:1189-1198.

Yang S, Zhang D, Yang Z, Hu X, Qian S, Liu J, Wilson B, Block M, Hong JS (2008) Curcumin protects dopaminergic neuron against LPS induced neurotoxicity in primary rat neuron/glia culture. Neurochem Res 33:2044-2053.

Yasuhara T, Shingo T, Date I (2004) The potential role of vascular endothelial growth factor in the central nervous system. Rev Neurosci 15:293-307.

Yau KW, Hardie RC (2009) Phototransduction motifs and variations. Cell 139:246-264.

Youdim KA, Shukitt-Hale B, Joseph JA (2004) Flavonoids and the brain: interactions at the blood-brain barrier and their physiological effects on the central nervous system. Free Radic Biol Med 37:1683-1693.

Zeiss CJ, Johnson EA (2004) Proliferation of microglia, but not photoreceptors, in the outer nuclear layer of the rd-1 mouse. Invest Ophthalmol Vis Sci 45:971-976.

Zeiss CJ, Neal J, Johnson EA (2004) Caspase-3 in postnatal retinal development and degeneration. Invest Ophthalmol Vis Sci 45:964-970.

Zeng HY, Zhu XA, Zhang C, Yang LP, Wu LM, Tso MO (2005) Identification of sequential events and factors associated with microglial activation, migration, and cytotoxicity in retinal degeneration in rd mice. Invest Ophthalmol Vis Sci 46:2992-2999.

Zhu J, Nathan C, Ding A (1999) Suppression of macrophage responses to bacterial lipopolysaccharide by a non-secretory form of secretory leukocyte protease inhibitor. Biochim Biophys Acta 1451:219-223.

List of Tables

Table 1	List of CLN genes which carry NCL causing mutations	p.19
Table 2	List of animals used in study, origin, mutation, genetic background and reference	p.27
Table 3	Primer and probes for TaqMan assays	p.27
Table 4	Enzymes: use and firm of purchase	p.28
Table 5	Primary antibody, species, dilution and firm of purchase	p.28
Table 6	Secondary antibody, species, dilution and firm of purchase	p.28
Table 7	Chemicals: use and firm of purchase	p.29
Table 8	Kit system: use and firm of purchase	p.29
Table 9	Diet, supplements and firm of purchase	p.30
Table 10	ERG materials and firm of purchase	p.30
Table 11	Buffers and solutions: composition, use and firm of purchase	p.31
Table 12	Basic materials, use and firm of purchase	p.32
Table 13	Machines: use and firm of purchase	p.33
Table 14	Software: use and firm of purchase	p.33
Table 15	PCR solution for *Cln3* mouse genotyping	p.35
Table 16	Primer pair for *Cln3* genotyping	p.35
Table 17	PCR program for CLN3 genotyping	p.35
Table 18	Method for DNA sequencing	p.36
Table 19	10 µl TaqMan solution	p.45

List of Figures

Figure 1	Gross anatomy of the eye ball and detailed cross-section of the human retina	p.1
Figure 2	Microglia activation occurs in a graded manner	p.5
Figure 3	Schematic representation of the Optomotor machine	p.33
Figure 4	The principle of TaqMan technology	p.36
Figure 5	Histological and immunohistological evaluation of 18 month old *Cln3*$^{\Delta ex7-8}$ retina	p.40
Figure 6	Histological and immunohistological evaluation of 12 months old *Cln3*$^{\Delta ex7-8}$ retina	p.41
Figure 7	Optokinetic tracking measurement of visual acuity using the OptoMotor system	p.42
Figure 8	Dark adapted (scotopic) ERG response of wild type and *Cln3*$^{\Delta ex7-8}$ mice at 6, 12 and 18 months of age	p.43
Figure 9	Histological and immunohistological characterization of wild type and aging *Cln6*^{nclf} mouse retina	p.46
Figure 10	TUNEL stains of *Cln6*$^{+/+}$ and *Cln6*^{nclf} retinas	p.47
Figure 11	Retinal morphometry measurements of *Cln6*$^{+/+}$ and *Cln6*^{nclf} whole retina and photoreceptor membrane	p.48
Figure 12	Optokinetic tracking measurement of aging wild type and *Cln6*^{nclf} mice	p.49
Figure 13	Rotarod performance of wild type and *Cln6*^{nclf} mice aged 4, 6 and 8 months	p.50
Figure 14	Dark adapted (scotopic) ERG response amplitudes, implicit times and b/a-wave amplitude ratios of age-matched wild type and *Cln6*^{nclf} mice	p.51
Figure 15	Quantitative real-time RT-PCR expression analysis of *Cln6*^{nclf} retinas compared to age-matched wild type controls	p.53
Figure 16	Weekly body weight of control-fed and supplemented mice	p.54
Figure 17	Histological and immunohistological comparison of control-fed	

	mice supplemented with 0.6% curcumin, 0.6% luteolin and 5% DHA	p.55
Figure 18	Retinal morphometry measurements of total retina and photoreceptor membrane layer	p.56
Figure 19	Optokinetic tracking of control and supplemented mice	p.57
Figure 20	Dark adapted ERG response amplitude, implicit time and b/a-wave amplitude ratio of age-matched *Cln6*^{nclf} control and supplemented mice	p.58
Figure 21	Quantitative real-time RT-PCR expression analysis of curcumin, luteolin, DHA-supplemented retinas compared to control	p.59

List of Abbreviations

AAP	Antartctic Phophatase
abcr$^{-/-}$	ATP-binding cassette, sub-family A (ABC1), member 4 knock out mouse
AD	Alzheimer's disease
ALS	amyotrophic lateral sclerosis
AMD	Age-related Macular Degeneration
ANCL	Adult neuronal ceroid lipofuscinosis
ATP	Adenosine-5'-triphosphate
ATP13A2	ATPase type 13A2
ATPase	Adenosintriphosphat Synthase
B.D.	Big Dye
bp	Base pairs
BSA	Bovine serum albumin
c	Concentration
c/d	Cycles per degree
C1qa	Complement C1q subunit a
Casp8	Caspase 8
CD11b	CD11b ligand
CD18	CD18 ligand
CD200	CD200 ligand
CD200R	CD200 receptor
Cd68	CD68 antigen
Cd95	CD95 antigen
cDNA	copy DNA
cDNA	Complementary DNA
CLN	Ceroid lipofuscinosis
Cln3$^{-/-}$	Cln3 knock out mouse
Cln3$^{+/+}$	Cln3 wild type mouse
Cln3$^{\Delta ex7/8}$	Cln3 exon 7-8 knock-in mouse
Cln6$^{+/+}$	*Cln6* wild type mouse
Cln6^{nclf}	*Cln6 nclf* mouse

CLN6p	CLN6 protein
CNS	Central nervous system
CO_2	Carbon dioxide
CRB1	Crumbs homolog 1
CRB1^{rd8}	Rd8 mutation in CRB1 gene mouse model
CRMP-2	collapsin response mediator protein-2
CSPα	Cysteine-string protein alpha
CT	Cycle Threshold
CTSD	Cathepsin D
CTSF	Cathepsin F
CX3CL1	chemokine (C-X3-C motif) ligand 1
CX3CR1	chemokine (C-X3-C motif) receptor 1
d	thickness
DAB	3,3'-Diaminobenzidine
DAPI	4',6-Diamidino-2-phenylindol
DHA	Docosahexaenoic acid
DNA	Deoxyribonucleic Acid
DNAJ	DNAJ chaperone
DNAJC5	DnaJ homolog subfamily C member 5
DNAse	deoxyribonuclease
dNTPs	Deoxynucleotide Triphosphates
dUTP	2´-Deoxyuridine, 5´-Triphosphate
E	extinction
EDN2	Endothelin 2
EDTA	Ethylenediaminetetraacetic acid
EEG	Electroencephalogram
EGR1	Early growth response 1
ER	Endoplasmic reticulum
ERG	Electroretinogram
EtOH	Ethanol
Exol	Exonucleaase
F4/80	surface glycoprotein F4/80
FRET	Fluorescence resonance energy transfer

GCL	Ganglion cell layer
gDNA	Genomic DNA
GFAP	glial fibrillary acidic protein
H2O	Water
H2O2	Hydrogen peroxide
HCl	Hydrogen chloride
HE	Hematoxylin-Eosin
Iba1	*ionized calcium binding adaptor molecule 1*
IFNγ	interferon-γ
IgG	Immunglobulin G
IL1	Interleukin 1
IL-10	interleukin-10
IL-1β	Interleukin -1β
IL6	Interleukin 6
INCL	Infantile neuronal ceroid lipofuscinosis
INL	Inner nuclear layer
IPL	Inner plexiform layer
IS	Inner segment
JNCL	Juvenile neuronal ceroid lipofuscinosis
kb	Kilo base
KCTD7	Potassium channel tetramerization domain-containing protein 7
LED	Light-emitting diode
Lipo	Lipofuscin
LPS	Lipopolysaccharide
LSD	lysosomal storage disorder
MCP	Monocyte chemoattractant protein
M-CSF	Macrophage colony stimulating factor
MFSD8	Major facilitator superfamily domain containing 8
MgCl	Magnesium Chloride
MHC	Major histocompatibility markers
mnd	Motor neuro degeneration
mRNA	Messenger RNA
n.d.	Not determined

Na_2HPO_4	Sodium hydrogen phosphate
NaAC	Sodium Acetate
NaCl	Sodium Chloride
NaN_3	Sodium Azide
NaOH	Sodium hydroxide
NCL	Neuronal ceroid lipofuscinosis
NFkB	nuclear factor kappa B
NPC	Neimann-Pick disease type C
O.C.T	optimum cutting temperature
OKT	Optokinetic tracking
OMIM	*Online Mendelian Inheritance in Men*
ON	Over night
ONL	Outer nuclear layer
OPL	Outer plexiform layer
OS	Outer segment
p	P value
PAMPs	pathogen-associated molecular patterns
PBS	Phosphate buffered saline
PCR	Polymerase chain reaction
PFA	paraformaldehyde
POD	Peroxidase
PPT1	Palmitoyl protein thioesterase 1
Ppt1$^{-/-}$	Ppt1 knock out mouse
PR	Photoreceptor
PUFA	polyunsatturated fatty acid
qRT-PCR	quantitative real time RT-PCR
rd	retinal degeneration 1
rds	retinal degeneration slow
Retnet	Retinal Information Network
RNA	Ribonucleic Acid
RP	Retinitis Pigmentosa
RPE	Retinal pigment epithelium
rpm	Rotation per minute

Rs1h-/Y	Retinoschisis-deficient mouse
RT	Reverse transcription
RT	Room temperature
RT-PCR	Reverse transcription polymerase chain reaction
SD	standard deviation
SDS	Sodium dodecyl sulfate
SEM	Standard error of mean
SEP	Somatosensory evoked potential
Taq	Thermus aquaticus
TBE	TRIS-Borat-EDTA
TdT	terminal transferase
TGFβ	Transforming growth factor beta
TNF	tumor necrosis factor
TNFR	tumor necrosis factor-R
TNFα	Tumor necrosis factor α
TPP1	Tripeptidyl peptidase 1
Tris	Tris(hydroxymethyl)-aminomethan
TUNEL	terminal deoxynucleotidyl transferase dUTP nick end labelling
UPL	Universal Probe Library
VEGF	vascular endothelial growth factor
VEP	Visual evoked potential
vLINCL	Variant late neuronal ceroid lipofuscinosis
w/v	Weight by volume
WT	Wild type
ε	Extinction factor

List of Publications

MIRZA M, VOLZ C, KARLSTETTER M, LANGIU M, SOMOGYI A, RUONALA MO, TAMM ER, JÄGLE H, LANGMANN T. Progressive retinal degeneration and glial activation in the *Cln6^{nclf}* mouse model of neuronal ceroid lipofuscinosis: a beneficial effect of DHA and Curcumin supplementation. In Submission to PLos One.

GROH J, KÜHL TG, IP CW, NELVAGAL HR, SRI S, DUCKETT S, **MIRZA M**, LANGMANN T, COOPER JD, MARTINI R. Immune cells perturb axons and impair neuronal survival in a mouse model of infantile neuronal ceroid lipofuscinosis. Brain. 2013 Apr;136(Pt 4):1083-101

SAMPSON HM, LAM H, CHEN PC, ZHANG D, MOTTILLO C, **MIRZA M**, QASIM K, SHRIER A, SHYNG SL, HANRAHAN JW, THOMAS DY. Compounds that correct F508del-CFTR trafficking can also correct other protein trafficking diseases: an in vitro study using cell lines**.** Orphanet J Rare Dis. 2013 Jan 14;8:11. doi: 10.1186/1750-1172-8-11.

KARLSTETTER M, LIPPE E, WALCZAK Y, MOEHLE C, ASLANIDIS A, **MIRZA M**, LANGMANN T. Curcumin is a potent modulator of microglial gene expression and migration. J Neuroinflammation. 2011 Sep 29;8:125. doi: 10.1186/1742-2094-8-125.

OUSINGSAWAT J, **MIRZA M**, TIAN Y, ROUSSA E, SCHREIBER R, COOK DI, KUNZELMANN K. Rotavirus toxin NSP4 induces diarrhea by activation of TMEM16A and inhibition of Na+ absorption. Pflugers Arch. 2011 May;461(5):579-89. doi: 10.1007/s00424-011-0947-0. Epub 2011 Mar 12.

SCHREIBER R, ULIYAKINA I, KONGSUPHOL P, WARTH R, **MIRZA M**, MARTINS JR, KUNZELMANN K. Expression and function of epithelial anoctamins**.** Journal of Biological Chemistry. 2010;285(10):7838-45

GORDON, DE*, **MIRZA M**,* SAHLENDER DA, JAKOVLESKA J AND PEDEN AA. Coiled-coil interactions are required for post-Golgi R-SNARE trafficking. EMBO Reports. 2009; 10(8):851-6. *Co-First Authors

Conferences

2010
Annual Meeting of the European Macrophage and Dendritic Cell Society (EMDS)
Edinburgh, UK (Attendee)

2011
22nd Meeting of the German Society of Human Genetics
Regensburg, Germany
Retinal degeneration and microglial activation in mouse models of neuronal ceroid lipofuscinosis (Poster)

Pro Retina Research-Colloquium
Potsdam, Germany
Retinal degeneration and microglial activation in mouse models of neuronal ceroid lipofuscinosis (Poster)

1st JNCL PhD Symposium
Hamburg, Germany
Retinal degeneration and microglial activation in mouse models of neuronal ceroid lipofuscinosis (Speaker)

10th European meeting on Glial Cells in Health and Disease
Prague, Czech Republic
Retinal degeneration and microglial activation in mouse models of neuronal ceroid lipofuscinosis (Poster)

2012
13th International Congress on The Neuronal Ceroid Lipofuscinoses (Batten Disease)
London, England
Retinal degeneration and microglial activation in mouse models of neuronal ceroid lipofuscinosis (Poster, Poster awardee)

The Association for Research in Vision and Ophthalmology (ARVO) 2012
Fort-Lauderdale, USA
Retinal degeneration and microglial activation in mouse models of neuronal ceroid lipofuscinosis (Poster)

XX Biennial Meeting of the International Society of Eye research (ISER)
Berlin, Germany
Retinal degeneration and microglial activation in mouse models of neuronal ceroid lipofuscinosis (Poster, Novartis Travel Grant)

Jahrestreffen der NCL-Gruppe Deutschland
Barsinghausen, Germany
Retinal degeneration and microglial activation in mouse models of neuronal ceroid lipofuscinosis (Speaker)

2013
2nd JNCL PhD Symposium together with the Brains 4 Brains workshop
Frankfurt, Germany
Curcumin, Luteolin and DHA Supplementation Abates Microglia Activation and Retinal Degeneration in the CLN6^{nclf} Neuronal Ceroid Lipofuscinosis Mouse Model (Speaker)

39th Annual Meeting of the Society of Neuropaediatrics
Innsbruck, Austria
Retinal degeneration and Inflammation in neuronal ceroid lipofuscinosis (NCL) (Speaker)

The Association for Research in Vision and Ophthalmology (ARVO) 2013
Seattle, USA
Curcumin, Luteolin and DHA Supplementation Abates Microglia Activation and Retinal Degeneration in the CLN6^{nclf} Neuronal Ceroid Lipofuscinosis Mouse Model (Poster)

Curriculum Vitae

Myriam Mirza, M.Sc.

August 20, 1985, Montreal, Canada

Education

Diploma of Collegial Studies, International Baccalaureate Program in Health Sciences. Champlain College, St-Lambert, CANADA. August 2002-June 2004

Bachelor of Science: Honors Biochemistry. McGill University, Montreal CANADA. August 2004 - June 2007.

Master of Science: Biochemistry and Chemical Biology. McGill University, Montreal CANADA. August 2007 - June 2009. Title: Characterization of New CFTR Monoclonal Antibodies

Doctor of Philosophy in Science: Biology, Human Genetics. Regensburg University, Regensburg, GERMANY. May 2010 – present. Title: Characterization of the retinal degeneration and glial activation of neuronal ceroid lipofuscinosis mouse models *Cln3*$^{\Delta ex7\text{-}8}$ and *Cln6*^{nclf} and the beneficial effects of dietary supplementation

Distinctions and Credentials

Chemical Biology Scholarship, CIHR, Canada, Effective: 09/2008, Ending: 09/2009

National Contest for Life_NCL Stiftung Hamburg, Germany, Effective: 05/2010, Ending: 10/2011

Novartis Travel Fellowship to ISER Berlin July 2012

Work Experience

Research Assistant 10/2009-04/2010

Regensburg University, Regensburg, GERMANY

Under the supervision of Prof. Dr. Karl Kunzelmann I studied electro-physiology of siRNA knocked down elements and their effect on CFTR. Additionally, I improved the western blotting system in the lab. I also studied TMEM16a and anoctamin mutations via western blot.

Research Assistant 06/2009-10/2009

Université de Montreal, Montreal, CANADA

Dr. Katherine Borden is a leading scientist in the field of leukemia and is running a nationwide clinical trial on M4/M5 acute myeloid leukemia. I assisted in doing real time PCR on tissue samples collected from patients in the clinical trial as well as western blots by looking for changes in specific markers in these patients.

Research Assistant 05/2007 - 08/2007

Cambridge University, Cambridge, U.K.

Under the supervision of Dr. Andrew Peden, I studied the role of VAMPs and SNAREs in post-golgi trafficking. The main objective was to learn how vesicles trafficked to the plasma membrane and back through the lysosomes to the Trans-Golgi Network. This was done by creating mutant cell lines and studying the effects by immunofluorescence.

Summer Student 05/2006 - 08/2006

Université de Poitiers, Poitiers, FRANCE

The cystic fibrosis laboratory of Dr. Frederic Becq works on better understanding CF and finding drugs which can correct the trafficking of the mutated protein CFTR. My project consisted of testing the drug Miglustat on different cell lines as well as improving and teaching the western blotting technique to the mostly patch-clamp laboratory.

Summer Student 05/2005 - 08/2005

McGill University, Montreal, CANADA

Dr. David Y Thomas had recently started working on CF when I joined the group and started undertaking a major compound screen in search for compounds which could push mutated CFTR to the plasma membrane. I assisted in the screen by western blotting the positive hits and observing effects through confocal microscopy.

Research Assistant 10/2004 - 03/2005

Montreal Children's Hospital, Montreal, CANADA

- Working in collaboration with the Toronto's Sick Kids Hospital on The Gene Modifier project
- Conducting thorough research on the medical history of patients with Cystic Fibrosis
- Combining data on Excel databases

Summer Student Lab Bench Learner 06/2003 - 08/2003

Montreal Children's Hospital, Montreal, CANADA

Cystic Fibrosis specialist Dr. Larry Lands studies the relationship between CF, chemokines and oxidation in cells. As a learning student I was given a simple project of determining which was the best way to normalize CF assays in papers, either using cell number or protein content. Through protein assays and cell counting it was concluded that cell number was the best form of normalization. The published abstract is mentioned below.

Acknowledgements

First and foremost, I would like to thank *Prof. Dr. Thomas Langmann* for giving me the opportunity to work in his lab and be part of his group. Prof. Langmann and I met when I nearly gave up on science and through his patience, kindness, great ideas, encouragement and friendly openness, restored my love and passion for science. He gave me a wonderful Ph.D. project and allowed me to explore my strengths as a scientist and become a better person. I could not envision working with a better supervisor or scientist and I am deeply grateful that our paths crossed when they did.

I would like to thank *Prof. Dr. Stephan Schneuwly* and *Prof. Dr. Rudolf Martini* for being my mentors, committee members and for their support. I would also like to thank P*rof. Dr. Ernst Tamm* for allowing me to work in his lab and sharing his equipment and wonderful lab technicians as well as being the chairman of my thesis committee.

Thank you for *Prof. Dr. Bernhard Weber* for giving me a place to work in the Institute of Human Genetics as well as allowing me to stay and continue my work when my lab moved away.

Thank you to *Dr. Klaus Rüther* for providing the *Cln3*$^{\Delta ex7\text{-}8}$ and *Cln6*^{nclf} mice without which my Ph.D. would not be possible.

Thank you to *Dr. Frank Stehr* from the NCL Stiftung in Hamburg for his endless support, advice and networking. Also, thank you to the NCL Stiftung for supporting part of my work and giving me the wonderful opportunity to work on NCL. Thank you to *Iris Dyck* from the NCL Gruppe Deutschland for supporting the supplementation study and giving me the opportunity to meet children and parents affected by NCL. It really changed my perspective on my research and what it means to be a scientist.

A big thank you for *Prof. Dr. Herbert Jägle* for the ERG experiments and putting up with my endless emails. A special thanks to *Dr. MD Cornelia Volz* for doing the ERG experiments and for playing Sherlock Holmes/Dr. Watson when results and experiments went funny. With her fantastic sense of humour, I always looked forward to her visits in the lab and I am glad we became good friends.

A heartfelt thanks to my lab mates *Alex Aslanidis* and *Dr. Marcus Karlstetter* for being wonderful, funny and helpful colleagues. They made coming to the lab a pleasure. A special thanks to *Yana Walczac* for putting up with me when I had no idea how the lab worked and teaching me so many techniques.

I would like to thank the animal care takers, *Engelbert Meier* and *Stephan Garbowski* for taking such good care of my mice and for their endless friendliness, jokes and occasional coffee.

I would like to extend my sincerest thanks to all the wonderful people in the Institute of Human Genetics for being so kind, helpful and friendly. A particular thanks to *Andrea Milenkovic* and *Kerstin Meier* who would always listen to my dramatic problems of life and lab. A special thanks to secretary *Regina Gellner* for understanding my broken German and helping me with all my paper work when I didn't know what to do.

A special personal thanks to my partner in crime, *Kerstin Rückl*, for being the best technician I have ever met and worked with. She was the first person I went to see when I had any problems or favours. I could not have gone through my last year of Ph.D. sane if she was not with me. She was always in a good mood, always smiling and always up for a new experiment. I will miss you so much. If I ever have a lab of my own, I will steal you!!

I would like to thank my partner and best friend, *Markus Reichold*, for his patience, support and encouragement, not only through my Ph.D., but also through my difficult journey in Germany. He is always there for me with advice, motivation and love, through good and bad times. I could not have made it without him by my side and I am very grateful to have him in my life.

I would like to thank my wonderful, supportive family. My uncles, aunts and cousins have always encouraged me and wished me the best. Special thanks to my cousin *Amber Mirza*, for waking up at 3am when I needed someone to talk to and my brother *Ismaël Mirza*, for being so ambitious and inspiring in everything he does and wants to accomplished.

Finally, I would like to thank my father, *Aftab Mirza* and my mother, *Nancy Chapados*. My father immigrated to Canada when he was a young man, with little education but very big dreams of building an incredible life for his family. I would not be where I am now, if my father didn't work so

hard and long hours to support us through good and bad times. He has always pushed me to do my best and go as far with my education as I possibly can because he believes that education is the most important thing a person can have. My mother has been my rock and my wings throughout my life. She has supported everything I do without question and I cannot think of another person who is braver or stronger than her. I would not be here if she did not push me to be the very best I am every day. Her wisdom and love have guided me through everything in my life, even from an ocean away. I am very grateful that my parents gave me every opportunity I needed to succeed with unconditional love and support.